INTERACTION OF CONSERVATIVE DESIGN PRACTICES, TESTS AND INSPECTIONS IN SAFETY OF STRUCTURAL COMPONENTS

By

AMIT ANAND KALE

A DISSERTATION PRESENTED TO THE GRADUATE SCHOOL
OF THE UNIVERSITY OF FLORIDA IN PARTIAL FULFILLMENT
OF THE REQUIREMENTS FOR THE DEGREE OF
DOCTOR OF PHILOSOPHY

UNIVERSITY OF FLORIDA

2005

This dissertation is dedicated to my parents

ACKNOWLEDGMENTS

I want to express my appreciation and special thanks to Dr. Raphael T. Haftka, chairman of my advisory committee. He has been a great mentor and constant source of inspiration and encouragement during my doctoral studies, and I want to thank him for providing me with the excellent opportunity and financial support to complete my doctoral studies under his exceptional guidance. He encouraged me to attend several conferences in the area of reliability based design optimization and helped me gain industrial experience in my research area through an internship during my doctoral studies. I am especially impressed by his unlimited zeal to explore new research areas, encourage new ideas and share his knowledge and experience with me. The interaction I have had with Dr. Haftka has helped me improve my personal and professional life.

I would also like to thank the members of my advisory committee, Dr. Bhavani V. Sankar, Dr. Nam Ho Kim, Dr. Nagaraj K. Arakere and Dr. Stanislav Uryasev. I am grateful for their willingness to serve on my committee, provide me with help whenever required, involvement with my oral qualifying examination, and for reviewing this dissertation. Special thanks go to Dr. Bhavani V. Sankar for his guidance with several technical issues during my research and Dr. Nam Ho Kim for his comments and suggestions during group presentations which helped me improve my work.

I would also like to thank Dr. Ben H. Thacker and Dr. Narasi Sridhar who gave me the excellent opportunity to work with them on an industrial project at Southwest Research Institute.

My colleagues in the Structural and Multidisciplinary Optimization Research Group at the University of Florida also deserve thanks for their help and many fruitful discussions. Special thanks go to Dr. Melih Papila and Erdem Acar who collaborated with me on several research papers.

The financial support provided by NASA CUIP (formerly URETI) Grant NCC3-994 to the Institute for Future Space Transport (IFST) at the University of Florida and NASA Grant NAG1-02042 is fully acknowledged.

My parents deserve my deepest appreciation for their constant love and support and for encouraging me to pursue a Ph.D.

TABLE OF CONTENTS

LIST OF TABLES

LIST OF FIGURES

KEY TO SYMBOLS

a = Crack size, *mm*

a_c = Critical crack size, *mm*

a_{cH} = Critical crack length due to hoop stress, *mm*

a_{cL} = Critical crack length for transverse stress, *mm*

a_{cY} = Critical crack length causing yield of net section of panel, *mm*

a_h = Crack size at which probability of detection is 50%, *mm*

a_i = Initial crack size, *mm*

$a_{i,0}$ = Crack size due to fabrication defects, *mm*

a_N = Crack size after N cycles of fatigue loading, *mm*

A_s = Area of a stiffener, $meter^2$

A_{Total} = Total cross sectional area of panel, $meter^2$

b = Panel length, *meters*

B_k = Error bounds on error in stress, k

cov = Coefficient of variation, (standard deviation divided by mean)

C = Distance from neutral axis of stiffener to skin, *meters*

C_{kb} = Cost of inspection schedule developed using k^{th} inspection type, dollars

C_{min} = Minimum cost of inspection schedule, dollars

C_{tot} = Total life cycle cost, dollars

d = Fastener diameter, *mm*

D = Paris model parameter, $meters^{1-\frac{m}{2}}(MPa)^{-m}$

e = Error in crack growth rate

E = Elastic modulus, MPa

F = Force at a rivet on intact stiffener, N

F_c = Fuel cost per pound per flight, dollars

$F^{\max}_{FirstStiffener}$ = Maximum stress on first stiffener, MPa

$F^{\max}_{SecondStiffener}$ = Maximum stress on second stiffener, MPa

$F^{\max}_{ThirdStiffener}$ = Maximum stress on third stiffener, MPa

g = Limit state function used to determine structural failure

h = Panel width, $meters$

H_1 = Fastener shear displacement parameter

H_2 = Fastener shear displacement parameter

i = Subscript used to denote indices

I = Stiffener inertia, $meter^4$

I_c = Inspection cost, dollars

I_{ck} = Cost of inspection of k^{th} type, I_{c1}, I_{c2},, I_{c3}, I_{c4}, dollars

I_k = Inspection of k^{th} type, $k = 1\ldots4$

k = Error in stress calculation

K = Stress intensity factor, $MPa\sqrt{meters}$

K_F = Stress intensity due to fastener forces, $MPa\sqrt{meter}$

K_{IC} = Fracture toughness, $MPa\sqrt{meters}$

K_{Total} = Total stress intensity on stiffened panel, $MPa\sqrt{meter}$

L = Frame spacing, *meters*

l = Fuselage length, *meters*

m = Paris model exponent, Eq. 3-1

M_{A_i} = Average bending moment between the i^{th} and i-1^{st} fastener, *N-meter*

M_c = Material manufacturing cost per pound for aluminum, dollars

n = Number of fastener on a side of crack centerline on a single stiffener

N = Number of cycles of fatigue loading

N_f = Fatigue life, flights (Flights, time and cycles are used interchangbly)

N_i = Number of Inspections

N_p = Number of panels

N_s = Number of stiffeners

N_{ub} = Number of intact stiffeners

p = Fuselage pressure differential, *MPa*

P = Force at a rivet on broken stiffener, *N*

P_c = Probability of failure after certification testing

P_d = Probability of detection

P_d^{rand} = Random number for probability of detection

P_f = Failure probability

Pf_{th} = Threshold probability of failure, reliability constraint

P_{nc} = Probability of failure without certification testing

r = Fuselage radius, *meters*

r_1 = Distance of a point from crack leading tip, *meters*

r_2 = Distance of a point from crack tailing tip, *meters*

r_3 = Parametric distance of a point ahead of *y* axis by a distance *b, meters*

r_4 = Parametric distance of a point behind of *y* axis by a distance *b, meters*

R = Batch rejection rate

s = Fastener spacing, *mm*

S_{FL} = Safety factor on life

S_F = Safety factor on load

S_l = Service Life (40,000 flights)

S_n = n^{th} inspection time in number of cycles or flights

t = Panel thickness, *mm*

t_2 = Thickness of the stiffener flange, *meters*

t_{cert} = Thickness of certified structures

t_{design} = Thickness of designed structures

t_s = Stiffener thickness, *mm*

V_1 = Displacement anywhere in the cracked sheet caused by the applied gross stress, *meters*

V_2 = Displacement in the uncracked sheet resulting from fastener load *F, meters*

V_3 = Displacement in the uncracked sheet resulting from broken fastener load *P, meters*

V_4 = Displacement in the cracked sheet resulting from stress applied to the crack face equal and opposite to the stresses caused by rivet loads, *meters*

V_F = Displacement at a point in and infinite plate due to a point force *F*

W = Structural weight, *lb*

Y = Yield stress, *MPa*

β = Inspection parameter

β_d = Reliability index

δ_{D_i} = Stiffened displacement due to direct fastener load at i^{th} fastener location, *meters*

δ_{G_i} = Stiffener displacement due to applied stress at i^{th} fastener location, *meters*

δ_{M_i} = Stiffener displacement due to bending at i^{th} fastener location, *meters*

δ_{R_i} = Fastener displacement due to elastic shear, *meters*

μ_{ai}-RSA = Response surface for estimating mean of crack size distribution, *mm*

ν = Poisson's ratio

ϕ = Cumulative density function of standard normal distribution

ψ = Geometric factor due to stiffening

ρ = Density of aluminum, lb/ft^3

σ = Hoop stress, *MPa*

σ_{ai}-RSA = Response surface estimating standard deviation of crack size distribution, *mm*

θ = Angle at a point as measured from origin (The x axis lies along the crack and y axis is perpendicular to crack with origin at crack center)

θ_1 = Angle at a point as measured from leading crack tip.

θ_2 = Angle at a point as measured from tailing crack tip.

Abstract of Dissertation Presented to the Graduate School
of the University of Florida in Partial Fulfillment of the
Requirements for the Degree of Doctor of Philosophy

INTERACTION OF CONSERVATIVE DESIGN PRACTICES, TESTS AND INSPECTIONS IN SAFETY OF STRUCTURAL COMPONENTS

By

Amit Anand Kale

December 2005

Chair: Raphael T. Haftka
Cochair: Bhavani V. Sankar
Major Department: Mechanical and Aerospace Engineering

Structural safety is achieved in aerospace application and other fields by using conservative design measures like safety factors, conservative material properties, tests and inspections to compensate for uncertainty in predicting structural failure. The objective of this dissertation is to clarify the interaction between these safety measures, and to explore the potential of including the interaction in the design process so that lifetime cost can be reduced by trading more expensive safety measures for less expensive ones. The work is a part of a larger effort to incorporate the effect of error and variability control in the design process. Inspections are featured more prominently than other safety measures.

The uncertainties are readily incorporated into the design process by using a probabilistic approach. We explore the interaction of variability, inspections and structural sizes on reliability of structural components subjected to fatigue damage growth. Structural sizes and inspection schedule are optimized simultaneously to reduce

operational cost by trading the cost of structural weight against inspections to maintain desired safety level.

Reliability analysis for fatigue cracking is computationally challenging. The high computational cost for estimating very low probabilities of failure combined with the need for repeated analysis for optimization of structural design and inspection times makes combined optimization of the inspection schedules and structural design prohibitively costly. This dissertation develops an efficient computational technique to perform reliability based optimization of structural design and inspection schedule combining Monte Carlo simulation (MCS) and first-order reliability method (FORM). The effect of the structural design and the inspection schedule on the operational cost and reliability is explored. Results revealed that the use of inspections can be very cost effective in maintaining structural safety.

Inspections can be made more effective if done at critical locations where likelihood of failure is maximum and the information obtained from inspections can be used to improve failure prediction and update reliability. This aspect is studied by developing a probabilistic model for predicting locations of maximum corrosion damage in gas pipelines. Inspections are done at these locations and failure probabilities are updated based on data obtained from inspections.

CHAPTER 1
INTRODUCTION

Motivation

Computation of life expectancy of structural components is an essential element of aircraft structural design. It has been shown that the life of a structure cannot be accurately determined even in carefully controlled conditions because of variability in material properties, manufacturing defects and environmental factors like corrosion.

Safety of aircraft structures is largely maintained by using conservative design practices to safeguard against uncertainties involved in the design process and service usage. Typically, conservative material property, scatter factor in fatigue life and conservative loads are used to design structures. This is further augmented by quality control measures like certification testing and inspections. Safety measures compensate for uncertainty in load modeling, stress analysis, material properties and factors that lead to errors in modeling structural failure. These safety measures were gradually developed based on empirical data obtained from service experience and are usually geared to target specific types of uncertainty. For example, the use of conservative material properties provide protection against variability in material properties, using machined crack for certification and conservative initial defect provide protection against flaws induced during manufacturing and fabrication, and inspections protect against uncertainty in damage growth and accidental damage that cannot be predicted during the service life.

The use of multiple safety measures along with quality control measures is costly. With a view of reducing lifetime cost and maintaining structural safety, this dissertation

is a step towards understanding the interaction between inspections and structural design. Inspections serve as protection against uncertainty in failure due to damage growth and reliability based design optimization is used to incorporate these uncertainties and trade the cost of inspection against structural weight to reduce overall life cycle cost.

Objective

The objective of this dissertation is to explore the possibility of designing safe structures at lower lifetime cost by including the interaction between safety measures and trading inspection costs against the cost of additional structural weight. With the view to reducing cost of operation of aircraft structures and maintaining low risk of structural failure, we address the problem of developing optimum structural design together with inspection schedule. The approach is based on the application of methods of structural reliability analysis. Reliability based optimization is computationally expensive when inspections are involved because crack size distribution has to be re-characterized after each inspection to simulate replacement. Typically, the crack size distribution after an inspection will not have a simple analytical form and can only be determined using expensive numerical techniques. A second objective of this dissertation is to develop an efficient computational method to estimate reliability with inspection.

Outline

This dissertation uses a combination of reliability methods, Monte Carlo simulation (MCS), first-order reliability method (FORM) and response surface approximations (RSA's), to perform reliability based optimization of structural design and inspection schedule. Typical examples of aircraft structures designed for fatigue crack growth and inspection plans are used to demonstrate the application of this methodology.

Most of the chapters in the dissertation are revised versions of conference or journal papers with multiple authors. The outline below gives the chapter description and an acknowledgement of the role of the other authors.

Chapter 2 presents the background and a literature survey on current methods used to design aircraft structures for damage growth. Uncertainty is a critical component in aircraft structural design and probabilistic methods are used to incorporate uncertainty in designing structures. This chapter also reviews reliability based methods used to design for structural safety.

Chapter 3 is close to Kale *et al.* (2005). It presents the simultaneous optimization of structural design and inspection schedule for fatigue damage growth. The computational methodology for efficient reliability calculation in the presence of inspections is described here. A typical aircraft structural design of fuselage stiffened panel is used to demonstrate application of the proposed method.

Chapter 4 is close to Kale *et al.* (2004). It presents the optimization of inspection schedule with multiple inspection types which are typically used in aerospace applications. This work was done in collaboration with Dr. Melih Papila, who provided inputs on cost of inspections and structural weight. A simple unstiffened panel design is used to obtain optimal structural design and inspection sequence. A mixture of different inspection types is used to generate the inspection schedule.

Chapter 5 is close to Kale *et al.* (2005). It presents the interaction among various safety measures recommended by the Federal Aviation Administration (FAA) to design aircraft structures for damage tolerance. Interaction among safety measures, uncertainty and certification tests is studied. In particular it sheds light on the effectiveness of

certification testing for fatigue. The computational method used in this chapter was developed in collaboration with Erdem Acar.

Chapter 6 is close to Kale *et al.* (2004). It shows how information obtained from in-service inspections can be used to update failure models and reliability using Bayesian updating. The methodology is applied to reliability assessment of gas pipelines subjected to corrosion damage. Risk based inspection plans are developed to determine optimal inspection locations where probability of corrosion damage is maximum. This work was done in collaboration with Dr. Ben H. Thacker, Dr. Narasi Sridhar and Dr. Chris Waldhart at the Southwest Research Institute.

CHAPTER 2
BACKGROUND

Structural Design Methodology

Aerospace structural design philosophy has been evolving continuously based on feedback from operational experience. The major drive in this evolution has been improving safety throughout the service life of the structure while reducing weight. Consequently, in the past few years there has been growing interest in reliability-based design and optimization of structures.

The loss of structural integrity with service usage is associated with propagation of damage such as fatigue cracks in metal structures or delamination in composite structures. In addition, damage may be inflicted by corrosion, freeze-thaw cycles, and accidents such as a turbine blade tearing through the structure or damage due to impact from birds or other objects. The effect of damage may be to reduce the residual strength of the structure below what is needed to carry the flight loads (limit loads or the design load). Alternatively, the damage may be unstable and propagate quickly resulting in the destruction of structural components.

In case of damage due to fatigue, a designer must consider damage initiation and damage growth. The potential for damage initiation and growth in structures has led to two concepts in structural design for safety: safe-life and fail-safe. Niu (1990) and Bristow (2000) have characterized the safe-life and fail-safe design methodologies in that, reliability of a safe-life structure is maintained by replacing components if their design life is less than the service life. Inspections or repairs are not performed. In

contrast, structural safety in a fail-safe design is maintained by means of design for damage containment or arrestment and alternative load-paths that preserve limit-load capabilities. These mechanisms are complemented with periodic inspections and repairs. Bristow (2000) provided historical insight on the evolution of structural design philosophy from safe-life in the early 50's to damage-tolerance used in present time.

The current practice to design structures using damage tolerance has gained widespread acceptance because of uncertainty in damage initiation and growth. Here we assume that cracks are always present in the structure due to manufacturing and fabrication and grow due to applied loads, corrosion and impacts. The Federal Aviation Administration (FAA) requires that all structures designed for damage tolerance be demonstrated to avoid failure due to fatigue, manufacturing defects and accidental damage (FAR 25.571, damage tolerance and fatigue evaluation of civil and transport category airplanes).

The purpose of damage tolerant design is to ensure that cracks will not become critical until they are detected and repaired by means of periodic inspections. Inspections play an important role in maintaining structural integrity by compensating for damage that cannot be predicted or modeled during the design due to randomness in loading, accidental impact damage and environmental factors. In today's practice both safe-life and fail-safe structural design concepts are necessary to create a structurally safe and operationally satisfactory components. These two concepts have found application in structural design of airplanes, bridges and other engineering structures for different structural parts based on the functionalities and associated redundancy level. For instance, nose landing gear and main landing gear do not employ any redundancy and

exhibit a short fatigue life. Therefore they are designated as safe-life structures. Wing skin-stringer and fuselage skin-stringer panels have a substantial fatigue life and usually offer structural redundancy, so they are designated as fail-safe structures.

Estimating Fatigue Life and Crack Sizes

Structural components experience numerous repetitive load cycles of normal flight conditions during their service life. In addition, less frequent but higher loads originating from strong atmospheric gusts or unexpected maneuvers during the life of aircraft are inevitable. Flaws and imperfections in the structure, such as micro cracks or delamination, may propagate under such service experience. Estimating fatigue life and crack size is a challenging task as there are no physical models available to determine crack growth as a function of the numerous factors that affect it.

The load spectrum of an aircraft gives first hand information on the expected service load for which the airplane should be designed. The load history of aircraft is generated by load factor measurements from accelerometer placed at the center-of gravity. The number of times a load factor is exceeded for a given maneuver type (cruise, climb, etc.) is recorded for 1000 hours of flight. This load factor data are converted into stress histories, which can be used in fatigue calculations (Nees and Canfield, 1998; Arietta and Striz, 2000, 2005). Load histories are converted into number of cycles at given load levels and then a damage accumulation rule can be used with stress-fatigue life (S-N curve) to estimate fatigue life. The Palmgren-Miner linear damage accumulation rules (Miner, 1945) has been popular in aerospace application since the early 1950s to the present day. This rule computes the fatigue life as the summation of ratios of applied load cycles at a given level divided by the allowable number of load cycles to failure at the same stress level which can be obtained from S-N curve (e.g., Tisseyre *et al.*, 1994).

An alternative fatigue life estimation method involves using crack propagation models obtained by fitting empirical models to experimental data. A breakthrough in damage growth rate prediction was achieved when Paris and Erdogan (1960) showed that damage grows exponentially as a function of crack tip stress intensity with each load cycle. Several modifications of the Paris model have been suggested to make the prediction more accurate and suitable for a specific set of loading condition; however the basic nature of the equations have remained unaltered. For instance Walker (1970) modified the Paris model by introducing an additional parameter to make it more accurate for variable amplitude loading when the history has both tensile and compressive stresses. Elber (1970) introduced the fatigue crack closure effect due to tensile overload effect in variable amplitude loading. Later crack growth retardation effects observed in variable amplitude loading were also introduced. Wheeler (1972) used the plastic zone size to modify the Paris model. These damage growth models have been widely used for life prediction with some modifications in structural design applications; e.g., Harkness (1994) and Tisseyre *et al.* (1994) used it in aerospace applications, and Enright and Frangopol (2000) used it for bridge design.

Probabilistic Approach for Fatigue Life Prediction

Aircraft structural design is still done by and large using code-based design rather than probabilistic approaches. Safety is improved through conservative design practices that include use of safety factors and conservative material properties. It is also improved by tests of components and certification tests that can reveal inadequacies in analysis or construction. These safety measures listed in FAR 25 for civil and transport category airplanes and Joint Service Specification Guide-2006 (JSSG). Use of large safety measures increases the structural weight and operational cost.

The main complexity for designing damage tolerant structures via safe-life and fail-safe concepts in design is due to uncertainties involved. These include uncertainty in modeling physical phenomena affecting structural integrity (e.g., loading, crack growth) and uncertainty in data (e.g., material properties). Inspection and replacement add additional uncertainty because damage detection capabilities depend on random factors such as location of the damages or labor quality and equipments. It has been demonstrated that small variations in material properties, loading and errors in modeling damage growth can produce huge scatter in fatigue life, (e.g., Harkness, 1994; Sinclair and Pierie, 1990) which makes it inevitable to use large safety measures during the design process.

Uncertainties are inevitable and past service experience in the design of new structures have become a key factor in modern damage tolerant design approaches. Statistical data are collected for material properties, load histories (by the use of accelerometers) and damage initiation and growth by scheduled inspections. Then the associated uncertainties may be introduced into the design procedure by probabilistic approaches.

A reliability-based approach towards structural design requires us to account for uncertainty in damage initiation, damage growth with time, residual strength and damage detection. In probabilistic formulation uncertainty is incorporated into the design process by representing random variables by probability distributions and unacceptable design is determined by calculating probability of failure of the damage state exceeding critical allowable state. The combination of probabilistic approach and fracture mechanics in fatigue life prediction has been demonstrated by Provan *et al.* (1987) and Belytschko *et*

al. (1992). Uncertainty in damage initiation and growth has been introduced into life prediction by Rahman and Rice (1992); Harkness (1994); Brot (1994) and Backman (2001). Uncertainty in loading has been incorporated by Nees and Canfield (1998) and Arietta and Striz (2005) by using load history. Tisseyre *et al.* (1994) and Enright and Frangopol (2000) used reliability based formulation to predict fatigue failure of structural components subjected to uncertainty in loading, damage initiation and growth. Backman (2001) studied reliability of aircraft structures subjected to impact damage.

Environmental factors like corrosion, enhance crack growth rates. The effect of environmental factors has been studied by fitting empirical models to experimental data. Weir *et al.* (1980) developed a linear model to describe the enhancement in fatigue crack growth in the presence of aggressive environment due to hydrogen enhanced embrittlement. Recently there has been advancement in estimating corrosion-fatigue growth rates. Harlow and Wei (1998) obtained empirical model for rate of corrosion fatigue in aggressive environment by fitting experimental results to linear models.

Probabilistic analysis is also very useful when there is no single model that can completely describe the crack growth phenomena for given set of conditions. When there are wide range of competing models, Bayesian updating techniques can be used to identify the most appropriate model that accurately predict the physical phenomenon. Zhang and Mahadevan (2000) used this method to determine the better of two competing crack growth models based on observed data.

Reliability Based Design

Fluctuations in loads, variability in material properties and errors in analytical models used for designing the structure contribute to a chance that the structure will not perform its intended function. Reliability analysis deals with the methods to calculate the

probability of structural failure subjected to such uncertainty. A typical reliability analysis problem can be defined as

$$P_f(d,x) = \int_{g(d,x)<0} f_x(x)dx$$
$$\textit{where} \qquad (2\text{-}1)$$
$$g(d,x) = R - S$$

where d is the vector of design variables, x is the vector of random variables, P_f is the failure probability as function of design variables and random variables, f_x is the joint probability density function of random variables and g is the performance function which decides if the structure has failed in terms of load S and resistance R. The reliability is defined as the complement of failure probability. Calculation of structural reliability is computationally expensive because many evaluations of the performance function (e.g., fatigue life, stresses or displacements) are needed for accurate computations. Ang and Tang (1975) and Madsen *et al.* (1986) have presented good review of various methods of structural reliability analysis. Here the two most extensively used methods, the Monte Carlo simulation (MCS) and the first-order reliability method (FORM), are presented.

Monte Carlo Integration

The Monte Carlo integration is by far the simplest and potentially most accurate method to obtain failure probability, although it can be computationally very expensive. A key aspect of Monte Carlo method is random number generation which provides a basis for selecting random realization of uncertain variables in the structural model (e.g., Melchers, 1987). The event of failure is evaluated by checking if the response of the structural design for each random realization of the set of uncertain variable is greater than the allowable response defined by the performance function. If N is the total number

of simulations of random variables and N_f the number of failed simulations then the probability of structural failure is estimated by

$$P_f \cong \frac{N_f}{N} \tag{2-2}$$

The accuracy of the probability calculated from Equation 2-2 increases with the number of simulations. An estimate of the accuracy in failure probability is obtained by calculating the standard deviation in P_f

$$\sigma_{Pf} = \sqrt{\frac{P_f\left(1-P_f\right)}{N}} \tag{2-3}$$

First-Order Reliability Method (FORM)

Monte Carlo method can be computationally very expensive for evaluating very low probabilities because large number of simulations is required for accuracy. The first-order reliability method is an efficient alternative. The FORM method is presented in several references (Madsen *et al.,* 1986 and Melchers, 1987). The key idea of FORM is to make a linear approximation to the failure surface between safe and failed realization in the standard Gaussian space (all random variables are transformed to standard normal variables). This linear approximation is made at a point where the distance of the origin of standard space and the limit surface is minimum. This point is referred to as the most probable point and the shortest distance is termed as reliability index β. The probability of failure is the area of tail beyond β under the standard normal distribution.

$$P_f = \phi(-\beta) \tag{2-4}$$

and ϕ is the cumulative density function of standard normal distribution. This method gives accurate results when the limit state function is linear. For nonlinear function, FORM underestimates failure probability for concave function and overestimates it for

convex function. Higher order method like the second-order reliability method (SORM) can be used to improve the accuracy.

Reliability Based Inspection Scheduling

Designing structure for damage containment can lead to overly conservative design which will be cost prohibitive in terms of manufacturing and operation. Reliability based inspection and maintenance can be used instead to detect and repair damage at periodic intervals. Inspections serve as protection against damage that cannot be modeled or predicted during design process (e.g., environmental, accidental impacts etc.). Designing inspection schedule is challenging for two reasons. First, the ability of the inspection to detect damage is limited because of human and mechanical errors, so that probabilistic models of inspection detection are needed. The function used to represent the probability of detection represents a common characteristic that small cracks will have low chance of detection and large cracks will be almost certainly detected. Palmberg *et al.* (1987); Tober and Klemmt (2000); Tisseyre *et al.* (1994) and Rummel and Matzkanin (1997) developed/used empirical equations to model probability of detection based on experimental data. Another reason for the computational expense is that damage size distribution changes with time due to crack growth and also after inspections because components with damage are replaced by new components. Re-characterizing crack size distribution after inspections is computationally challenging.

Reliability centered maintenance focuses on scheduling inspections when the failure probability exceeds a threshold probability level. The reliability level is computed by determining the probability that damage becomes too large and remains undetected in all the previous inspections. The simplest and potentially most accurate method is to use Monte Carlo simulations, MCS (e.g., Harkness *et al.,* 1994; Enright and Frangopol,

2000). MCS is computationally expensive as it requires large samples for estimating low probability of failure. Moment based techniques have been used to reduce the computational expense of reliability calculations with inspections. The first-order reliability method (FORM) and second-order reliability method (SORM) have been used to obtain probability after inspection by Rahman and Rice (1992); Harkness (1994); Fujimoto *et al.* (1998); Toyoda-Makino (1999) and Enright and Frangopol (2000). The main problem with the use of moment based method is that the damage size distribution cannot be updated explicitly after each inspection using these techniques. Some modification and simplifying assumptions have been used in the moment based methods to make the calculations less time consuming. For instance Rahman and Rice (1992) developed a methodology to update crack size distribution after inspections using Bayesian updating. Harkness (1994) modified the FORM to directly calculate reliability with inspections without updating the crack size distribution.

Reliability Based Design Optimization

Structural optimization is a reasonable tool for helping a designer address the challenge of designing complex structures, at least in the preliminary design stage. For instance, Nees and Canfield (1998) and Arietta and Striz (2000, 2005) optimized F-16 wing panels subject to constraints on damage growth. Reliability based design optimization further increases the cost of reliability analysis because several iterations on design variables are required to obtain optimum design that will satisfy the specified reliability constraint. The main reason for the computational expense is when the objective function and\or the constraints do not have simple analytical form and have to be evaluated numerically (e.g., finite element model). In these circumstances the numerically expensive function can be replaced by an approximation or surrogate model

having lower computational cost such as response surface approximation. Response surface methodology can be summarized as a collection of statistical tools and techniques for constructing an approximate functional relationship between a response variable and a set of design variables. This approximate functional relationship is typically constructed in the form of a low order polynomial by fitting it to a set of experimental or numerical data. The unknown coefficients of a response surface approximation are estimated from experimental data points by means of a process known as linear regression. These coefficients are estimated in such a way as to minimize the sum of square of the error between the experimental response and the estimated response (e.g., Myers and Montgomery, 1995). The accuracy of a response surface is expressed in terms of various error terms and statistical parameters that represent the predictive capability of the approximation. Response surfaces have been widely used in structural optimization to reduce computational cost. NESSUS © (Riha *et al.*, 2000) and DARWIN © (Wu *et al.*, 2000) use response surface approximations for reducing computational cost of probabilistic finite element analysis. Venter (1998) proposed methods to improve accuracy of response surface approximation and used them for optimizing design of composites. Papila (2001) also used response surfaces in structural optimization for estimation of structural weight. Qu (2004) used RSA's to minimize cost of reliability based optimization.

CHAPTER 3
EFFICIENT RELIABILITY BASED DESIGN AND INSPECTION OF STIFFENED PANELS AGAINST FATIGUE

Introduction

Reliability based optimization is computationally expensive when inspections are involved because crack size distribution has to be re-characterized after each inspection to simulate replacement. Inspections improve the structural safety through damage detection and replacement. However, inspections cannot detect all damage with absolute certainty due to equipment limitations and human errors. Probabilistic model of inspection effectiveness can be used to incorporate the uncertainty associated with damage detection. Typically, the crack size distribution after an inspection will not have a simple analytical form and can only be determined numerically during reliability analysis. Exact evaluation of failure probability following an inspection can be done by Monte Carlo simulation (MCS) with large population which is computationally expensive. The high computational cost for estimating very low probabilities of failure combined with the need for repeated analysis for optimization of structural design and inspection times make MCS cost prohibitive.

Harkness (1994) developed a computational methodology to calculate structural reliability with inspections without updating the crack size distribution after each inspection. He assumed that repaired components will never fail again and incorporated

this assumption by modifying the first order reliability method (FORM).* This expedites reliability computations which require only the initial crack size distribution to be specified. In previous papers (Kale *et al.,* 2003, 2004), we used the same methodology to optimize inspection schedule.

When inspections are needed earlier than half the service life, repaired components can have large probability of failure. In this case Harkness's method may not be accurate enough. In this chapter we propose an approximate method to simulate inspection and repair using Monte Carlo simulation (MCS) and estimate the failure probability using the first order reliability method (FORM). MCS is computationally very expensive for evaluating low failure probabilities due to large population requirement but is very cheap for estimating probability distribution parameters (e.g., mean and standard deviation). We use the data obtained from MCS to obtain the mean and standard deviation of crack size distribution. Subsequently, FORM is used to calculate the failure probabilities between inspections. The combined MCS and FORM approach to calculate failure probability with inspection removes the computational burden associated with using MCS alone.

This method is applied to combined optimization of structural design and inspection schedule of fuselage stiffened panels. Stiffened panels are popular in aerospace applications. Stiffeners improve the load carrying capacity of structures subjected to fatigue by providing alternate load path so that load gets redistributed to stiffeners as cracks progress. Typical stiffening members include stringers in the longitudinal directions and frames, fail-safe-straps and doublers in the circumferential direction of the fuselage. Fracture analysis of stiffened panels has been performed by

* FORM is a moment based technique which calculates the failure probability using a first order approximation about the point on the limit state where failure is most probable.

Swift (1984) and Yu (1988). They used displacement compatibility to obtain the stress intensity factor due to stiffening. Swift (1984) studied the effect of stiffener area, skin thickness and stiffener spacing on the stress intensity factor. He also discussed failure due to fastener unzipping and effect of stiffening on residual strength of the panel. Yu (1988) also compared the results with finite element simulation.

Our previous paper Kale *et al.* (2003) demonstrated the combined structural design and optimization of inspection schedule of an unstiffened panel. The main objective of the present chapter is to develop a cost effective computational methodology to perform reliability based optimization of structural design and inspection schedule. The methodology is demonstrated by performing structural optimization and inspection scheduling of stiffened structures against fatigue. To reduce the computational time associated with fatigue life calculation and reliability analysis, response surface approximations are developed for tracking crack growth.

Crack Growth and Inspection Model

Fatigue Crack Growth

The rate of fatigue crack propagation can be expressed as a function of applied stress intensity factor, crack size and material constants (which are obtained by fitting empirical model to experimental data). For the example in this chapter we use the Paris law.

$$\frac{da}{dN} = D(\Delta K)^m \tag{3-1}$$

where a is the crack size in *meters*, N is the number of cycles of fatigue loading in flights, da/dN is the crack growth rate in *meters/cycles*, the stress intensity factor range ΔK is in $MPa\sqrt{meters}$ and m is obtained by fitting the crack growth model to empirical data.

More complex models account for load history effects. The stress intensity factor range ΔK for cracked stiffened panel can be calculated using finite element or analytical method as a function of stress σ and crack length a.

$$\Delta K = \psi \sigma \sqrt{\pi a} \tag{3-2}$$

The effect of stiffening on the stress intensity is characterized by the geometric factor ψ which is the ratio of stress intensity factor for the cracked body to that of stress intensity factor at the crack tip of an infinite plate with a through the thickness center crack. The calculation of ψ usually requires detailed finite element analysis. Here, ψ is calculated using a method due to Swift (1984). The number of fatigue cycles accumulated in growing a crack from the initial size a_i to the final size a_N can be obtained by integrating Equation 3-1 between the initial crack a_i and final crack a_N. Alternatively, the final crack size a_N after N fatigue cycles can be determined by solving Equation 3-3. This requires repeated calculation of ψ as the crack propagates. The computational approach for integrating Equation 3-3 is illustrated in Appendix B.

$$N = \int_{a_i}^{a_N} \frac{da}{f\left(\Delta K\left(\psi\right), m\right)} \tag{3-3}$$

Here we focus on designing a fuselage panel for fatigue failure caused by hoop stresses. The hoop stress is given by Equation 3-4 and crack grows perpendicular to the direction of hoop stress given by

$$\sigma = \frac{rph}{th + N_s A_s} \tag{3-4}$$

where r is the fuselage radius, p is the pressure differential inside the fuselage, h is the panel width, t is panel thickness, N_s is the number of stiffeners and A_s is the area of single stiffener (See Figure 3-1).

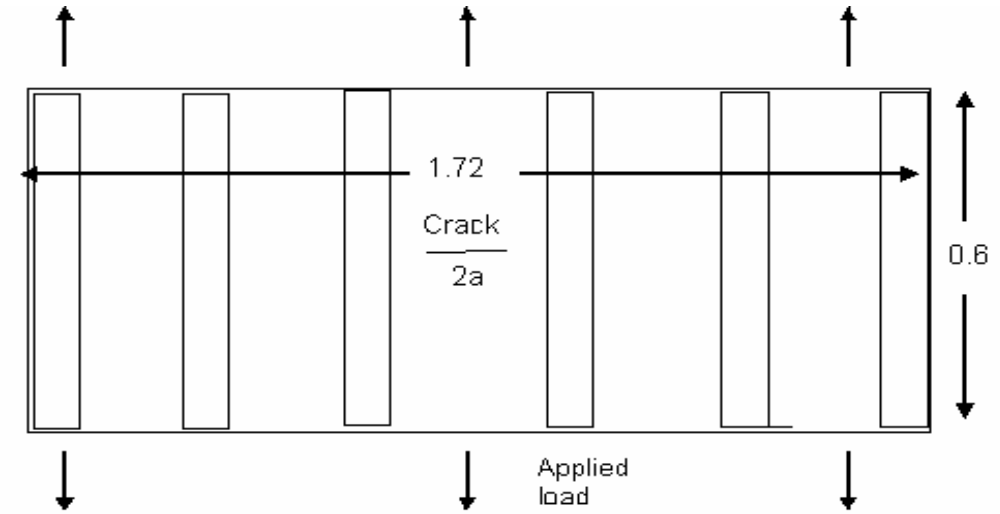

Figure 3-1: Fuselage stiffened panel geometry and applied loading in hoop direction (crack grows perpendicular to the direction of hoop stress)

Critical Crack Size

We consider optimizing the design of a typical fuselage panel for fatigue failure due to hoop stress. The fail-safe stiffening members in circumferential direction such as frames, fail-safe straps and doublers are modeled as equispaced rectangular rods discretely attached to the panel by fasteners. The panel size is assumed to be small compared to the fuselage radius so it is modeled as a flat panel following Swift (1984). We assume that only three stiffeners adjacent to crack centerline are effective in reducing the stress intensity factor. So we model the aircraft fuselage structure by a periodic array of through-the-thickness center cracks with three stiffeners on either sides of centerline as show in Figure 3-1. The critical crack length a_c at which failure will occur is dictated by considerations of residual strength or crack stability. Structural failure occurs if the crack size at that time is greater than critical crack. The crack length causing net section failure is given by

$$a_{cY} = 0.5\left(h - \left[\frac{rph}{Yt} - \frac{N_{ub} A_s}{t} \right] \right) \tag{3-5}$$

Equation 3-5 gives the crack length a_{cY} at which the residual strength of the panel will be less than yield stress Y and N_{ub} is the number of intact stiffeners.

$$a_{cH} = \left(\frac{K_{IC}}{\psi \sigma \sqrt{\pi}} \right)^2 \tag{3-6}$$

$$a_{cL} = \left(\frac{K_{IC}}{\frac{pr}{2t} \sqrt{\pi}} \right)^2 \tag{3-7}$$

Equation 3-6 determines the critical crack length for failure due to hoop stress σ and Equation 3-7 determines the critical crack length for failure due to transverse stress. This is required to prevent fatigue failure in longitudinal direction where skin is the only load carrying member (effect of stringers in longitudinal direction is not considered because hoop stress in more critical for fatigue). The critical crack length for preventing structural failure is given by Equation 3-8 and the fatigue life N_f of structure is determined by integrating Equation 3-3 between the initial crack a_i and critical crack a_c.

$$a_c = \min\left(a_{cY}, a_{cH}, a_{cL}\right) \tag{3-8}$$

Typical material properties for 7075-T651 aluminum-alloy most commonly used in aerospace application are presented in Table 3-1. The applied load due to fuselage pressurization is assumed to be 0.06 *MPa* (maximum pressure differential, 8.85 psi, Niu, 1990). The Joint Service Specification Guide-2006 specifies design assuming a minimum initial crack of 0.127 *mm* to exist in structure at all times. However we consider more conservative value of initial crack distribution (mean of 0.2 *mm*) to account for uncertainties associated with damage initiation and growth associated with corrosion, environmental effects and accidental damage. The structural design parameters obtained

for B747 series aircraft from Niu (1990) and Jane's all the world's aircraft (Jackson, 1996) are listed in Table 3-2.

Table 3-1: Fatigue properties of 7075-T651 Aluminum alloy

Property	Yield stress *Y, MPa*	Initial crack $a_{i,0}$ *meters* Mean. Standard deviation	Paris exponent *m* Mean. Standard deviation	Fuselage radius, *r, meters*	Pressure load, *p*, (*MPa*)	Fracture toughness, K_{IC} $MPa\sqrt{meters}$
Distribution type	500.0	Lognormal 0.0002, 0.00007	Lognormal 2.97 1.05	3.25	Lognormal 0.06 0.003	36.58

(Source: Sinclair and Pierie, 1990 and Niu, 1990)

Table 3-2: Structural design for fuselage

Fastener diameter, *d*	4.8 *mm*
Fastener spacing, *s*	3.1 *cm*
Fuselage length, *l*	68.3 *m*
Fuselage radius, *r*	3.25 *m*
Number of panels, N_p	1350
Number of fasteners per stiffener	20
Number of stiffeners, N_s	6
Panel length, *b*	0.6 *m*
Panel width, *h*	1.72 *m*
Stiffener thickness, t_s	5 *mm*

(Source: Swift, 1984; Jackson, 1996 and Niu, 1990)

Probability of Failure at a Given Time

The probability of failure after *N* cycles of loading is defined as the event that fatigue life (number of cycles accumulated in growing a crack from initial crack to critical crack) is less that *N*. The purpose of reliability analysis is to determine the probability that the structure will not fail for a random realization of uncertain variables (a_i, *m* and σ). The equation which define the failure boundary is known as the limit state function, *g*. So for our case

$$g(a_i, m, \sigma) = N_f(a_i, m, \sigma) - N \tag{3-9}$$

where the fatigue life N_f is determined by integrating Equation 3-3 between the initial crack a_i and the critical crack a_c. The failure probability corresponding to Equation 3-9 is calculated using the first-order reliability method (FORM). In this method the limit state function is represented in the transformed standard normal variables (a_i, m and σ are transformed to normal distributions with mean = 0 and standard deviation = 1) and the point on the limit surface closest to origin is determined. This point is known as design point or most probable point and the shortest distance is called reliability index, β_d. The calculation of reliability index is an optimization problem requiring repeated calculation of Equation 3-9 for several iterations in the random variables. In this chapter the MATLAB© fmincon function (which employs sequential quadratic programming) is used to determine the reliability index. The main reason for using reliability index instead of directly calculating failure probability is that FORM is computationally cheaper compared to MCS. A second reason is that reliability index is more suitable for generating accurate surrogate models because it varies over much smaller range compared to the failure probability. Failure probability is determined from the reliability index using the cumulative density function, ϕ of the standard normal distribution.

$$P_f = \phi(-\beta_d) \tag{3-10}$$

For an unstiffened panel analytical expression of fatigue life is available; however for stiffened panels, determining fatigue life requires computationally expensive calculation of the geometric factor ψ. The computational procedure for calculating fatigue life is described in Appendix B.

Inspection Model

When the structure is subjected to periodic inspections, cracks are detected and repaired or the structural part is replaced. We assume that the probability P_d, of detecting a crack of length a is given by Palmberg's equation (Palmberg *et al.,* 1987).

$$P_d(a) = \frac{(a/a_h)^\beta}{1+(a/a_h)^\beta} \tag{3-11}$$

Where a_h is the crack size that will be detected with 50% probability and β is inspection parameter. An approximate values of a_h of 1 *mm* was obtained by rounding off data from the probability of detection curves in Rummel and Matzkanin (1997) for eddy current inspection. They obtained the probability of detection curves by machining artificial cracks in panels and counting the number of times they were detected after inspecting several times. The value of the other inspection parameter β of 3 was obtained by fitting Equation 3-11 to the inspection data in that reference and increasing it slightly (to account for improvement in inspection technology since 1997). It is assumed that once a crack is detected, the panel is replaced by newly manufactured panel with the fabrication defect distribution.

Computational Method to Perform Reliability Based Optimization with Inspections

When inspection and replacement of structural components are scheduled, the damage size distribution changes because defective parts are replaced with new parts having a smaller damage sizes (fabrication defects, $a_{i,0}$). Reliability computation is very expensive when inspections are involved because crack size distribution has to be re-characterized after each inspection to simulate replacement and exact computation of failure probability using MCS requires large sample size.

Harkness (1994) developed an approximate method to expedite reliability computation with inspection by assuming that repaired components will never fail again and incorporated this assumption by modifying the first order reliability method (FORM). The failure probability at any time following an inspection is the probability that the crack size is greater than the critical crack size at that time and that it is not detected in any of the previous inspections. Using an empirical crack growth model like Equation 3-3 to predict crack size at any time, a probabilistic model for inspection probability of detection and a specified value of critical crack size, he calculated the structural reliability using the FORM method. The effect of inspections is incorporated into the FORM by integrating the (probability density function) PDF of undetected cracks over the failure region using numerical integration. The assumption that detected cracks are replaced and the new component will not fail during the remainder of service life greatly simplifies the numerical computation by considering only the PDF of undetected cracks.

When inspections are needed earlier than half the service life, repaired components may have large probability of failure and Harkness's method may not be accurate enough. Kale *et al*. (2005) proposed an approximate method to simulate inspection and repair using Monte Carlo simulation (MCS) with small sample size to update the crack size mean and standard deviation after an inspection and first order reliability method (FORM) to calculate the failure probability between inspections. The procedure described below expedites the reliability calculations by removing the need of exact MCS analysis with large sample size.

Searching for Next Inspection Time Using FORM

The main computation associated with determining inspection schedule for a given structure is to find the next inspection time at which the structural reliability will be lower

than the specified threshold value. The probability of failure after N cycles of loading since the most recent inspection is defined as the event that fatigue life N_f is less than N.

$$P_f\left(N, a_i, m, \sigma\right) = P\left(N_f\left(a_i, m, \sigma\right) - N\right) \tag{3-12}$$

where a_i is the crack size distribution at the beginning of inspection period and the fatigue life N_f is the number of cycles accumulated in growing a crack from initial crack a_i to critical crack a_c. For a given structural thickness, the next inspection time is obtained such that the probability of failure before the inspection is just equal to the maximum allowed value (Pf_{th}, reliability constraint). The next inspection time S_n for a given threshold reliability level is obtained by solving Equation 3-13.

$$P\left(N_f\left(a_i, m, \sigma\right) - N\right) - Pf_{th} = 0 \tag{3-13}$$

Equation 3-13 is solved for time interval N by using bisection method between previous inspection time S_{n-1} and service life S_l and for each of the bisection iteration, the first term is calculated by FORM. For an unstiffened panel FORM is very cheap; however for stiffened panel it is computationally expensive because calculation of fatigue life is expensive and additional computational burden is added because of the bisection search between previous inspection time S_{n-1} and service life S_l.

Updating Crack Size Distribution after Inspection using MCS

The algorithm for simulating crack growth and inspections is shown in Table 3-3. After obtaining the next inspection time, the crack size distribution has to be updated after that inspection. This updated crack size distribution serves as initial crack size distribution for the following inspection interval. The damage distribution after an inspection can easily be updated by using Monte Carlo simulation (MCS) with a small sample size and is computationally very cheap compared to calculating probabilities. The

crack size a_N after N cycle of fatigue loading is obtained by solving Equation 3-3. To obtain the crack size mean and standard deviation after an inspection, we produce 50,000[†] random numbers for each random variable in Equation 3-3 (a_i, m, σ) and obtain the final crack size a_N. We then simulate the inspection by using Equation 3-11 with another random number for probability of detection. If the crack is detected the panel is replaced by a new one with a random crack size picked from the distribution of manufacturing defects $a_{i,0}$. After all cracks are analyzed for detection, the updated crack sizes are used to fit a distribution and to obtain its mean and standard deviation. This serves as the initial crack distribution for the next inspection. For the data used in this chapter the fabrication crack distribution is lognormal, and the distribution after inspections was also found to be best approximated by lognormal distribution out of 12 analytical distributions in ARENA software © (Takus and Profozich, 1997).

Table 3-3: Pseudo code for updating crack size distribution after N cycles from previous inspection

(1) Generate a panel by a random vector of uncertain variables (a_i, m, and σ)
(2) Solve Equation 3-3 for crack size a_N after N cycles of fatigue loading for the panel using Newton's method or bisection (if Newton's method does not converge).
(3) Compute the probability of detection of crack a_N from Equation 3-11, $P_d(a_N)$.
(4) Generate a random number from a uniform distribution with bounds (0, 1) P_d^{rand}
(5) If $P_d(a_N) \geq P_d^{rand}$ then simulate replacement of defective component by generating a random crack $a_{i,0}$ for a new panel and set $a_N = a_{i,0}$ else keep a_N
(7) Store a_N for fitting probability distribution to crack sizes after inspection and go back to (1)
(8) Stop after 50,000 random panels have been simulated and fit distribution to crack sizes

[†] A large sample size was used to get accurate estimate of mean and standard deviation. This makes the optimization results insensitive to MCS seed. For the unstiffened panel 100,000 samples are used.

The crack size probability distribution after the inspection is estimated by fitting probability distribution to the crack size samples obtained from MCS. The goodness of fit of this distribution affects the accuracy of probability calculations. To illustrate this we calculate the actual probability of failure for two inspection times calculated for a 2.00 *mm* thick unstiffened panel using the proposed method. The first inspection time of 9288 flights is calculated using FORM with a lognormal initial crack size distribution with mean of 0.20 *mm* and coefficient of variation of 0.35. The crack size distribution after this inspection is updated by Table 3-3 using a crack growth time N of 9288 flights. The updated crack distribution is found to be lognormal with mean = 0.30 *mm* and cov = 0.86. The next inspection time of 15,540 flights is obtained from FORM using the updated crack distribution.

The actual and best fitted (cumulative distribution function) CDF of crack size distribution after 9288 flights are shown in Figure 3-2. The corresponding p-value is less than 0.005 indicating a bad fit; however for low failure probabilities (e.g., 10^{-7}) this fit ensures accurate structural design calculation at very low computational expense. To validate this claim, failure probability is calculated for the inspection schedule (first inspection = 9,288, second inspection = 15,540 flights) using MCS with 10^8 samples. The exact failure probability after 9288 flights is 4.0×10^{-7} and after 15,540 flights is 2.7×10^{-7} which are close to the value of 10^{-7} calculated using the proposed method. The square error between actual PDF and lognormally fitted PDF is 0.00029 and the maximum error between CDF's is 0.06 at crack size of 0.28 *mm*

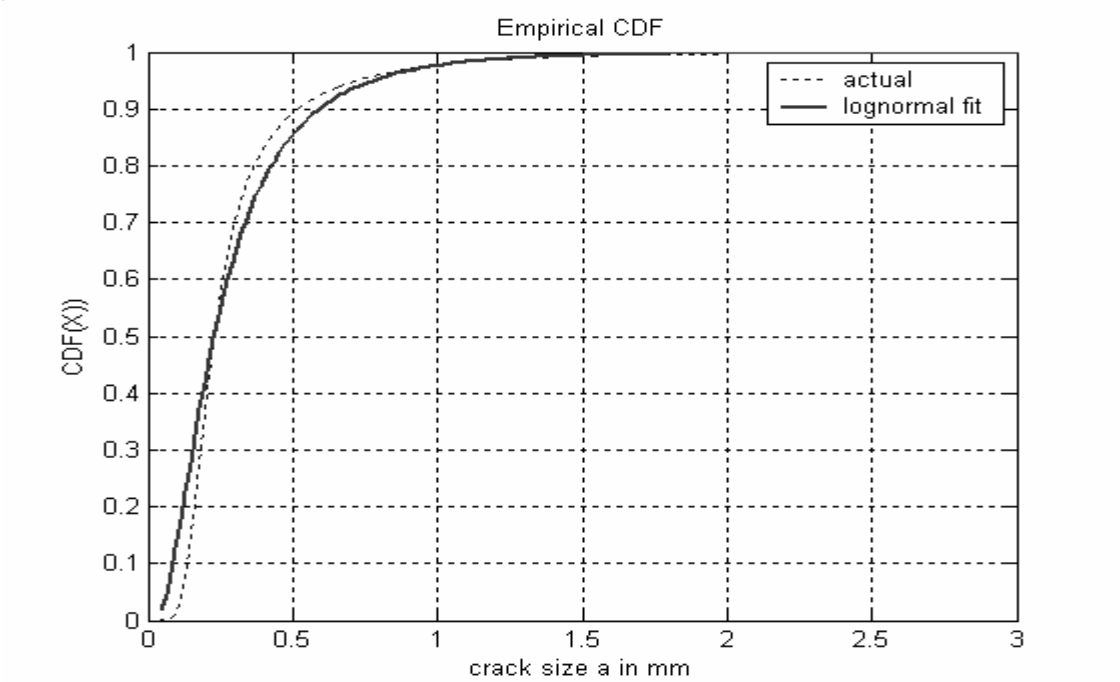

Figure 3-2: Comparison of actual and lognormally fitted CDF of crack sizes after an inspection conducted at 9288 flights

Calculation of Inspection Schedule for a Given Structure

For a given structural design optimum inspections are added one by one until the probability at end of service life is less than the specified threshold reliability level. Example 3-1 illustrates the approach described in previous sections for a 2.0 *mm* thick unstiffened plate and a required reliability level of 10^{-7}. Solving Equation 3-13 for *N*, the first inspection time is 9288 flights. Crack growth simulation using the MCS pseudo code in Table 3-3 is performed with initial crack sizes $a_{i,0}$ and crack growth time of 9288 flights giving the updated crack size distribution after the first inspection. The lognormal distribution fitted after inspection has a mean of 0.30 *mm* and coefficient of variation 86.0%. This serves as the initial crack size distribution for the second inspection. Again, the second inspection time of 15,540 flights is obtained solving Equation 3-13. This cycle of scheduling inspections is continued until the failure probability at the end of service life is less than the specified value.

Figure 3-3 illustrates the variation of the probability of failure with and without inspection. Table 3-4 presents the inspection schedule during the service life and the crack size distribution parameters after each inspection. It can be seen that inspections are very helpful in maintaining the reliability of the structure. From Table 3-4 it can be seen that first inspection interval is the largest. After the first inspection the repaired components are replaced with the same initial crack distribution (mean = 0.20 *mm* and cov = 35%); however some cracks escape detection, leading to smaller inspection intervals. From the crack size distribution parameters shown in last column of Table 3-4 we can conclude that the crack size distribution after each inspection essentially remains unchanged after a certain number of inspections, leading to uniform inspection intervals. We can infer that towards the end of service the rate at which unsafe cracks are introduced in the structure due to replacement is same as the rate at which cracks are detected by the inspections.

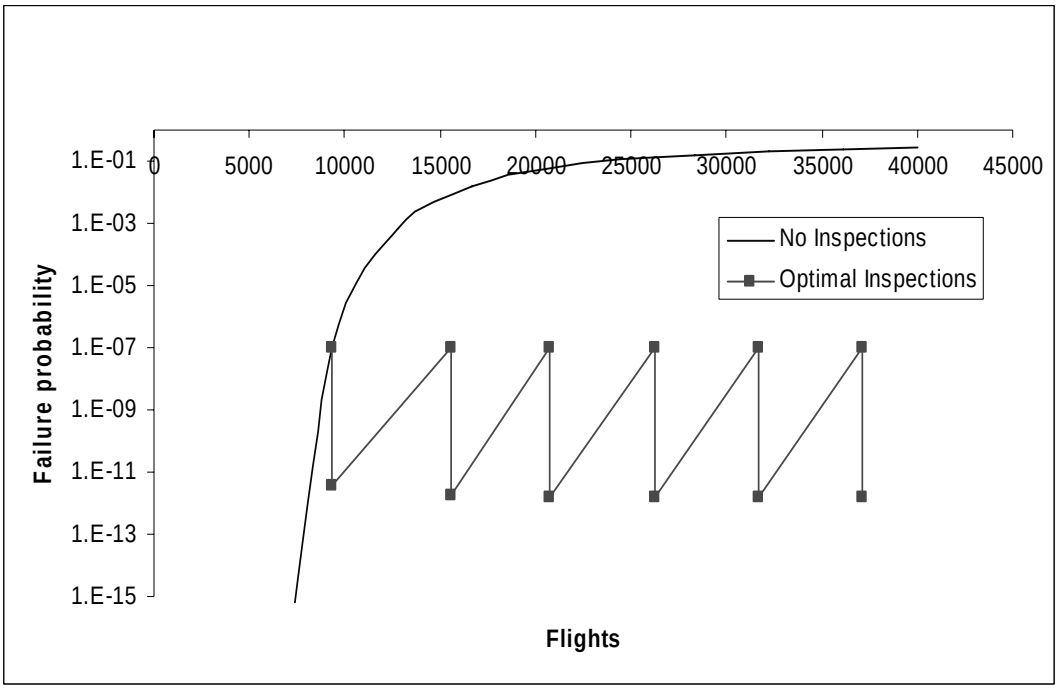

Figure 3-3: Example 3-1, Variation of failure probability with number of cycles for a 2.00 *mm* thick unstiffened panel with inspections scheduled for $Pf_{th} = 10^{-7}$

Table 3-4: Example 3-1, Inspection schedule and crack size distribution after inspection for an unstiffened plate thickness of 2.00 *mm* and a threshold probability of 10^{-7}

Number of inspections	Inspection time, S_n (flights)	Inspection interval (flights) $S_n - S_{n-1}$	Crack size distribution after inspection (mean, *mm* cov)
0	--	--	Initial crack distribution (0.200, 35%)
1	9,288	9,288	(0.300, 86%)
2	15,540	6,252	(0.326, 90%)
3	20,741	5,201	(0.335, 87%)
4	26,223	5,482	(0.342, 87%)
5	31,649	5,426	(0.345, 86%)
6	37,100	5,451	(0.347, 86%)

Optimization of Structural Design

The cost associated with change in the structural weight for aluminum and the fuel cost is taken from Venter (1998). He assumed a fuel cost of $0.89 per gallon and that a pound of structural weight will cost 0.1 pound of fuel per flight. From this we calculated that a pound of structural weight will cost $0.015 in a flight for fuel. The structural

weight is assumed to be directly proportional to the plate thickness and a pound of structural weight is assumed to cost $150 for material and manufacturing. Appendix D shows the details of material and fuel cost calculations. A typical inspection cost of about a million dollars was obtained from Backman (2001). Following Backman (2001) the service life is assumed to be 40,000 flights. The structural design parameters obtained for B747 series aircraft and cost factors are summarized in Table 3-5.

Table 3-5: Cost of inspection, material and fuel

Density of aluminum (ρ)	166 lb/ft^3
Fuel cost per pound per flight (F_c)	$ 0.015
Inspection cost (I_c)	$ 1,000,000
Material and manufacturing cost per *lb* (M_c)	$ 150.0
Number of panels, N_p	1350
Service life, S_l	40,000 flights

(Source: Venter, 1998 and Backman, 2001)

The life cycle cost C_{tot} for N_i inspections is

$$C_{tot} = M_c W + F_c W S_l \quad + N_i I_c \tag{3-14}$$

Where W is the total weight of all the panels in the fuselage, given as

$$W = N_p \left(N_s A_s b + thb \right) \rho \tag{3-15}$$

The parameters in Equations 3-14 and 3-15 are defined in nomenclature.

Reliability based design optimization is computationally very expensive when inspections are involved because several iterations on structural design variables and inspection times are required to find an optimum combination of structural sizes and inspections that will minimize total cost. For an unstiffened panel, analytical expression for crack growth is available and exact computations using the combined MCS and FORM technique is very cheap. For stiffened panel, the crack growth has to be determined numerically and reliability computations are very expensive even with the combined MCS and FORM approach. The key factor responsible for computational time

is the calculation of geometric factor ψ due to stiffening, which can be determined using detailed finite element analysis or displacement compatibility method due to Swift (1984). In this chapter we used Swift's approach which takes about 0.5 second for evaluating single value of ψ for a given structural design and crack length. Table 3-6 explains the various RSA's used to make computations faster and Table 3-7 gives the breakdown of computational cost for calculation of exact inspection time and updating crack size distribution.

Table 3-6: Description of response surface approximations used in optimization

Name of response surface	Description	Function of variables
ψ -RSA	Geometric factor due to stiffeners	Skin thickness t_s, Stiffener area A_s, Crack length a
μ_{ai}-RSA	Crack size mean after inspection	Skin thickness t_s, Stiffener area A_s, mean crack length μ_a, mean crack length σ_a, time N, standard deviation in stress σ_p
σ_{ai}-RSA	Crack size standard deviation after inspection	Skin thickness t_s, Stiffener area A_s, mean crack length μ_a, mean crack length σ_a, time N, standard deviation in stress σ_p
β_d-RSA	Reliability index	Skin thickness t_s, Stiffener area A_s, mean crack length μ_a, mean crack length σ_a, time N, standard deviation in stress σ_p

Table 3-7: Computational time spent in exact calculation of next inspection time and error due to ψ-RSA usage

Variable	*Computational method*	*Number of function evaluation*	*Total time, seconds*	*Typical error due to use of RSA*
Geometric factor, ψ	*Displacement compatibility*	*1*	*0.5*	*0.02 approximately*
Fatigue life, N_f	*Numerical integration using MATLAB's adaptive Simpson's quadrature*	*100 evaluation of* ψ	*50*	*600[‡] flights (error in* N_f *due to error in* ψ*)*
Reliability index, β_d	*Iterative search using MATLAB's fmincon*	*100 evaluation of* N_f	*5,000*	*0.2, average fitting error from* β_d*-RSA + 0.1[§] from error in* N_f
Next inspection time, S_N	*Bisection between* S_N *-1 and service life* S_l	*15 evaluation of* β_d	*75,000 (0.86 days)*	--

Computational time spent in exact updating of crack size distribution using MCS and error due to ψ-RSA usage				
Crack size a_N after N cycles	Iterative search using Newton's method	20 evaluation of N_f	1,000	--
Crack size distribution using step F	MCS	50,000 evaluations of a_N	5,000,000,0 (578 days)	Less that 0.1 % from μ_{ai}-RSA and σ_{ai}-RSA.

When structural design and inspections schedule are optimized together, the computational cost will be several hundred times that shown in Table 3-7 because of iterative search on structural sizes and number of inspections in a schedule required to

[‡] Assuming that the structure is designed for inspection interval of 10,000 flights (typical results obtained in this chapter), the error in fatigue life calculation due to error in ψ will be 10,000/ $(1.02)^m$, where m is the Paris law exponent. Using the mean value of m = 2.97 an error of 600 flights in fatigue life is obtained

[§] The fatigue life has an error of 600 flights because of which the inspection time has the same error. The reliability calculated at the next inspection time plus the error in N_F , that is S_n+ 600 will have error in reliability index of about 0.1 (2%); however this translates to error in probability of 200 % for a reliability level of the order of 10^{-7}.

maintain the specified reliability level. To overcome this we develop surrogate models based on response surface approximations shown in Table 3-6. The last columns of Table 3-7 show the errors made by the use of RSA's in calculations. An error of 0.02 is the typical fitting error in construction of RSA for ψ. Table 3-8 gives the overview of the methodology describing the computational challenge in its implementation and explains the approach used to perform reliability based optimization of structural design and inspection schedule.

The computational procedure is explained first followed by the computational challenge associated with implementation of this procedure. The surrogate models used to remove the computational burden involved in this method are also explained. It is to be noted that the main cause of using the surrogate models is because there is no analytical expression available to calculate crack growth for stiffened panel. If analytical expression for crack growth is available then exact computations will become feasible.

For an unstiffened panel the computational cost for calculating crack size distribution after inspection is very low and is calculated by Monte Carlo simulation with 100,000 samples during the optimization. However, for stiffened panel, calculation of crack growth is expensive and we use response surface approximation (RSA) to estimate the crack size mean and standard deviation after an inspection. This RSA is constructed by fitting data obtained from MCS at some sampled locations in design domain (skin thickness, initial crack size mean, initial crack size standard deviation, stiffener area, standard deviation in stress and number of cycles of loading) as shown in Appendix C.

Table 3-8: Pseudo code for combined optimization of structural design and inspection schedule

(A) Optimization of structural design: For a given structural design calculate inspection schedule using step B and obtain cost of structural weight and inspections. Stop if convergence on minimum cost is obtained otherwise update the structural design.
(B) Optimization of inspection schedule: Add one inspection at a time using step C, update crack size distribution using step D. Check if the number of inspections is sufficient for maintaining the given reliability level during the service using FORM, if not add one additional inspection.
(C) Searching for next inspection time: Given structural sizes, probability distribution of random variables, find when the next inspection is needed by calculating the time S_n at which the probability of failure equals the required reliability level Pf_{th} using the first order reliability method (FORM). This is a computationally intensive optimization problem which requires repetitive computation of reliability index. A rough estimate of computer time is described in Table 3-7. To reduce the computational burden associated with repeated reliability calculation during optimization we generate design response surface to estimate reliability index. Appendix C explains the details of this response surface approximation (β_d-RSA).
(D) Updating crack size distribution after inspection: After obtaining the next inspection time from step C, use Monte Carlo simulation (MCS) to update the crack size distribution after this inspection by growing cracks between the inspection time S_n and the previous inspection time S_{n-1}. The MCS method is described in Table 3-3 and the computational expense associated with it is described in Table 3-7. The computational burden associated with estimating crack size distribution parameters after an inspection is solved by using RSA's to estimate the crack size mean μ_{ai}-RSA and standard deviation σ_{ai}-RSA after an inspection. Appendix C explains the details of these RSA's.

During the optimization the structural thickness t and the stiffener area A_s are changed, which changes the structural weight according to Equation 3-15. The optimum inspection schedule is determined for this structural design using Table 3-8 and the total

cost of structural weight and inspection is obtained from Equation 3-14. The optimization iteration is stopped after a specified convergence tolerance is achieved. The convergence tolerance on minimum cost is assumed to be $10,000 in this chapter and MATLAB © is used to perform optimization of the design. Using the RSA's, entire calculations can be done in about 3 days on a Windows Pentium 4 processor.

Results

Structural design can have large effect on operational cost and weight of the structure. When inspections and maintenance are not feasible, safety can be maintained by having conservative (thick) structural design. To demonstrate this we first obtain safe-life design required to maintain desired level of reliability throughout the service life for unstiffened and stiffened structures. Table 3-9 shows the safe life design of unstiffened panel and Table 3-10 shows the safe-life design of a stiffened panel.

Table 3-9: Safe–Life design of an unstiffened panel

Required probability of failure, Pf_{th}	Minimum required skin thickness , t (mm)	Life cycle cost C_{tot} $\$ \times 10^6$	Structural weight, lb
10^{-7}	4.08	25.42	33902
10^{-8}	4.20	26.16	34880
10^{-9}	4.24	26.34	35129

Table 3-10: Safe–Life design of a stiffened panel

Required probability of failure, Pf_{th}	Total stiffener area 10^{-3} m^2, A_s	Skin thickness , t (mm)	$\frac{A_s}{A_{Total}}100\%$	Life cycle cost, C_{tot} $\$ \times 10^6$	Structural weight, lb
10^{-7}	2.23	2.31	35.85	22.42	29900
10^{-8}	2.26	2.33	36.00	22.68	30248
10^{-9}	2.30	2.35	36.22	22.91	30555

An unstiffened panel is a single load path structure without load transfer capability. Comparing Table 3-9 to Table 3-10, we see that if structure is designed with multiple

load transfer capability then the weight and cost can be reduced by about 10 %. Stiffeners improve the load carrying capacity and reduce crack growth rates allowing greater crack length safely. This issue is further explored in Appendix A.

Next we demonstrate the effect of inspections on structural safety and operational cost. Inspections improve the reliability by detecting and removing cracks. By optimizing the structural design together with inspection schedule, we can trade structural weight against inspection cost to reduce overall life cycle cost. To demonstrate the effectiveness of inspections, optimum structural design and inspection schedule were first obtained for an unstiffened panel design with results shown in Table 3-11.

Table 3-11: Optimum structural design and inspection schedule of an unstiffened panel (in all cases the optimum number of inspection is 3)

Required probability of failure, Pf_{th}	Skin thickness, t (mm)	Optimum inspection times, S_n (flights)	Life cycle cost C_{tot} $\$ \times 10^6$	Structural weight, lb
10^{-7}	2.30	12346,22881,31365	17.28	19109
10^{-8}	2.43	13158,23496,31496	18.15	20199
10^{-9}	2.56	13927,24016,31682	18.97	21295

It can be seen that inspection and repair lower the life cycle cost by about 25% over safe-life unstiffened panel design and by 20% over to stiffened panel safe-life design. The corresponding reductions in structural weight are 40% and 30%, respectively. There is an additional incentive for conducting inspections in that they protect against other types of damage like that due to accidental impacts and corrosion. Next we optimize the structural design and inspection schedule for stiffened panel design (Table 3-12) and illustrate the tradeoff of structural weight in skin and stiffeners against inspection cost.

Table 3-12: Optimum structural design and inspection schedule for stiffened panel

Required probability of failure, Pf_{th}	Total stiffener area, A_s $\times 10^{-4}$ $meter^2$	Required skin thickness , t (mm)	$\frac{A_s}{A_{Total}}100$ %	Optimal inspection times, S_n (flights)	Life cycle cost , C_{tot} $\$ \times 10^6$	Structural weight, lb
10^{-7}	7.11	1.71	19.40	10844,18625, 25791, 32908	17.20	17659
10^{-8}	7.30	1.81	18.95	11089,18758, 25865, 32943	17.87	18504
10^{-9}	13.74	1.67	32.29	12699,22289, 31163	18.33	20443

Comparing Table 3-10 to Table 3-12 we see that inspections lower the life cycle cost of stiffened panel design by about 20% compared to safe-life design. Comparing Tables 3-11 and 3-12 we see only a small gain (about 3%) in designing stiffened structures when inspections are involved and cost can be minimized by designing single load path structures (unstiffened) with inspections. Comparing Table 3-12 to Table 3-11, the increased design flexibility allows additional tradeoff of structural weight against inspections by having one additional inspection over the unstiffened panel design. About 20% to 30 % of the structural weight is transferred from skin to stiffeners.

In aircraft operation the inspection intervals are dictated by practical considerations and regulation which are based on service experience. The Joint Service Specification Regulations-2006 requires all airlines to conduct major depot level inspection four times during the service life. These inspections are conducted at uniform intervals. Table 3-13 shows the design with fixed inspection schedule.

Table 3-13: Optimum structural design for regulations based inspections conducted at four constant interval or 8000 flights for stiffened panel

Required probability of failure, Pf_{th}	Total stiffener area A_S 10^{-4} $meter^2$	Required skin thickness, t (mm)	$\frac{A_s}{A_{Total}} 100\,\%$	Inspection times, S_n	Life cycle cost, C_{tot} \$ $\times$ 10^6	Structural weight, lb
10^{-7}	13.41	1.38	35.94	8000, 16000,24000, 32000	17.44	17927
10^{-8}	13.80	1.47	35.12	8000, 16000,24000, 32000	18.16	18878
10^{-9}	14.85	1.49	36.60	8000, 16000,24000, 32000	18.61	19491

It is seen that inspections done at constant interval are only marginally less cost effective than the optimized inspection schedule. From Tables 3-11, 3-12 and 3-13 we can conclude that when inspections are used to maintain safety there is less gain in using stiffeners for stable fatigue crack growth. However, stiffeners might be very useful in maintaining structural rigidity to resist buckling and pillowing. Also, from Table 3-10 when structures are designed without any inspections, stiffeners can be very helpful in reducing crack growth rate. Appendix A discusses the effect of stiffening on structural design and crack growth rates. Next we obtain optimum structural design and inspection times for fixed number of inspections. Through this we seek to demonstrate the tradeoff of inspection cost against cost of structural weight

Table 3-14: Tradeoff of inspection cost against cost of structural weight required to maintain fixed reliability level for stiffened panel

Required probability of failure, Pf_{th}	Number of inspection	Total stiffener area $A_s \times 10^{-4}$ $meter^2$	Required skin thickness (mm)	$\frac{A_s}{A_{Total}}100$ %	Optimal inspection times (flights)	Life cycle cost \$ $\times 10^6$
10^{-7}	5	7.05	1.60	20.26	9497,16029,22064, 28060,34036	17.53
10^{-7}	4	7.11	1.71	19.40	10844,18625,25791, 32908	17.20
10^{-7}	3	7.23	1.88	18.14**	12743,22435,31212	17.35
10^{-8}	5	7.00	1.70	19.18	9933,16406,22363, 28271,34145	18.14
10^{-8}	4	7.30	1.81	18.95	11089,18758,25865, 32943	17.87
10^{-8}	3	13.29	1.63	32.04	12514,22178, 31110	18.03
10^{-9}	5	7.50	1.74	19.92	10091,16428,23260, 29268, 34412	18.53
10^{-9}	4	7.89	1.88	19.51	11546,19064,26064, 33044	18.59
10^{-9}	3	13.74	1.67	32.29	12699,22289,31163	18.33

From Table 3-14 we see that the optimum structural weight decreases monotonically with the number of inspections because structural weight is traded against inspections. However, the stiffener areas show sudden jump with the required number of inspections (decreasing inspections from four to three). The main reason for this is the presence of several local minima because the inspection cost is a discrete variable and any change in number of inspection will lead to huge jump in either the skin thickness or stiffener area if total cost is minimized. In this case the stiffener areas show sudden change because of the reason that stiffeners break during crack growth reducing reliability so that when the number of inspections are large, minimum cost can be

** There exist another local minimum with $A_s = 14.64\ mm^2$, $t_s = 1.505\ mm$ and inspection times of 12375, 22097 and 31083 flights. However this design has slightly higher cost (2%), hence it is not shown in Table 3-14.

achieved by reducing stiffener areas and increasing structural thickness. Because of this there are several local optimums for structural sizes. The cost difference between these optimums is very small. Actual failure probability was calculated for each of the local optimums and the design whose failure probability was closest to threshold value was selected. Exact evaluation of failure probability for some designs is shown below. The ratio of stiffener area to skin area is constant at about 20% when the number of inspections is large. For lesser number of inspections about 30% of the structural weight is transferred to stiffeners. As more inspections are added the structural weight is traded against inspection cost until a minimum is reached, beyond this any further reduction in structural weight will lead to faster crack growth rate requiring frequent inspections to maintain reliability.

Table 3-15 presents the exact evaluation of failure probability without any RSA for the optimum obtained from Table 3-12. This is done by calculating reliability using FORM without using β_d-RSA reliability index.

Table 3-15: Exact evaluation of structural reliability for optimum obtained from RSA for stiffened panel with inspection

Required reliability level, Pf_{th}	Optimum design (skin thickness *mm*, $\frac{A_s}{A_{Total}}100\,\%$)	Inspection times, flights	Actual Pf / Pf_{th} before each inspection
10^{-7}	1.71, 19.40	10844,18625,25791, 32908	2.89, 2.26, 1.98 , 3.90, 1.87
10^{-8}	1.81, 18.95	11089,18758, 25865, 32943	0.98, 3.75, 3.35, 3.18, 3.06
10^{-9}	1.67, 32.29	12699,22289, 31163	2.12, 5.27, 1.47, 1.44

It can be seen that RSA's can be used to predict the optimum with sufficient accuracy. The error in actual reliability versus calculated reliability using approximations can comes from the RSA for ψ which can affect the accuracy in calculation of inspection

time by 600 flights. Additional error is introduced because of convergence tolerance for calculation of reliability index (0.1 used in the chapter) and randomness in MCS seed for calculating crack size distribution. The effect of RSA on accuracy of results and computational cost is explained in detail previous section. Typically the optimum obtained from RSA will be slightly different from the true optimum because of error in RSA. To get more accurate results, optimum obtained from RSA's can be iteratively calibrated so that the actual failure probabilities are close to the threshold value. The entire calculations can be done in about 3 days on a Windows Pentium 4 processor.

Summary

A computational method was developed using a combination of MCS and FORM to perform combined optimization of structural design and inspection schedule. The method was found to be computationally cheap and accurate in determining structural reliability with inspection. Response surface approximations were used to obtain fatigue life to reduce computational cost associated with life calculations. Optimum combination of structural design and inspection schedule was obtained that will maintain the desired reliability level during service at minimum cost.

CHAPTER 4
TRADEOFF OF WEIGHT AND INSPECTION COST IN RELIABILITY-BASED STRUCTURAL OPTIMIZATION USING MULTIPLE INSPECTION TYPES

Introduction

The integrity of structural components is affected by damage due to fatigue, corrosion and accidental impact. Damage may reduce the residual strength of the structure below what is needed to carry the service loads. In a fail-safe design, structural safety can be maintained by inspecting the components and repairing the detected damage. Alternatively, stresses can be lowered by increasing structural sizes so that damage never grows to a critical length during service life.

Structural component safety checks have gained widespread acceptance because of uncertainty in damage initiation and propagation. The damage tolerance approach to structural integrity assumes that damage is present in the structure at all times and sufficient safety measures should be employed to ensure that it will not grow to a critical length during the operational life of the structure. The Federal Aviation Administration (FAA) requires that all structures designed for damage tolerance be demonstrated to avoid failure due to fatigue, environmental effects, manufacturing defects and accidental damage.

It is easier to perform reliability-based structural optimization of safe-life structures than of fail-safe structures because the optimization of the former involves only structural sizes while for the latter the inspection regime also needs to be optimized. Nees and Canfield (1998) and Arietta and Striz (2000, 2005) performed safe-life structural

optimization of F-16 wing panels to obtain the minimum structural weight for fatigue crack growth under a service load spectrum.

For aircraft fail-safe design, reliability-based design optimization has been applied to the design of inspection schedules. Harkness *et al.* (1994) developed an approximate method to evaluate reliability with inspections, Provan and Farhangdoost (1994) used Markov-chains to estimate the failure probability of a system of components and Brot (1994) demonstrated that using multiple inspection types could minimize cost.

Fujimoto *et al*. (1998); Toyoda-Makino (1999); Enright and Frangopol (2000); Wu *et al*. (2000); Garbatov and Soares (2001) and Wu and Shin (2003) developed optimum inspection schedules for a given structural design to maintain a specified probability of failure. Wu and Shin (2005) developed a methodology to improve the accuracy of reliability calculations with inspections.

Reliability-based optimization of the structural design and inspection schedules has also been applied to pipelines subjected to corrosion damage. Hellevik *et al.* (1999) optimized the pipeline thickness together with the inspection regime to minimize the total operational cost. Using Bayesian updating and a decision tree, they obtained the optimum inspection regime in times and types of inspection. The corrosion information obtained from the inspection was used to update the corrosion model and corrosion probabilities.

Backman (2001) also used multiple inspection types to develop an optimum inspection schedule. However, he also considered the tradeoff between the cost of inspection and the cost of additional structural weight for maintaining the same probability of failure. Using an approximate relationship between structural weight and

damage propagation, he concluded that increasing the structural weight is more cost effective than increasing the inspection frequency.

Reliability based optimization is computationally very expensive when inspections are involved because crack size distribution has to be re-characterized after each inspection to simulate replacement. Exact computation using Monte Carlo simulation (MCS) is very expensive for estimating a low probability of failure due to the large sample size. Harkness (1994) developed a computational methodology to calculate reliability with inspections without updating the crack size distribution after each inspection. He assumed that repaired components will never fail again and incorporated this assumption by modifying the first-order reliability method (FORM).[††] This leads to fast and accurate reliability computations that require only the specification of the initial crack size distribution. In previous papers (Kale *et al.,* 2003, 2004), we used the same methodology to optimize the inspection schedule.

When inspections are scheduled before half the service life, repaired components can have a large probability of failure. In this case, Harkness's method may not be accurate enough because the repaired components can fail during the remainder of the service life. In Chapter 3 we proposed and approximate method to simulate inspection and repair using Monte Carlo simulations (MCS) and calculate the failure probability using FORM. In this chapter we use the approximate method from Chapter 3 for combined optimization of structural design and inspection schedule using multiple inspection types. MCS is computationally very expensive for evaluating low failure

[††] FORM is a moment based technique which calculates the failure probability using a first order approximation about the point on the limit state closest to origin and is computational very cheap compared to MCS

probability, but is cheap for estimating probability distribution parameters (e.g., mean and standard deviation). We use the data obtained from MCS to approximate the probability distribution of crack size after inspection, and obtain the mean and standard deviation. Subsequently, FORM is used to calculate the failure probabilities between inspections. The combined MCS and FORM approach to calculate failure probability with inspection removes the computational burden associated with calculating the failure probability using MCS for low failure probabilities.

The main objective of the present chapter is to use this methodology to optimize aircraft structural design together with inspection schedules using multiple inspection types. The optimization parameters are structural thickness, inspection times and inspection types. The application of the proposed methodology is demonstrated by using an example of an aircraft structure modeled as an unstiffened panel designed for fatigue. A second objective of this chapter is to demonstrate that if structures are designed together with the inspection schedule, then the cost of additional structural weight can be traded against the cost of additional inspections in order to achieve an overall minimum operational cost.

Structural Design and Damage Growth Model

Fatigue Crack Growth

We consider fatigue crack growth in a fuselage panel with an initial crack size a_i subjected to load cycles with constant amplitude. We assume that the main fatigue loading is due to pressurization, with stress varying between a maximum value of σ to a minimum value of zero in one flight. One cycle of fatigue loading consist of one flight. Like many other researchers (e.g., Tisseyre *et al*., 1994; Harkness *et al*., 1994 and Lin *et al*., 2000), we assume that damage growth follow the Paris equation

$$\frac{da}{dN} = D(\Delta K)^m \tag{4-1}$$

where a is the crack size in *meters*, N is the number of cycles (flights), da/dN is the crack growth rate in $meters/cycle$, and the stress intensity factor range ΔK is in $MPa\sqrt{meters}$. For 7075-T651 aluminum alloy, D and m are material parameters related by Equation 4-2 obtained from Sinclair and Pierie (1990). D has units in $meters^{1-\frac{m}{2}}(MPa)^{-m}$

$$D = e^{(-3.2m-12.47)} \tag{4-2}$$

The stress intensity factor range ΔK for a center cracked panel is calculated as a function of the stress σ and the crack length a in Equation 4-3, and the hoop stress due to the pressure differential p is given by Equation 4-4

$$\Delta K = \sigma\sqrt{\pi a} \tag{4-3}$$

$$\sigma = \frac{pr}{t} \tag{4-4}$$

where r is the fuselage radius and t is the skin thickness. The number of cycles of fatigue loading N accumulated in growing a crack from the initial crack size a_i to the final crack a_N can be obtained by integrating Equation 4-1 between the initial crack a_i and the final crack a_N. Alternatively, the crack size a_N after N cycle of fatigue loading can be obtained by solving Equation 4-5

$$N = \int_{a_i}^{a_N} \frac{da}{D\left(\sigma\sqrt{\pi a}\right)^m} = \frac{a_N^{1-\frac{m}{2}} - a_i^{1-\frac{m}{2}}}{D\left(1-\frac{m}{2}\right)\left(\sigma\sqrt{\pi}\right)^m} \tag{4-5}$$

The fatigue life of the panel can then be obtained by substituting the critical crack length a_c in place of a_N in Equation 4-5

$$N_f = \frac{a_c^{1-\frac{m}{2}} - a_i^{1-\frac{m}{2}}}{D\left(1-\frac{m}{2}\right)\left(\sigma\sqrt{\pi}\right)^m} \tag{4-6}$$

Here we assume that the critical crack length a_c is dictated by considerations of crack stability, so that

$$a_c = \left(\frac{K_{IC}}{\sigma\sqrt{\pi}}\right)^2 \tag{4-7}$$

and K_{IC} is the fracture toughness of the material. Typical material properties for 7075-T651 aluminum alloy are presented in Table 4-1. A conservative distribution of initial defects was chosen following the Department of Defense Joint Service Specification Guide for aluminum alloys to account for uncertainties in damage initiation and growth. The applied fuselage pressure differential is 0.06 *MPa*, obtained from Niu (1990) and the stress is given by Equation 4-4.

Table 4-1: Fatigue properties of 7075-T651 Aluminum alloy

Property	Initial crack $a_{i,0}$, *mm*	Paris exponent, *m*	Pressure, *p* (*MPa*)	Fracture toughness, K_{IC} $MPa\sqrt{meters}$	Fuselage radius, *r* *Meters*
Distribution type, mean, standard deviation	Lognormal 0.2,0.07	Lognormal 2.97, 1.05	Lognormal 0.06, 0.003	36.58 Deterministic	3.25

(Source: Sinclair and Pierie, 1990 and Niu, 1990)

Inspection Model

When the structure is subjected to periodic inspections, cracks are detected and repaired or the structural part is replaced. We assume that the probability P_d, of detecting a crack of length *a* is given by Equation 4-8 (Palmberg *et al*., 1987)

$$P_d(a) = \frac{(a/a_h)^{\beta}}{1+(a/a_h)^{\beta}} \tag{4-8}$$

Where a_h is the crack size that will be detected with 50% probability and β is inspection parameter. Values of a_h of 0.63 *mm*, 0.80 *mm* and 1.27 *mm* were obtained from the probability of detection curves from Rummel and Matzkanin (1997) for eddy current inspection and a_h of 2.00 *mm* was obtained from Tober and Klemmt (2000) for ultrasonic inspection. The three versions of eddy current inspections differ in terms of the instruments used and the number of operators inspecting the component. They all obtained the probability of detection curves by artificially machining cracks in panels and counting the number of times that they were detected after being inspected. The value of the other inspection parameterβ, as shown in Figure 4-1, was obtained by fitting Equation 4-8 to the inspection data in these references. The probability of detection curves for different inspection types are shown in Figure 4-1. Type 1 is the most effective inspection followed by type 2, and so on. It is assumed that once a crack is detected, the panel is replaced by a newly manufactured panel with a smaller defect size distribution (fabrication defects).

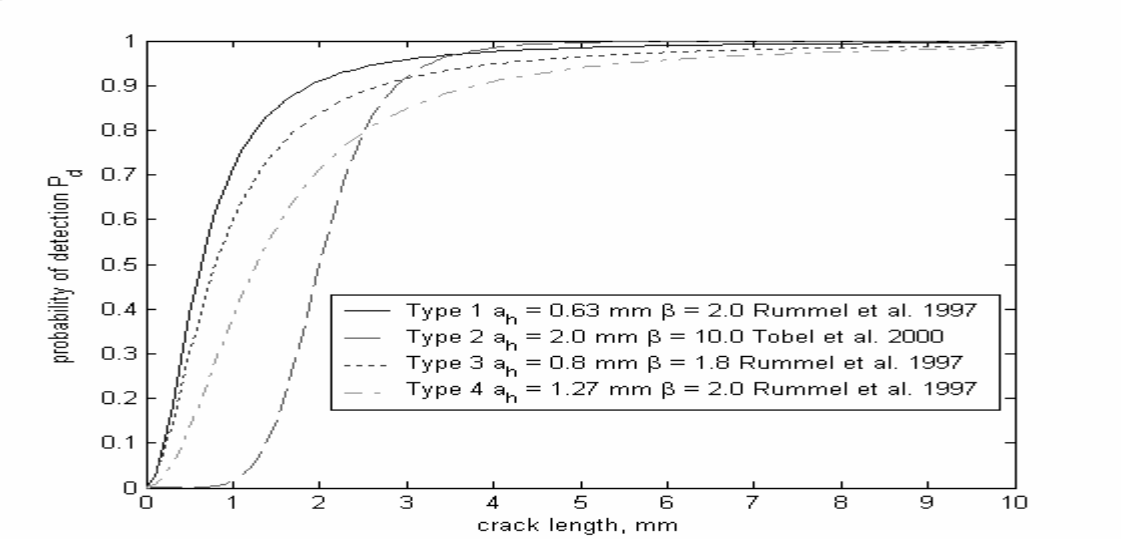

Figure 4-1: Probability of detection curve for different inspection types from Equation 4-8

Calculating an Inspection Schedule

Estimating Crack Size Distribution after Inspection

When inspection and replacement of structural components are scheduled, the damage size distribution changes because defective parts are replaced with new parts having a smaller value of the damage size (fabrication defects). Reliability-based optimization is computationally very expensive when inspections are involved, because crack size distribution has to be re-characterized after each inspection to simulate replacement and exact computation using Monte Carlo simulation (MCS) is very expensive for estimating low probability of failure due to large sample size. Harkness (1994) developed a computational methodology to calculate reliability with inspections without updating the crack size distribution after each inspection. He assumed that repaired components will never fail again and incorporated this assumption by modifying the first-order reliability method (FORM). Using this method, FORM is updated over the failure region after each inspection using numerical integration. This expedites the

reliability computations, which require only that the initial crack size distribution be specified.

When inspections are scheduled after half the service life, this method gives accurate results because the repaired component will not fail until the end of service. However when inspections are scheduled before half the service life, the repaired components can have a large probability of failure and Harkness's method may not be accurate enough compared to exact probability of failure obtained from MCS.

Kale *et al.* (2005) developed an approximate method to account for inspection and repair using Monte Carlo simulation (MCS) and evaluated the failure probability using the first-order reliability method (FORM). Evaluating low failure probability using MCS requires a large sample size, which makes reliability-based optimization expensive; instead MCS is used to estimate the mean and standard deviation of probability distribution using small sample size, which is computationally cheap. The data obtained from MCS are used to fit a probability distribution of crack size after inspection and then FORM is used to calculate the failure probabilities at any time following the inspection. This greatly expedites the reliability computations.

Here we assume that inspections do not change the type of distribution and that damaged components are replaced by new components with damage distribution due to fabrication. The damage distribution after an inspection can easily be updated by using MCS with a small sample size. The crack size a_N after N cycle of fatigue loading is obtained by solving Equation 4-5. To obtain the crack size mean and standard deviation after an inspection is conducted, we produce 100,000[‡‡] random numbers for each random

[‡‡] A large sample size was used to get accurate estimate of mean and standard deviation. This makes the optimization results insensitive to MCS seed.

variable in Equation 4-5 (a_i, m, σ) and obtain the final crack size a_N. We then simulate the inspection by using Equation 4-8 with another random number for probability of detection. If the crack is detected, the panel is replaced by a new one with a random crack size picked from the distribution of manufacturing defects $a_{i,0}$. After all cracks are analyzed for detection, the updated crack sizes are used to fit a distribution and to obtain its mean and standard deviation. This serves as the initial crack distribution for the next inspection. For the data used in this chapter, the fabrication crack distribution is lognormal, and the distribution after inspections was also found to be best approximated by lognormal distribution out of 12 analytical distributions in ARENA software © (Takus and Profozich, 1997). If better accuracy is needed then a distribution with more parameters can be fitted to the data. Even though this distribution may not represent the data accurately, it provides a conservative fit to data. The algorithm for simulating crack growth and inspections is shown in Table 4-2.

Table 4-2: Pseudo code for updating crack distribution after N cycles from previous inspection

Generate a panel by a random vector of uncertain variables (a_i ,m , σ)
Solve Equation 4-5 for crack size a_N after N cycles of fatigue loading corresponding to the random vector (a_i, m, σ)
Compute the probability of detection of crack a_N from Equation 4-8, $P_d\ (a_N)$
Generate a random number from a uniform distribution with bounds (0, 1) P_d^{rand}
If $P_d(a_N) \geq P_d^{rand}$ then simulate replacement of defective component by generating a random crack $a_{i,0}$ for a new panel and set $a_N = a_{i,0}$ else keep a_N
Store a_N for fitting probability distribution to crack sizes after inspection
Stop after 100,000 random panels have been simulated and fit distribution to crack sizes

Calculating the Failure Probability Using the First-Order Reliability Method (FORM)

It would be possible to use the same MCS procedure as described in the previous step in order to calculate the probabilities of failure needed for scheduling inspections.

However, since the required probabilities of failure are of the order of 10^{-8}, this would require a prohibitively large MCS. So instead we use FORM, taking advantage of the characterization of the crack distribution as lognormal, as described in the previous section and in Table 4-2. The probability of failure after N cycles of fatigue loading since the most recent inspection is

$$P_f(N, a_i) = P(a(N, a_i) \geq a_c) \tag{4-9}$$

where a_i is the crack size distribution (either initial or updated) at the beginning of the inspection period and a_c is the critical crack given by Equation 4-7. This probability is calculated by the first-order reliability method (FORM). For a given structural thickness, optimum inspection times are obtained such that the probability of failure before the inspection is just equal to the maximum allowed value (Pf_{th}, reliability constraint). The probability of failure decreases after the inspection, because cracks are detected and repaired. With the number of cycles of loading (flights), the failure probability increases until it hits the threshold value again, defining the next inspection. The n^{th} inspection time S_n is obtained by solving Equation 4-9 using a bisection method between the previous inspection time[§§] S_{n-1} and the service life S_l (40,000 flights). To ascertain whether the number of inspections is adequate, the probability of failure at the end of service is calculated. If this failure probability is greater than the threshold value, additional inspections must be added. The combined MCS and FORM approach removes the computational burden associated with calculating the failure probability using MCS for very low failure probabilities.

[§§] Time, cycle and flights are used interchangeably in this chapter because for one cycle of fatigue loading is equal to one flight in a fuselage and time is measured in number of flights.

To demonstrate the application of the combined FORM and MCS method to calculate the failure probability we calculate the inspection time for a threshold reliability level of $Pf_{th} = 10^{-7}$ in Table 4-3 for a 2.48 *mm* thick panel. Calculating $P(a(N, a_i) \geq a_c)$ using FORM in Equation 4-9 with $a_i = a_{i,0}$ and solving for N, the first inspection time is 14569 flights. To update the crack size distribution after this inspection, crack growth simulation using the MCS pseudo code is performed with initial crack sizes $a_{i,0}$ and a crack growth time of 14569 flights. This gives the updated crack size distribution after the first inspection a_i (mean = 0.264 *mm*, cov = 1.04). This serves as the initial crack size distribution for the second inspection. The second inspection time is obtained by solving Equation 4-9 using FORM with the updated initial crack size distribution a_i (mean = 0.264 *mm*, cov = 1.04). This is continued until the failure probability at the end of service life is less than the specified value.

Figure 4-2 illustrates the variation of the probability of failure with and without inspection. It can be seen that inspections are very helpful in maintaining the reliability of the structure. From Table 4-3 it can be seen that the first inspection interval is the largest. After the first inspection, damaged components are replaced with the same initial crack distribution (mean = 0.20 *mm* and cov = 0.35); however some cracks may have escaped detection. The fact that some cracks (larger than the initial cracks) may have escaped detection and will grow faster leads to smaller intervals.

Table 4-3: Example 4-1, inspection schedule and crack size distribution after inspection (a_h = 0.63 *mm*) for an unstiffened plate thickness of 2.48 *mm* and a threshold probability of 10^{-7}

Number of inspections	Inspection time (flights)	Inspection interval (flights) $S_n - S_{n-1}$	Crack size distribution after inspection (mean, *mm*, cov)
0	--	--	(0.200,0.35)
1	14569	14569	(0.264,1.04)
2	26053	11484	(0.271,1.11)
3	35576	9523	(0.245,1.10)

*Inspection times may differ by a maximum value of 100 flights due to MCS seed; the corresponding error in probability calculation is negligible.

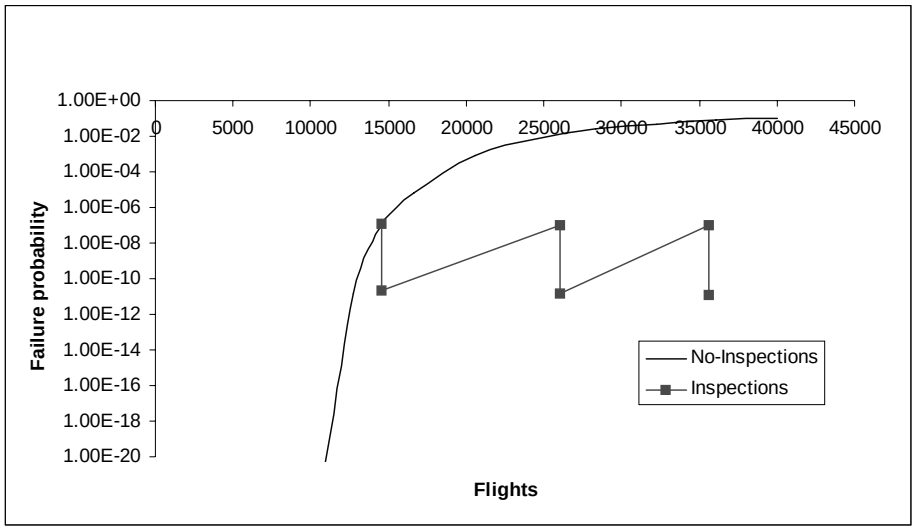

Figure 4-2: Variation of failure probability with number of cycles for a 2.48 *mm* thick unstiffened panel with inspections scheduled for $Pf_{th} = 10^{-7}$

The previous example showed how an optimum inspection schedule can be developed for a single inspection type. The same procedure is followed for scheduling the inspection sequence with multiple inspection types. Here the probability of detection of each inspection type can be different and inspections are performed in the same order as specified in the sequence. If the specified reliability level cannot be maintained with the inspection sequence, then it is not feasible.

Cost Model

The cost associated with a change in the structural weight for aluminum and the fuel cost is taken from Venter (1998). He assumed a fuel cost of $0.89 per gallon and calculated that a pound of structural weight will cost 0.1 pound of fuel per flight. From this we calculate that a pound of structural weight will cost $0.015 in a flight for fuel. The structural weight is assumed to be directly proportional to the plate thickness and a pound of structural weight is assumed to cost $150 for material and manufacturing. Appendix D shows the details of material and fuel cost calculations. A typical inspection cost of about a million dollars was obtained from Backman (2001) and costs of other inspection types were adjusted such that the incentive for carrying less effective inspection decreases with the number of inspections. Thus, one inspection of the first type is more attractive than carrying two inspections of the second type, three inspections of the third type or four inspections of the fourth type. The structural design parameters for the B747 series aircraft obtained by Niu (1990) are also listed in Table 4-4. Following Backman (2001) the service life S_l is assumed to be 40,000 flights.

Table 4-4: Design details and cost factors

Density of aluminum ρ	166 lb/ft^3
Frame spacing b	0.6 m
Fuel cost per pound per flight F_c	$ 0.015
Fuselage radius r	3.25 m
Length l	68.3 m
Material and manufacturing cost per pound M_c	$ 150.0
Number of panels N_p	1350
Panel width h	1.72 m
Type 1 inspection cost I_{c1}	$ 1.35 million
Type 2 inspection cost I_{c2}	$ 1.23 million
Type 3 inspection cost I_{c3}	$ 0.98 million
Type 4 inspection cost I_{c4}	$ 0.85 million

(Source: Venter, 1998 and Backman, 2001)

The life cycle cost is calculated as

$$C_{tot} = M_c W + F_c W S_l + \sum_{k=1}^{4} I_{ck} N_k \tag{4-10}$$

$$W = N_p thb\rho \tag{4-11}$$

During the optimization, the structural thickness t changes, this in turn changes the structural weight according to Equation 4-11. The optimum inspection schedule (times and types) is determined for this structural design and the total cost is obtained from Equation 4-10.

Optimization of Inspection Types

The combined optimization of inspection times to minimize the cost for the specified reliability constraint is complicated because of the large number of permutations of inspection types that can occur in an inspection schedule. To reduce the number of permutations that need to be considered, we first calculate the inspection schedule and the cost of all the single type inspections. We then use the lowest cost as a bound that allows us to eliminate many possible sequences. Appendix E provides a detailed description of the algorithm.

(1) Determine optimum inspection times and costs using each of the four inspection types. This step provides (N_{kb}, C_{kb}), where N_{kb} is the number of required inspections of the k^{th} type (that is if only type k is used) and C_{kb} is the total cost of an inspection schedule developed using only the k^{th} inspection type. Determine the minimum cost, C_{min} = Min (C_{kb}, k = 1…4).

(2) Eliminate impossible or clearly suboptimal inspection sequences to seek a mix of inspection types with N_k inspections of type k. If we use more than one inspection type, the total number of inspections in the sequence should be at most equal to the number of

inspections required by the least effective inspection in the sequence. Also, the total number should be at least equal to the number of inspections required by most effective inspection in the sequence

$$\min_{N_k \neq 0}\left(N_{kb}\right) \leq \sum_{k=1}^{4} N_k \leq \max_{N_k \neq 0}\left(N_{kb}\right) \tag{4-12}$$

$$N_k < \left\lfloor \frac{C_{min}}{I_{ck}} \right\rfloor \tag{4-13}$$

(3) Generate the cheapest inspection sequence satisfying Equations 4-12 and 4-13.

(4) Generate the inspection times for the inspection sequence and check if the failure probability at the end of the service life is less than the specified reliability constraint. $P_f\left(S_l\right) - Pf_{th} \leq 0$ (i.e., whether the inspection sequence is feasible.)

(5) Stop if the sequence is feasible otherwise generate the next cheapest inspection sequence and go back to step 4.

Combined Optimization of Structural Design and Inspection Schedule

Our objective is to determine the optimum combination of the structural thickness, inspection types and inspection times that lead to a minimum life cycle cost for maintaining the specified reliability level (Pf_{th}) through the service life. To obtain the optimum thickness we first obtain the safe-life thickness, which is the minimum thickness necessary to maintain the threshold probability of failure without any inspection. In order to determine whether additional inspections reduce cost, we do a one-dimensional search on the thickness by reducing the thickness gradually and obtain optimum inspection schedule using the algorithm described in Appendix E until we get the optimum lifetime cost.

Safe-Life Design

When inspections and maintenance are not feasible, safety can be maintained by having a conservative (thicker) structural design. To demonstrate this, we first obtain the safe-life design required to maintain the desired level of reliability throughout the service life. Table 4-5 shows the safe-life design.

Table 4-5: Structural size required to maintain a specified reliability level without and inspection.

Threshold probability of failure, Pf_{th}	Minimum required skin thickness (*mm*)	Life cycle cost \$ × 10^6	Structural weight, *lb*	% Increase in cost of improving reliability by a factor of 10
10^{-7}	4.08	25.42	33902	--
10^{-8}	4.20	26.16	34880	2.91
10^{-9}	4.24	26.34	35129	0.68

From Table 4-5, comparing the minimum thickness to that used in Example 4-1 (Table 4-3), we see that the safe-life design must be very thick and heavy in order to maintain the required safety levels.

Cost Effectiveness of Combined Optimization

Next we demonstrate the effect of inspections on structural safety and operational cost. Inspections improve the reliability by detecting and removing cracks. If this effect is used to optimize the structural design together with the inspection schedule, then the structural weight could be traded against the inspection cost to reduce the overall operational cost. The results of combined structure and inspection optimization are shown in Table 4-6.

Table 4-6: Optimum structural design and inspection schedule required to maintain specified threshold reliability level

Threshold probability of failure, Pf_{th}	Optimum plate thickness (mm)	Optimum inspection type sequence	Optimum inspection time (flights)	Minimum cost \$ × 10^6	Cost factors %		
					F_c	M_c	I_c
10^{-7}	2.48	I_1, I_4, I_3	14569, 26023, 32706	18.66	66	16	18
10^{-8}	2.54	I_1, I_3, I_1	14321, 23780, 30963	19.47	64	16	20
10^{-9}	2.66	I_1, I_3, I_1	15064, 23532, 30023	20.27	65	16	19

From Table 4-6 we can see that if inspections are added, the structural thickness can be reduced to maintain the required reliability level at a lower cost. Inspections are very useful in maintaining the structural safety in that large cracks are detected and the damaged part is replaced with new components improving the fatigue life. In this chapter we optimize the inspection schedule for fatigue damage. However inspections are also used to detect other damage, such as tool drop, bird impact and corrosion, which makes them even more cost effective compared to the safe-life design.

The combined optimization of structural design and inspection schedule leads to tradeoff of the costs of structural weight against the inspection cost. Comparing Tables 4-5 and 4-6, we can see that adding inspection leads to a 25% saving in life cycle cost over the safe-life design. Also, we can see that as the safety requirement becomes more stringent, additional and\or more effective inspections become worthwhile. For a safety level of 10^{-7}, cheaper inspections can be used (I_4 and I_3), whereas for 10^{-9} more effective inspections are useful. We can see that only a single inspection type may not be the best choice for maintaining different reliability levels. For maintaining a reliability level of

10^{-7}, a structural size of 2.48 *mm* and three inspections of type one, four and three leads to minimum cost, but the same choice of inspection types is not suitable for a reliability level of 10^{-8}. The last columns of Table 4-6 show the cost factors in percentage of fuel cost (F_c), manufacturing cost (M_c) and inspection cost (I_c). It can be seen that the fuel cost is the major design driver and more inspections can be used to tradeoff cost if fuel cost increases. This issue is further explored below.

Next we compare the optimum inspection schedule developed using only a single inspection type for the structural thickness obtained in Table 4-6 for a reliability level of 10^{-7}.

Table 4-7: Comparison of optimum inspection schedule using a single inspection type for a fixed structural size

Threshold probability of failure, Pf_{th}	Optimum plate thickness (*mm*)	Optimum inspection type sequence using a single inspection type				Minimum cost $\$ \times 10^6$
		I_1	I_2	I_3	I_4	
10^{-7}	2.48	14569, 26053, 35576	14569, 24683, 33430	14569, 19596, 29502, 35156	14569, 18991, 25952, 30128, 38167	I_2 : 19.17
Inspection cost $\$ \times 10^6$		4.05	3.69	3.92	4.25	

Table 4-7 shows the inspection schedules and cost for the inspection sequence generated using individual inspection types for a fixed structural size. Compar ing Tables 4-6 and 4-7, it can be seen that for a fixed structure, multiple inspection types can reduce cost. For a given structure, the advantage of multiple inspection types is partly driven by the fact that at the end of the service life, each inspection schedule leads to a different probability of failure. That is, the cost differential is partly due to different safety margins at the end of service. With combined structural and inspection optimization, the margin at

the end of the service life is removed by a reduction in structural thickness. This leads to a smaller incentive for multiple inspection types, as shown in Table 4-8.

Table 4-8: Optimum structural design and inspection schedule using only a single inspection type

Threshold probability of failure, Pf_{th}	Optimum plate thickness (*mm*)	Optimum inspection time (flights)	Optimum inspection type	Minimum cost $\$ \times 10^6$
10^{-7}	2.39	13317, 18651, 26642, 32460	I_3	18.78
10^{-8}	2.50	13971, 22897, 31443	I_1	19.65
10^{-9}	2.64	14975, 19642, 26230, 32670	I_3	20.41

Comparing Tables 4-6 and 4-8 we can conclude that mixing inspections lead to only a small improvement in cost over a single inspection type design (1%) when structural optimization is done with inspection scheduling.

Effect of Fuel Cost

Fuel cost has a large effect on the optimization of the structural design and inspection schedule. To demonstrate the effect of the increase in fuel cycle cost since 1998, we double the fuel cost to $1.8 per gallon or $0.03 per pound per flight. For the optimum design in Table 4-6, the fuel cost is about 60% of the total life cycle cost and inspections accounted for 20%. Optimization of the structural design and inspection schedule is performed for a reliability level of 10^{-7}. The optimum plate thickness is 2.02 *mm* and a comparison of the optimum inspection schedule using different inspection sequences is shown in Table 4-9.

Table 4-9: Optimum structural design (plate thickness of 2.02 *mm*) and inspection schedule for $Pf_{th} = 10^{-7}$

Inspection type sequence	Optimum inspection time (flights)	Minimum cost $\$ \times 10^6$
I_1	9472, 14383, 20204, 25583, 31192, 36623	30.71
I_2	9472, 13431, 17315, 21659, 26191, 30784, 35359, 39917	32.45
I_3	9472, 11290, 17422, 20206, 25773, 29006, 34178, 37711	30.45
I_4	9472, 11001, 14575, 17130, 21277, 24231, 28099, 31225, 34907, 38178	31.11
$I_1, I_3, I_3, I_3, I_3, I_3, I_3$ (Optimum schedule)	9472, 14383, 18120, 22941, 26770, 31495, 35433	29.84

Comparing Table 4-9 to the first row of Tables 4-6 and 4-7 we can conclude that as fuel cost increases it becomes advantageous to schedule additional inspections and reduce weight to reduce the overall lifecycle cost. For the optimum structural design and inspection schedule in Table 4-9, the fuel cost is 66%, the manufacturing cost 8% and inspections are 26% of the total cost. It should be noted; however fatigue is not the only structural design driver, so that at lower thicknesses, other structural constraints may dominate.

Summary

A methodology for developing optimum inspection type sequences, time, and structural thickness was developed for fuselage panels. Uncertainty in material properties, crack sizes and loads were considered. The FORM method was used to determine the probability of failure at a given time and crack size distribution after inspection was updated using Monte Carlo simulation. Inspections and structural sizes were optimized so that a given threshold probability of failure was never exceeded.

CHAPTER 5
EFFECT OF SAFETY MEASURES ON RELIABILITY OF AIRCRAFT STRUCTURES SUBJECTED TO FATIGUE DAMAGE GROWTH

Introduction

Safety of aircraft structures is largely maintained by using conservative design practices to compensate for the uncertainties in the design process and service usage. Typically, conservative initial defect specification, A-basis material properties, safety factor in fatigue life and conservative loads are used to design structures for fatigue crack growth. This is further augmented by quality control measures like certification testing and inspections. The main reason for using several layers of safety measures is the uncertainties involved (e.g., loading, material properties, accidental impact etc.).

It has been shown that the life of a structure cannot be accurately determined even in carefully controlled conditions because of variability in material properties, manufacturing defects etc. (Sinclair and Pierie, 1990). Because of uncertainty in damage initiation and growth, a damage tolerance approach to assuring structural integrity has become popular in aerospace applications. Here we assume that damage is present in the structure at all times in the form of cracks and we make sure that these cracks will not grow to a critical length during the operational life before they are detected and removed by inspections. Inspections are scheduled at fixed time intervals to detect cracks and protect against unmodeled damage and unexpected accidental damage. The Federal Aviation Administration (FAA) requires that all structures designed for damage tolerance

should be shown to avoid failure due to fatigue, manufacturing defects and accidental damage.

As an example, we study here the design of fuselage structures for fatigue failure due to pressure loading and compute the service failure probability and the effect of safety measures and certification tests. Design of fuselage structures for fatigue is described in detail in Niu (1990). Ahmed *et al.* (2002) studied the initiation and distribution of cracks in fuselage panel by performing fatigue testing. Structural optimization and inspection scheduling of fuselage structure subjected to fatigue damage has been studied in our previous papers (Kale *et al.*, 2003, 2004). Vermeulen and Tooren (2004) designed fuselage structures for fatigue crack growth and found that damage growth and residual strength were two main design drivers. Widespread fatigue damage in fuselage structure has been investigated by testing panels according to FAA regulations (Gruber *et al.*, 1996, FAA/AR-95/47).

The combined effects of various safety measures used to design structures for static strength were studied by Acar *et al.* (2005). They studied the interaction of uncertainties, safety factors and certification tests on safety of aircraft structures designed for static strength. As in earlier studies, the effect of variability in geometry, loads, and material properties is readily incorporated here by the appropriate random variables. However, there is also uncertainty due to lack of knowledge (epistemic uncertainty), such as modeling errors in the analysis. To simulate these epistemic uncertainties, we transform the error into a random variable by considering the design of multiple aircraft models. As a consequence, for each model the structure is different. It is as if we pretend that there are hundreds of companies (Airbus, Boeing, Bombardier, Embraer etc.) each designing

essentially the same airplane, but each having different errors in their structural analysis. The objective of this chapter is to study the effect of individual safety measures used to design structures for fatigue damage growth. The effectiveness of certification testing as a function of magnitude of safety factors and errors is also explored.

Classification of Uncertainties

A good analysis of different sources of uncertainty is provided by Oberkampf *et al.* (2002). Here we simplify the classification, with a view to the question of how to control uncertainty. The classification in Table 5-1 distinguishes between (1) uncertainties that apply equally to the entire fleet of an aircraft model and (2) uncertainties that vary for individual aircraft. The distinction is important because safety measures usually target one or the other. While type 2 are random uncertainties that can be readily modeled probabilistically, type 1 are fixed for a given aircraft model (e.g., Boeing 737-400) but they are largely unknown.

For failure of a structural member this classification reflects distinction between systemic errors and variability. Systemic errors reflect inaccurate modeling of physical phenomena, errors in structural analysis, errors in load calculations, or use of materials and tooling in construction that are different from those specified by the designer. Systemic errors affect all the copies of the structural components made and are therefore fleet-level uncertainties. They can reflect differences in analysis, manufacturing and operation of the aircraft from an ideal. The ideal aircraft is designed assuming that it is possible to perfectly predict structural loads and structural failure for a given structure, that there are no biases in the average material properties and dimensions of the fleet with respect to design specifications, and that the operating environment agrees on average

with the design specifications. The other type of uncertainty reflects variability in material properties, geometry, or loading between different copies of the same structure.

Table 5-1: Uncertainty classification

Type of uncertainty	Spread	Cause	Remedies
Systemic error (Modeling errors)	Entire fleet of components designed using the model	Errors in predicting structural failure.	Testing and simulation to improve math model.
Variability	Individual component level	Variability in tooling, manufacturing process, and flying environment.	Improve tooling and construction. Quality control.

In this chapter, we focus on design of fuselage structures for fatigue damage growth due to pressure loading. To simulate the effect of these modeling errors we pretend that there are several aircraft companies designing the same airplane but each having some different stress calculations and crack growth model leading to different designs. Because these models are only approximate, the stress and crack growth rates calculated by the companies for structural design will be different from the true stress and true crack growth rate. We account for this difference between the "true" and "calculated" value by model error factors k and e for stress and crack growth, respectively. Following this, we calculate the failure probability by selecting random value of errors k and e fixed for an aircraft company.

Safety Measures

Aircraft structural design is still done largely using code-based design rather than probabilistic approaches. Safety is improved through conservative design practices that include use of safety factors and conservative material properties. It is also improved by certification tests that can reveal inadequacies in analysis or construction. In this section, we detail some of these safety measures listed in FAR 25.571 for civil and transport

airplanes and in the Department of Defense, Joint Services Specification Guide-2006 (JSSG).

Safety Margin on Load. Aircraft structures should be demonstrated to withstand 1.5 times the limit load without failure. For damaged fuselage structure, it should be demonstrated by tests that the structure has enough residual strength to withstand 1.15 times the differential pressure.

Conservative Material Properties. In order to account for uncertainty in material properties, the FAA recommends the use of conservative material properties. This is determined by testing a specified number of coupons selected at random from a batch of material. The A-basis property is defined as the value of a material property exceeded by 99% of the population with 95% confidence, and the B-basis property is that exceeded by 90% of the population with 95% confidence. For structures without redundancy, A-basis properties are used and for structures with redundancy, B-basis properties are used. The conservative material properties considered here are A-Basis values of crack growth exponent (leading to rapid crack propagation), yield stress Y and fracture toughness K_{IC}. Appendix H describes the methodology for obtaining these properties from coupon tests.

Conservative Initial Crack. The FAA requires all damage tolerant structures to be designed assuming initial flaw of maximum probable size that could exist because of manufacturing or fabrication. The JSSG-2006 damage tolerance guidelines specify this value as the B-basis crack size. This is the value that can be detected by an eddy current inspection with a 90% probability and 95% confidence.

Safety Factor on Life. Typically, transport aircraft are designed with a safety factor of two on the fatigue life. Fatigue tests are conducted to validate the structural

design and the FAA requires that no aircraft be operated for more than half the number of cycles accumulated on a full-scale fatigue test.

Inspections. Inspections provide protection against structural failure by detecting damage. The FAA requires that inspection schedule should be in place to detect and repair damage before it grows to unacceptable size causing structural failure. The JSSG-2006 damage tolerance guidelines specify that fail-safe multiple load path structures should be designed for depot-level inspections every one quarter of service life.

Component and Certification Tests. Component tests and certification tests of major structural components reduce stress and material uncertainties due to inadequate structural models. These tests are conducted in a building block procedure. First, individual coupons are tested, and then a sub-assembly is tested followed by a full-scale test of the entire structure. Since these tests cannot apply to every load condition, they leave uncertainties with respect to some load conditions. It is possible to reduce the probability of failure by performing more tests to reduce uncertainty or by extra structural weight to reduce stresses. Certification testing may be conducted in two ways. A panel may be randomly chosen out of a batch and subjected to fatigue test. Alternatively, the panel may be chosen and a larger crack can be machined so that tests become more conservative. For the latter, we simulate the panel with the B-basis value of crack size, which is also used to design the panel. A summary of fatigue testing of fuselage panels is documented in FAA/AR-95/47 (Gruber *et al.*, 1996).

Simulation Procedure for Calculation of Probability

We simulate the effect of these safety measures by assuming statistical distributions of uncertainties and incorporating them in Monte Carlo simulation. For variability, the simulation is straightforward. However, while systemic errors are uncertain at the time of

the design, they will not vary for a single structural component on a particular aircraft. Therefore, to simulate the uncertainty, we assume that we have a large number of nominally identical aircraft being designed (e.g., by Airbus, Boeing, Bombardier, etc.), with the errors being fixed for each aircraft. This creates a two-level Monte Carlo simulation, with different aircraft models being considered at the upper level, and different instances of the same aircraft at the lower level.

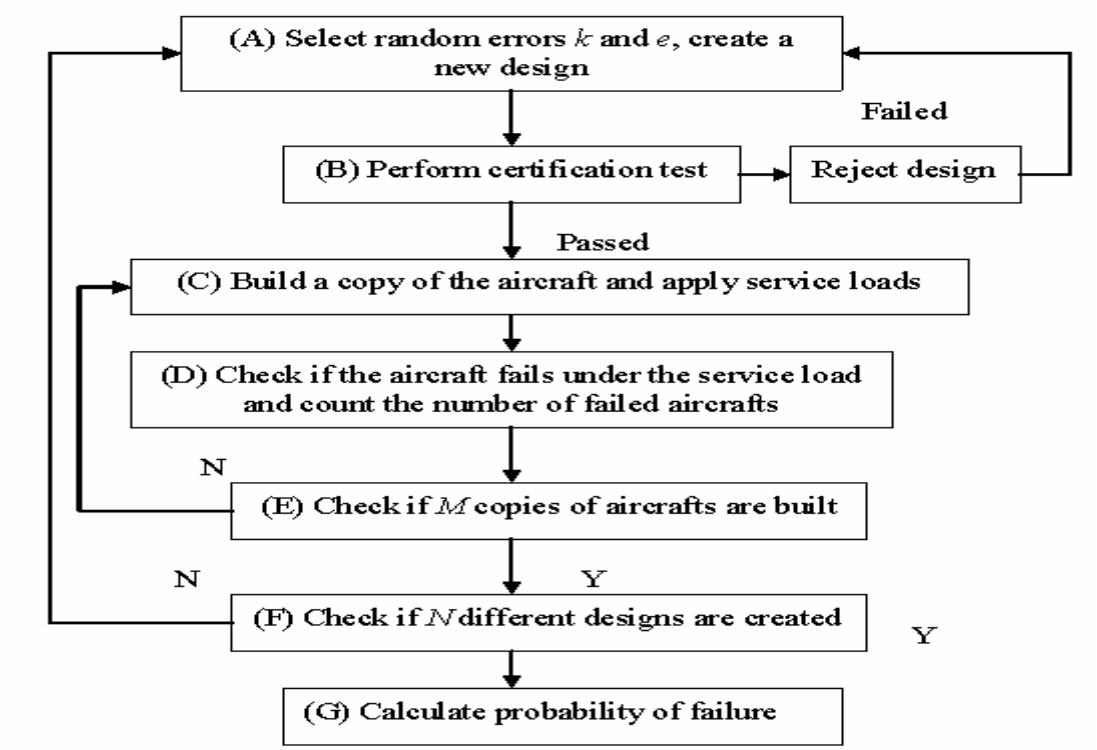

Figure 5-1: Flowchart for Monte Carlo simulation of panel design and failure

We consider a generic structural component characterized by thickness t. The random error parameters k and e account for the difference between the "true" and "calculated" value of stress and crack growth, respectively, and are fixed for each aircraft manufacturing company. We have N different aircraft companies designing essentially the same airplane but with different errors in their calculations. During the design process, the only random quantities are the conservative material properties and the

model errors k and e. In the outer loop of the Monte Carlo simulation (Figure 5-1, step A) we generate different values of k and e and obtain the structural design t_{design} for each company. This is the average thickness of the structure built by the company. The actual structural thickness t_{act} and material properties will be different because of manufacturing variability. We simulate the effect of this variability by producing M instances of the design obtained in step A (Figure 5-1) from assumed statistical distributions for material properties and thickness distribution.

Next we simulate certification testing in step B of Figure 5-1 by selecting a structure from each company and testing if it fails before the design life. If the design passes the test, each of the M structures produced by that aircraft company is assumed to be used in actual service. The failure probability is calculated by applying actual random service loads in step D (Figure 5-1) and counting the number of failed structures.

Damage Growth Model

The typical structural design process involves determining structural sizes that would be sufficient to meet given strength and crack growth requirements during the design life. Prototypes of these designs are then tested for fatigue crack growth by applying design loads in a test rig. These tests continue for several months until structural failure occurs. To illustrate the procedure we consider a simple example of fuselage structure modeled as unstiffened panel and designed for fatigue under uniaxial tensile loads. The stress varies from a maximum value of σ to a minimum value of zero in one flight. One cycle of fatigue loading consists of one flight. To model fatigue, we assume that crack growth follows the Paris model. Equation 5-1 represents the rate of crack growth da/dN in terms of stress intensity.

$$\left(\frac{da}{dN}\right)_{calc} = D(\Delta K)^m \tag{5-1}$$

where a is the crack size in *meters*, N is the number of cycles (*flights*), $\frac{da}{dN}$ is the crack growth rate in $meters/cycle$, and the stress intensity factor range ΔK is in $MPa\sqrt{meters}$. For 7075-T651 aluminum alloy, D and m are material parameters related by Equation 5-2 obtained from Sinclair and Pierie (1990). D has units in $meters^{1-\frac{m}{2}}(MPa)^{-m}$

$$D = e^{(-3.2m-12.47)} \tag{5-2}$$

We use the subscript "*calc*" to note that relations, (such as Equation 5-1), that we use in the analysis, provide only approximations to true values. For a center cracked infinite panel with far field stress σ and one cycle of fatigue loading per flight we have

$$\Delta K = \sigma_{calc}\sqrt{\pi a} \tag{5-3}$$

Equation 5-1 is integrated to obtain estimated fatigue life N_f^{calc}

$$N_f^{calc} = \frac{a_c^{1-\frac{m}{2}} - a_i^{1-\frac{m}{2}}}{D\left(1-\frac{m}{2}\right)\left(\sigma_{calc}\sqrt{\pi}\right)^m} \tag{5-4}$$

where the computed stress σ_{calc} (as obtained from finite element analysis) is different from the actual stress σ_{true} in the structure. Here a_i is the initial crack size and the critical crack length a_c is the crack length at which crack growth becomes unstable. The critical crack length can be obtained as a function of fracture toughness K_{IC} and σ from Equation 5-5.

$$a_c = \left(\frac{K_{IC}}{\sigma\sqrt{\pi}}\right)^2 \tag{5-5}$$

Equation 5-1 represents an approximate value of crack growth rate because it is obtained by fitting empirical model to observed crack growth data and calculated stress σ_{calc}. The true crack growth rate is different from that estimated by Equation 5-1. We include and error factor *e* in analysis and then Equations 5-1 and 5-4 become.

$$\left(\frac{da}{dN}\right)_{true} = eD\left(\Delta K\right)^m \tag{5-6a}$$

$$N_f^{true} = \left(\frac{1}{e}\right)\frac{a_c^{1-\frac{m}{2}} - a_i^{1-\frac{m}{2}}}{D\left(1-\frac{m}{2}\right)\left(\sigma_{true}\sqrt{\pi}\right)^m} \tag{5-6b}$$

The actual stress σ_{true} in the structure due to applied loading is different from the calculated stress σ_{calc} used to design the structure. Equation 5-7 represents the error in the calculated stress, through an error parameter *k*.

$$\sigma_{true} = (1+k)\sigma_{calc} \tag{5-7}$$

Values of *k* and *e* greater than the mean values (0 for *k* and 1 for *e*) yield conservative estimates of the true stress and fatigue life and those less than the means yield unconservative estimations.

Table 5-2: Distributions of errors, design and material parameters for 7075-T6 aluminum

Variables	Distribution	Mean	Coefficient of variation, (standard deviation/ mean)
a_i, initial crack	Lognormal	0.2 *mm*	35 %
e, error in crack growth	Lognormal	1.0	Variable
k, error in stress	Uniform	0.0	Variable
K_{IC}, fracture toughness	Lognormal	30.5 *MPa-m*$^{.5}$	10%
m, paris exponent	Lognormal	2.97	17%
N_l, service life	Deterministic	40,000 *flights*	--
N_s, design life	Deterministic	10,000 *flights*	--
p, pressure load	Lognormal	p_d 8.3 psi (0.057 *MPa*)	2.5 %
r, fuselage radius	Deterministic	3.25 *m*	--
S_{FL} safety factor on life	Deterministic	2	--
S_F, safety factor on load	Deterministic	1.5	--
t_{act}, actual thickness	Lognormal	t_{design} , *mm*	3%
Y, yield stress	Lognormal	495 *MPa*	5%

(Source: Sinclair and Pierie, 1990 and Niu, 1990. A lognormal distribution for error e in crack growth rate is chosen to reflect the lognormal distribution of crack sizes used in literature (e.g., Harkness, 1994 and Rahman and Rice, 1992). Uniform distribution for k is chosen to reflect lack of information)

Table 5-2 lists uncertainties in form of errors and variability in the life prediction and structural design model assumed here for 7075-T6-aluminum alloy. Typical service life of 40,000 flights is obtained from Backman (2001). In this chapter we demonstrate the effect of safety factors on two design criteria, (i) safe-life: structure is designed for safe crack growth for the entire service life of 40,000 flights; no inspections are performed (ii) fail-safe: structure is designed for safe crack growth until the next inspection (10,000 flights). The typical inspection interval of 10,000 flights was obtained from JSSG-2006.

Calculating Design Thickness

This section determines the design thickness calculation in step A of Figure 5-1. The calculated stress σ_{calc} on the structure is found from Equation 5-8 representing hoop stress due to pressure loading.

$$\sigma_{calc} = \frac{pC}{t} \tag{5-8}$$

where C is a function of the geometry, p is applied pressure differential and t is structural thickness. In subsequent calculations for stress in fuselage components in hoop direction, the parameter C was approximated for convenience by the value for a cylindrical pressure vessel.[***]

$$C = r \tag{5-9}$$

where r is the radius of fuselage. Combining Equations 5-7 and 5-8, the stress in the structure is calculated as

$$\sigma_{true} = (1+k)\frac{rp}{t} \tag{5-10}$$

To design a panel for fixed life we first obtain the stress level required to grow the initial crack a_i to critical crack a_c during the design life. This is obtained by solving Equation 5-6b with all the safety measures. The safety measures considered are using m_A, the A-Basis value of m, a_{iB} the B-basis value of a_i, the conservative value of critical crack a_{cA} obtained using A-basis value of K_{IC} in Equation 5-4, A-Basis value of yield stress, and S_{FL} of 2.0, the safety factor on fatigue life.

[***] The actual stress may be somewhat different, but for the purpose of this chapter it is only important to model the inverse relationship between stress and thickness.

$$1-\frac{1}{\left(\sigma_{design}^{fatigue}\sqrt{\pi}\right)^{m_A}}\left(\frac{S_{FL}N_s eD\left(1-\frac{m_A}{2}\right)}{\left(\frac{K_{IC}^{A}}{\sigma_{design}^{fatigue}\sqrt{\pi}}\right)^{2-m_A}-a_{iB}^{1-\frac{m_A}{2}}}\right)=0 \tag{5-11}$$

Solving Equation 5-11 for $\sigma_{design}^{fatigue}$ gives the stress that should not be exceeded so that the fatigue life does not fall below twice the service life. Further, 1.5 times the maximum load in any component should not exceed the yield stress of the material to prevent static failure. We assume that the A-Basis property of yield stress is used to design the structure for static strength.

$$\sigma_{design}^{yield}=\sigma_{A-Basis}^{yield} \tag{5-12}$$

Equations 5-11 and 5-12 give two different values of allowable design stress. Also the FAA requires that the damaged structure should have sufficient residual strength to withstand 1.15 times the limit load without failure. We assume that the net section area does not reduce below 80% until the crack is detected and repaired. The design thickness is determined so that all the three criteria are satisfied. For the undamaged structure, a safety factor S_F = 1.5 on design load is also specified, then structural thickness is designed with a design load p_d multiplied by a safety factor S_F, hence the design thickness of the structural is calculated from Equation 5-13 as

$$t_{design}^{mean} = \max\left(\begin{array}{l}(1+k)\dfrac{p_d r}{\sigma_{design}^{fatigue}}\\ (1+k)\dfrac{1.5\,p_d r}{\sigma_{design}^{yield}}\\ (1+k)\dfrac{1.15\,p_d r}{0.80\,\sigma_{design}^{yield}}\end{array}\right) \tag{5-13}$$

For the example considered here, the second and third components of Equation 5-13 are less critical than the first. The thickness obtained from Equation 5-13 is the average thickness for a given aircraft model. The actual thickness will vary due to individual–level manufacturing uncertainties, which are incorporated in calculation of failure probability using Monte Carlo simulation.

Calculating Failure Probability

Certification Testing

After the structure has been designed (that is, design thickness determined from Equation 5-13), we simulate certification testing for the aircraft. We assume that the structure will not be built with complete fidelity to the design due to manufacturing and fabrication variability. To check if the structure is fit for use, we conduct two tests in step B of Figure 5-1 (i) randomly selected structural design from each aircraft company is fatigue tested for pressure differential equal to the design load p_d for twice the design life (ii) another random structural design from the same company is loaded with 1.5 times the limit static load to check certification passage if the following inequalities are satisfied

$$\text{Fatigue certification test: } S_{FL}N_s - \frac{a_c^{1-\frac{m}{2}} - a_i^{1-\frac{m}{2}}}{D\left(1-\frac{m}{2}\right)\left(\frac{p_d r}{t_{act}}\sqrt{\pi}\right)^m} \geq 0 \qquad \text{(5-14a)}$$

$$\text{Static certification test: } \sigma - \sigma_f = \frac{S_F p_d r}{t_{act}} - \sigma_f \geq 0 \qquad \text{(5-14b)}$$

where the actual thickness t_{act} is uniformly distributed with mean equal to t_{design} and 3% bound. If the structural design fails either test than that design is rejected. Here the thickness t, initial crack a_i, fractures toughness K_{IC}, yield stress σ_f and Paris model constant m are random variables (see Table 5-2). This procedure of design and testing is

repeated (steps A-B, Figure 5-1) for N different aircraft models. For each new model, different random error factor k and e are picked for the design, and different allowable properties are generated from coupon testing (Appendix I). If the design passes the certification tests, then M instance of the design are generated to simulate variability in the aircraft fleet.

Service Simulation

To simulate failure in service we assume that the structure is required to withstand service stress for the specified design life N_s. The inner loop in Figure 5-1 (steps C-E) represents the simulation of a population of M fuselage designs that all have the same design. However, each structure is different due to variability in geometry (thickness t), material properties (K_{IC}, a_i, m, σ_f) and loading, p (step D, Figure 5-1). We subject the structure in each airplane to actual random maximum (over a lifetime) service loads (step E, Figure 5-1) and calculate whether it fails using Equation 5-15.

$$N_s - \frac{a_c^{1-\frac{m}{2}} - a_i^{1-\frac{m}{2}}}{D\left(1-\frac{m}{2}\right)\left(\frac{pr}{t_{act}}\sqrt{\pi}\right)^m} \geq 0 \qquad (5\text{-}15)$$

$$\sigma - \sigma_f = \frac{pr}{t_{act}} - \sigma_f \geq 0$$

where the actual thickness t_{act} is uniformly distributed with mean equal to t_{design} and 3% bound. If the structural design fails either test than that design is rejected. Here the thickness t, initial crack a_i, fractures toughness K_{IC}, yield stress σ_f and Paris model constant m are random variables (see Table 5-2). This procedure of design and testing is repeated (steps A-B, Figure 5-1) for N different aircraft models. For each new model, different random error factor k and e are picked for the design, and different allowable

properties are generated from coupon testing (Appendix H). If the design passes the certification tests, then M instance of the design are generated to simulate variability in the aircraft fleet. We add up the number of structures failed for each airplane, and calculate the failure probability by dividing the number of failures by the number of airplane models that passed certification times M. The values of N and M used here for calculation of failure probability are 2000 and 5000, respectively. The following symbols are used to describe the results

Table 5-3: Nomenclature of symbols used to calculate failure probability and describe the effect of certification testing

Symbol	Description
B_k	Bounds on error k
P_c	Probability of failure with certification
P_{nc}	Probability of failure without certification
R	Percentage of designs rejected by certification
SF_{eff}	Ratio of mean design thickness with safety measures to that without any safety measure
t_{cert}	Structural thickness of certified structures
t_{design}	Thickness of designed structures

In this chapter we demonstrate the effect of safety factors on two design criteria (i) safe-life: structure is designed for safe crack growth (fatigue life) for the entire service life of 40,000 flights; no inspections are performed (ii) fail-safe: structure is designed for safe crack growth until the next inspection (10,000 flights). Typical inspection interval of 10,000 flights was obtained from JSSG-2006.

Results

Effect of Errors and Testing on Structural Safety

Effects of All Safety Measures. We calculate first the failure probability of structures designed using all the safety measures. The safety measures considered are the A-Basis m, the B-basis a_i, the A-basis K_{IC}, the A-Basis yield stress, SF of 1.5, the safety factor on

static load and SF_L of 2, safety factor on fatigue life. Calculations are done for two levels of e and three levels of k. For small probability of failure, simulations performed using M = 10,000 can be inaccurate because some batches may have no failure at all. This can produce large scatter in failure probability among designs. We also performed calculations with N = 500 designs and M = 100,000 instances of each design. These are not necessarily more accurate, but they give an idea of the MCS errors for these low probabilities. Tables 5-4 and 5-5 show the fail-safe structures designed for fatigue life until the next inspection (10,000 flights) and Tables 5-6 and 5-7 demonstrate the calculation for safe-life structure designed for the entire service life (40,000 flights).

Table 5-4: Probability of failure for 10 % COV in e and different bounds on error k using all safety measures for fail-safe design for 10,000 flights. Simulations are performed with N= 5000 designs and M = 10000 instances of each design

B_k	P_c	P_{nc}	R %	t_{cert} (mean, standard deviation) mm	t_{design} (mean, standard deviation) mm	P_c/P_{nc}
0.1	$<10^{-8}$	$<10^{-8}$	0.0	2.08, 0.14	2.08, 0.14	--
0.3	6×10^{-6} (6.7)	6×10^{-6} (6.7)	0.4	2.08, 0.38	2.08, 0.38	1.0
0.5	3×10^{-3} (5.7)	7×10^{-3} (3.9)	6.0	2.14, 0.57	2.08, 0.60	0.42

*Using N = 500 designs and M = 100,000. For B_k = 0.3, we have $P_c = 5\times10^{-6}$ (5.9) and $P_{nc} = 5\times10^{-6}$ (5.6). The coefficient of variation among batches reduces because failure probability of each batch is computed more accurately because of larger M

Since calculation of failure probability is based on Monte Carlo simulation (MCS), there will be error because of finite sample size. The failure probability before and after certification tests presented in each row is the average failure probability of all the designs used in service. The standard error (estimate of standard deviation) in this value due to MCS is reduced by a factor of or 70.7 from the standard deviation of the probability. For example, in Table 5-4 the probability of failure is given as 6×10^{-6} with a coefficient of variation of 6.7. The coefficient of variation of the mean probability is

6.7/70.7 or approximately 10%. So we only present the number of significant digits consistent with the size of MCS. Accuracy can be improved by using larger sample sizes.

Table 5-5: Probability of failure for 50 % COV in e for different bounds on error k using all safety factors for fail-safe design for 10,000 flights. Simulations are performed with N= 5000 designs and M = 10000 instances of each design

B_k	P_c	P_{nc}	R %	t_{cert} (mean, standard deviation) mm	t_{design} (mean, standard deviation) mm	P_c/P_{nc}
0.1	8×10^{-5} (8.2)	9×10^{-5} (7.4)	1	2.05, 0.39	2.04, 0.40	0.88
0.3	8×10^{-4} (7.5)	2×10^{-3} (8.7)	3	2.07, 0.50	2.04, 0.51	0.4
0.5	3×10^{-3} (6.9)	2×10^{-2} (3.8)	12	2.17, 0.64	2.04, 0.70	0.15

Using N= 500 designs and M = 100,000. For B_k = 0.1, we have $P_c = 4\times10^{-5}$ (8.3) and $P_{nc} = 6\times10^{-5}$ (7.5) and for B_k = 0.3, we have $P_c = 8\times10^{-4}$ (6.9) and $P_{nc} = 3\times10^{-3}$ (7.7)

Table 5-6: Probability of failure for 10 % COV in e for different bounds on error k using all safety measures for safe-life design of 40,000 flights. Simulations are performed with N= 5000 designs and M = 10000 instances of each design

B_k	P_c	P_{nc}	R_B %	t_{cert} (mean, standard deviation) mm	t_{design} (mean, standard deviation) mm	P_c/P_{nc}
0.1	$<10^{-8}$	$<10^{-8}$	0	3.58, 0.24	3.58, 0.24	1.0
0.3	3×10^{-5} (5.2)	4×10^{-5} (4.8)	0.8	3.60, 0.64	3.59, 0.64	0.75
0.5	3×10^{-3} (4.3)	5×10^{-3} (3.6)	4	3.68, 0.98	3.61, 1.02	0.6

Using N= 500 designs and M = 100,000. For B_k = 0.1, we have $P_c = 1\times10^{-7}$ (8.1) and $P_{nc} = 1\times10^{-7}$ (8.1) and For B_k = 0.3, we have $P_c = 4\times10^{-5}$ (5.1) and $P_{nc} = 4\times10^{-5}$ (4.9)

Table 5-7: Probability of failure for 50 % COV in e for different bounds on error k using all safety factors for safe-life design of 40,000 flights. Simulations are performed with N= 5000 designs and M = 10000 instances of each design)

B_k	P_c	P_{nc}	R %	t_{cert} (mean, standard deviation) mm	t_{design} (mean, standard deviation) mm	P_c/P_{nc}
0.1	3×10^{-4} (6.2)	3×10^{-4} (5.7)	1	3.53, 0.74	3.52, 0.74	1.0
0.3	3×10^{-3} (6.7)	4×10^{-3} (5.7)	4	3.49, 0.87	3.44, 0.88	0.75
0.5	4×10^{-3} (4.8)	2×10^{-2} (3.6)	10	3.68, 1.17	3.49, 1.24	0.2

Using N = 500 designs and M = 100,000. For B_k = 0.1, we have $P_c = 3\times10^{-4}$ (7.2) and $P_{nc} = 5\times10^{-4}$ (6.9)

The second and third columns give the failure probabilities and the fourth column shows the percentage of designs rejected by the certification test. This number increases with error magnitude because large errors may produce less conservative designs which will be rejected by testing. The coefficient of variation in the probabilities is given in parentheses and represents the variation in failure probability between structures designed by different aircraft companies. The fifth column gives the mean and standard deviation in thickness of certified designs and sixth column gives the corresponding design thicknesses. The variability in design thickness is due to uncertainty in model errors. Certification testing increases the mean values and reduces the standard deviations because extremely thin designs will fail certification. We see that probability of failure is high when errors are high and it decreases with errors. The effectiveness of certification tests, measured by the ratio of probability improvement P_c / P_{nc}, is high when errors are high, indicating that testing is more important for large errors. Large errors produce some super-strong and some super-weak designs. The super-weak designs are mostly caught by the certification tests, leaving the super-strong designs to reduce the probability of failure. This is also indicated by large batch rejection rate for high errors.

Comparing Tables 5-4 and 5-5 with Tables 5-6 and 5-7 we see that there is a large difference in design thickness (about 40%) between fail-safe and safe-life design. The reason for this is that the safe-life structure is designed for entire service life (40,000 flights) which requires greater thickness for maintaining stable crack growth over a longer period of time. In contrast the fail-safe structure is designed for 10,000 flights only which require lower structural thickness. From the last columns, comparing the ratio P_c

/P_{nc} we see that certification tests are more effective for fail-safe structures than safe-life structures even though the batch rejection rates for the latter are higher.

Next, we perform simulations for structure designed without any safety measure for structure designed using fail-safe criteria.

Table 5-8: Probability of failure for different bounds on error k for 10 % COV in e without any safety measures for fail-safe design for 10,000 flights. Simulations are performed with N= 5000 designs and M = 10000 instances of each design

B_k	P_c	P_{nc}	R %	t_{cert} (mean, standard deviation) mm	t_{design} (mean, standard deviation) mm	P_c/P_{nc}
0.1	0.22 (1.1)	0.52 (0.2)	53	0.90, 0.05	0.88, 0.05	0.42
0.3	0.14 (1.5)	0.52 (0.6)	52	0.99, 0.11	0.88, 0.15	0.27
0.5	9×10^{-2} (2.0)	0.51 (0.7)	51	1.09, 0.16	0.88, 0.25	0.17

Table 5-9: Probability of failure for different bounds on error k for 50 % COV in e without any safety measures for fail-safe design for 10,000 flights. Simulations are performed with N= 5000 designs and M = 10000 instances of each design

B_k	P_c	P_{nc}	R %	t_{cert} (mean, standard deviation) mm	t_{design} (mean, standard deviation) mm	P_c/P_{nc}
0.1	0.16 (1.5)	0.56 (0.4)	56	0.95, 0.13	0.86, 0.14	0.28
0.3	0.13 (1.7)	0.57 (0.5)	56	1.01, 0.16	0.86, 0.19	0.22
0.5	9×10^{-2} (2.1)	0.54 (0.7)	54	1.10, 0.20	0.87, 0.28	0.16

Tables 5-8 and 5-9 shows that the probability of failure without testing is about 50%. This is expected because the structure is designed without any safety factors so that about 50% of the designs will fail below design life because of unconservative designs. Also we see that the probability of failure after certification decreases with increase in errors. When the errors are large, the average thickness of the designs that pass certification is high which leads to decrease in failure probability. Thus for this case we

get counterintuitive results that large errors produce safer designs. This phenomenon manifests itself when safety factors are low. We further explore the effectiveness of testing by testing components with artificially machined cracks in next section.

Effect of Certification Testing With Machined Crack

From Tables 5-4 and 5-5 we see that certification testing is not very effective in reducing the probability of failure. The primary reason for this is because of the non-linear damage growth model which is very sensitive to variability in material properties leading to huge scatter in fatigue life. Because of this, the structure passing certification tests will not closely represent entire fleet. As a result, copies of the certified structures will still fail in actual service because of variability in material properties. Testing only reduces model errors; variability in material properties of tested panels reduces the effectiveness of testing. The effectiveness of certification testing may be improved by machining a large crack in the structure. Such tests are documented in FAA/AR-95/47 (Gruber *et al.*, 1996) and are primarily used to determine material properties and understand component failure. Here we simulate this procedure by introducing a B-basis crack and checking if fatigue life is less than twice the design life. The use of machine cracks removes the uncertainty in certification testing associated with the distribution of initial crack sizes. Table 5-10 show the results for fail-safe structure designed for 10,000 flights and Table 5-11 show the calculations for design of safe-life structure for the service life of 40,000 flights.

Table 5-10: Probability of failure for different bounds on k and 10 % COV in e for structures designed with all safety measures for fail-safe for 10,000 flights and tested using a machine cracked panel. Simulations are performed with N= 5000 designs and M = 10000 instances of each design

B_k	P_c	P_{nc}	R %	t_{cert} (mean, standard deviation) mm	t_{design} (mean, standard deviation) mm	P_c/P_{nc}
0.1	$<10^{-8}$	$<10^{-8}$	1	2.08, 0.14	2.08, 0.14	--
0.3	1×10^{-6} (11.6)	4×10^{-6} (6.1)	10	2.13, 0.34	2.07, 0.36	0.25
0.5	7×10^{-6} (11.8)	6×10^{-3} (4.2)	26	2.35, 0.47	2.09, 0.61	1.16×10^{-3}

Using N = 500 designs and M = 100,000. For B_k = 0.3, we have $P_c = 2\times10^{-6}$ (7.1) and $P_{nc} = 6\times10^{-6}$ (4.9) For B_k = 0.5, we have $P_c = 1\times10^{-5}$ (11.7) and $P_{nc} = 6\times10^{-3}$ (3.9)

Table 5-11: Probability of failure for different bounds on k and 10 % COV in e for structures designed with all safety measures for safe-life of 40,000 flights and tested using a machine cracked panel. Simulations are performed with N= 5000 designs and M = 10000 instances of each design).

B_k	P_c	P_{nc}	R %	t_{cert} (mean, standard deviation) mm	t_{design} (mean, standard deviation) mm	P_c/P_{nc}
0.1	--	--	--	3.59, 0.25	3.59, 0.25	--
0.3	3×10^{-5} (6.5)	7×10^{-5} (7.0)	7	3.65, 0.63	3.59, 0.65	0.42
0.5	6×10^{-4} (8.9)	6×10^{-3} (3.3)	20	3.91, 0.90	3.57, 1.06	0.1

Using N= 500 designs and M = 100,000, For B_k = 0.1, we have $P_c = 2\times10^{-7}$ (8.6) and $P_{nc} = 3\times10^{-7}$ (8.1) , For B_k = 0.3, we have $P_c = 2\times10^{-5}$ (5.5) and $P_{nc} = 4\times10^{-5}$ (4.6). For B_k = 0.5, we have $P_c = 3\times10^{-4}$ (6.2) and $P_{nc} = 6\times10^{-3}$ (3.4)

Comparing Tables 5-4 and 5-6, to Tables 5-10 and 5-11 we note large improvement in effectiveness of certification and reduction probability of failure due to certification testing. Effectiveness of certification testing is largely affected by variability in material properties and using machined cracked panels reduces the variability in crack sizes, thereby improving effectiveness of tests. We see that failure probability can be reduced by a marginal amount (less than an order of magnitude) using certification for safe-life structures. For fail-safe structures certification is very effective and a large improvement

in failure probability can be achieved. We conclude that certification is more effective when structures are designed and certified for short fatigue life.

Effect of Variability in Material Properties on Structure Designed With all Safety Measures

Tables 5-4 through 5-11 used 17% COV in material parameter *m*. The COV in *m* was obtained from test data (reported by several different experimentalists) presented in Sinclair and Pierie (1990). In practice, aircraft companies employ stringent quality control on materials so that the variability in material properties is reduced. To demonstrate the effect of variability in material properties on fatigue life we obtain failure probabilities for 8.5% COV in *m* and compare it to the results for 17% COV in *m*.

Table 5-12: Probability of failure for different bounds on *k* and 10 % COV in *e* for structure designed with all safety measures for fail-safe for 10,000 flights and COV in material property *m* reduced to 8.5%. Simulations are performed with *N*= 5000 designs and *M* = 10000 instances of each design).

B_k	P_c	P_{nc}	R %	t_{cert} (mean, standard deviation) mm	t_{design} (mean, standard deviation) mm	P_c/P_{nc}
0.1	$<10^{-8}$	$<10^{-8}$	0	1.83, 0.12	1.83, 0.12	--
0.3	1×10^{-6} (11.7)	1×10^{-6} (11.7)	0	1.82, 0.32	1.82, 0.32	1.0
0.5	2×10^{-3} (9.4)	1.2×10^{-2} (4.2)	10	1.92, 0.48	1.83, 0.53	0.16

Using *N*= 500 designs and *M* = 100,000. For $B_k = 0.3$, we have $P_c = 1\times10^{-6}$ (7.6) and $P_{nc} = 1\times10^{-6}$ (7.4)

Table 5-13: Probability of failure for different bounds on *k* and 50 % COV in *e* for structures designed with all safety measures for fail-safe criteria for 10,000 flights and COV in material property *m* reduced to 8.5%. Simulations are performed with *N*= 5000 designs and *M* = 10,000 instances of each design

B_k	P_c	P_{nc}	R %	t_{cert} (mean, standard deviation) mm	t_{design} (mean, standard deviation) mm	P_c/P_{nc}
0.1	3×10^{-5} (13.8)	4×10^{-5} (11.7)	0.4	1.80, 0.31	1.80, 0.32	0.75
0.3	5×10^{-4} (12.3)	3×10^{-3} (8.7)	4	1.85, 0.41	1.82, 0.42	0.16
0.5	1×10^{-3} (9.6)	3×10^{-2} (3.8)	12	1.92, 0.53	1.80, 0.58	0.03

Using *N* = 500 designs and *M* = 100,000. For $B_k = 0.1$, we have $P_c = 2\times10^{-6}$ (8.3) and $P_{nc} = 2\times10^{-5}$ (8.6). For $B_k = 0.3$, we have $P_c = 7\times10^{-4}$ (11.1) and $P_{nc} = 2\times10^{-3}$ (7.3)

Comparing Tables 5-4 and 5-5 to Tables 5-12 and 5-13, we see that certification testing becomes more effective when variability is low. This is reasonable because large variability increases the chance of large difference between the tested design and the actual structures used in service. Also we see that failure probability reduces when variability is lesser. This is because of the use of conservative value of *m* in design.

Effect of Conservative Material Properties. Failure probability is calculated next for structures designed using only conservative material specification. In Table 5-14 we calculate the failure probability for structure designed using A-Basis property for *m* only. Tables 5-15 and 5-16 present the results using A-Basis property for fracture toughness K_{th} and crack growth parameter *m* (17% COV), B-basis value of crack size and A-Basis value of yield stress. All other safety measures have a value of 1.0.

Table 5-14: Probability of failure for different bounds on *k* and 10 % COV in *e* for structures designed using only A-Basis *m* for fail-safe criteria for 10,000 flights. Simulations are performed with *N*= 5000 designs and *M* = 10,000 instances of each design

B_k	P_c	P_{nc}	*R* %	t_{cert} (mean, standard deviation) mm	t_{design} (mean, standard deviation) mm	P_c/P_{nc}
0.1	2×10^{-2} (1.3)	2×10^{-2} (1.2)	2	1.23, 0.08	1.23, 0.08	1.0
0.3	6×10^{-2} (1.8)	1×10^{-1} (1.5)	10	1.26, 0.20	1.23, 0.22	0.6
0.5	6×10^{-2} (2.6)	2×10^{-1} (1.4)	23	1.37, 0.29	1.23, 0.36	0.3

Compared to Table 5-9 where structure is designed without any safety measures, we see from Table 5-14 that using A-basis *m* improves the failure probability by an order of magnitude. However, comparing Table 5-14 to Table 5-13 we see that reducing the variability in material property *m* by 50% is more effective than using conservative material property for *m*.

Table 5-15: Probability of failure for different bounds on *k,* 10 % COV in *e* for structure designed using conservative properties for fail-safe design for 10,000 flights. Simulations are performed with *N*= 5000 designs and *M* = 10000 instances of each design).

B_k	P_c	P_{nc}	R %	t_{cert} (mean, standard deviation) mm	t_{design} (mean, standard deviation) mm	P_c/P_{nc}
0.1	3×10^{-5} (3.1)	3×10^{-5} (3.1)	0	1.61, 0.10	1.61, 0.10	1.0
0.3	3×10^{-3} (3.3)	3×10^{-3} (3.2)	0.7	1.64, 0.28	1.64, 0.28	1.0
0.5	3×10^{-2} (3.0)	7×10^{-2} (2.3)	6	1.67, 0.44	1.61, 0.47	0.42

Using N = 500 designs and M = 100,000. For B_k = 0.1, we have $P_c = 3\times10^{-5}$ (2.8) and $P_{nc} = 3\times10^{-5}$(2.8)

Table 5-16: Probability of failure for different bounds on *k*, 50 % COV in *e* for structures designed using conservative properties for fail-safe criteria for 10,000 flights. Simulations are performed with *N*= 5000 designs and *M* = 10000 instances of each design

B_k	P_c	P_{nc}	R %	t_{cert} (mean, standard deviation) mm	t_{design} (mean, standard deviation) mm	P_c/P_{nc}
0.1	4×10^{-3} (4.8)	6×10^{-3} (4.8)	0.6	1.59, 0.28	1.58, 0.28	0.66
0.3	1.6×10^{-2} (3.4)	2×10^{-2} (3.2)	2	1.59, 0.33	1.56, 0.34	0.8
0.5	4×10^{-2} (3.0)	0.10 (2.2)	10	1.65,0.48	1.57, 0.51	0.4

Comparing Tables 5-4 and 5-5 with Tables 5-15 and 5-16 it can be seen that failure probability is very sensitive to structural design. When all safety measures are used, the effective safety factor (ratio of design thickness with safety measures to that without any safety measures) is about 2.36, while when only conservative material properties are used the effective safety factor is about 1.8. For this 20% decrease in effective safety factor the failure probability increases by more than an order on magnitude when errors are high and about four orders of magnitude when errors are low.

To illustrate the interaction between safety measures, errors and variability we obtain the effective safety factor in Table 5-17 for two levels of error bounds. The ratio

P_{SF}/P_{NSF} indicates the effectiveness of safety factors in reducing failure probability. The other ratio P_c/P_{nc} is the ratio of probability of failure with certification test to that without any test and measures the effectiveness of certification testing only.

Table 5-17: Effective safety factor and measures of probability improvement in terms of individual safety measures and error bounds for structure designed using fail-safe criteria of 10,000 flights. A = conservative properties, C = certification, M = machined crack certification, S = design safety factors, SF_{eff} = ratio of structural thickness with all safety measure to that without any safety measure, P_{SF}/P_{NSF} = ratio of probability of failure of structure designed using safety measure to that designed without any safety measure.

Safety measure	Error bounds (k = 10%, e = 10%)			Error bound (k = 50%, e = 50%)		
	SF_{eff}	P_{SF}/P_{NSF}	P_c/P_{nc}	SF_{eff}	P_{SF}/P_{NSF}	P_c/P_{nc}
S+A+M	2.36	2×10^{-8}	1.0	2.69	4×10^{-5}	7×10^{-4}
S+A+C	2.36	2×10^{-8}	1.0	2.50	6×10^{-3}	0.4
S+A	2.36	2×10^{-8}	--	2.34	4×10^{-2}	--
C+A	1.83	6×10^{-5}	1.0	1.90	0.08	0.4
A	1.83	6×10^{-5}	--	1.80	0.2	--
C	1.02	0.4	0.4	1.26	0.16	0.16

We can see that certification tests are not very useful when errors are low. The effective safety factor is almost the same with or without certification for low error bounds (k = 10%, e = 10%). For high errors certification tests become more useful as indicated by column seven of Table 5-17. All the tables indicate that the when the errors increase, (P_c/P_{nc}) decreases revealing that the efficiency of testing increases. Another way of looking at this effect is to note that when there are no errors, there is no point to the tests. The ratio P_{SF}/P_{NSF} in Table 5-17 shows that safety measures are most effective when errors are lower and greater improvement in failure probability can be achieved as compared to that at high errors. From P_{SF}/P_{NSF} we see that among all the safety measure the conservative material properties (A) contribute the most to probability improvement when errors are low, for high errors, testing is more effective. This is expected because fatigue is very sensitive to material properties and using conservative material properties

reduces the effect of variability. The other safety measures provide less protection. We can see that certification testing is most effective when safety factors are low, errors are high and variability is low and effectiveness of tests can be improved by using panels with machined cracks. The combined effect of all safety measures can reduce the failure probability to about 10^{-7}.

CHAPTER 6
A PROBABILISTIC MODEL FOR INTERNAL CORROSION OF GAS PIPELINES

Introduction

Internal corrosion in a pipeline leads to reduction of pipe wall thickness and ultimately to leak or burst failure. The presence of electrolytes such as water and species such as CO_2, H_2S, and O_2 are some of the prominent factors causing internal corrosion. Consequently, periodic inspections and repairs are necessary to maintain pipeline integrity and prevent failure. Despite recent advances in inline inspection (ILI) technology, not all portions of a pipeline can typically be inspected due to various geometrical and economic constraints. The surest way to determine the location and extent of internal corrosion is to excavate and examine the pipe. However, typical oil and gas pipelines are hundreds of miles long and extensive excavation is impractical given the negative economic consequence of shutting the pipeline down to perform the excavation. Recently, an internal corrosion direct assessment (ICDA) methodology has been developed for essentially dry gas lines to prioritize locations for excavation and detailed examination by Burwell *et al.* (2004). This chapter addresses the uncertainties entailed in the ICDA method using a probabilistic framework.

Bich and Eng (2002) and Nguyen and Heaver (2003) conducted corrosion measurements at a few discrete locations along a pipeline. Predicted corrosion rates were compared with observed corrosion rates and factors related to corrosion (CO_2, H_2S, O_2, Sulfides, etc.) were identified and matched to morphology and location of observed damage. Preventive measures like thermal regulation, increased inhibitor use, inspection

pig runs, and reduction of corrosion enhancing species were recommended to reduce corrosion damage. Philipchuk (1998) developed a regression equation to forecast the number of leaks per year in terms of annual leak histories and other measured variables driving corrosion growth. He also determined the most significant variables affecting leak. An important limitation of these approaches is that they are local in nature because the analysis is made on few discrete locations. However, since these corrosion models are not coupled to models that identify locations along a pipeline where corrosive electrolyte could accumulate, they provide no information about the location where excavation should be performed to perform inspections. Without incorporating this information into a predictive model, it is unclear how what is learned in one area can be applied to another. For a specific area, it is not possible for a pipeline operator to identify all other areas that are similar in size, age and conditions and examine the corrosion depth.

Previous work on dry gas pipelines conducted at Southwest Research Institute (SwRI) used deterministic flow analysis to identify locations in a pipeline where water is likely to accumulate first. Internal corrosion is considered to be present at these locations and is most severe where the inclination angle[†††] of the pipe is greater than the critical flow angle.[‡‡‡] Excavations can be performed at these locations, and other locations can be inspected if substantial corrosion is detected at these locations. Although this method gives a reasonable idea about the presence of corrosion, no account of the inherent variations in flow information (pressure, temperature, and species concentration),

[†††] The inclination angle is the angle between horizontal and the current section of pipe

[‡‡‡] Water is assumed to accumulate if the inclination angle is greater than the critical angle.

elevation data, and modeling error are taken into account. Furthermore, the simplified flow modeling is not adequate for wet gas lines.

Probabilistic analysis can be used to incorporate uncertainty in data and obtain the relative likelihood of failure in a pipeline subjected to corrosion growth. Here the model parameters are represented as random variables, each with a probability distribution. The state of failure is represented by the probability that the corrosion depth will exceed a critical amount at a specified location and time of operation of the pipeline. The combination of physics-based modeling, associated parameter and model uncertainties, and inspection-based model updating provides a more rational framework for making inspect/repair/replace decisions that does traditional deterministic analysis. An example application of probabilistic analysis to the prediction of life governed by mechanical failure in gas distribution pipelines is given in Thacker *et al*. (1992).

Muhlbauer (1996) developed a risk indexing system that relies on establishing subjective weighing factors derived from judgment of the corrosivity of the product and presence/absence of mitigation methods (monitoring coupons, ILI, inhibitor injection, gas treatment, and internal coating). Other risk assessment methods use a fault-tree/event-tree approach but assign subjective probabilities to various processes leading to a leak. These approaches are limited by the fact these indices or probabilities are fixed, subjective, and do not allow updated pipeline information.

Ahammed and Melchers (1995) used the First Order Reliability Method (FORM) to predict the pipe leak probability at a single location subjected to pitting corrosion. Ahammed and Melchers (1997) performed reliability analysis to incorporate uncertainty in data and obtain failure probability of a single section of pipe subjected to widespread

corrosion growth. Ahammed and Melchers (1997) and Caleyo *et al.* (2002) assumed that the number and location of defective sites were known and used a probabilistic approach to compute the reliability of a pipeline segment subjected to corrosion growth in the presence of multiple defects. Vinod *et al.* (2003) used Markov chains and FORM to estimate inspection time for a pipe segment for maintaining a specified probability of failure. They used the erosion-corrosion growth model to estimate the time required for corrosion depth to exceed a critical depth. Hong (1999) also used Markov chains to develop a method for obtaining optimum inspection time for a pipeline subjected to corrosion growth including generation of new defects during the service life of a pipeline. All of these methods are based on calculating the reliability estimate of a single section of pipe, which is assumed to govern the overall structural integrity of the pipeline. Consequently, they provide no framework to identify the critical location in the pipeline itself.

Gartland *et al*. (2003) developed a model to predict the corrosion profile throughout the length of a pipeline. The model combines pipeline profile and flow information into multiphase flow modeling software to obtain water wetting factors at different locations along pipe length. This is combined with a point corrosion model and inhibitor effect to estimate CO_2 corrosion along the pipe length. They also developed a framework to combine the model predictions with inspection and monitoring data to obtain updated estimates. However they did not account for uncertainty in pipeline profile information in calculating water wetting factors. Also their results are conditioned upon predictions of a single model, which may not be suitable for all conditions in pipelines.

The proposed approach is aimed at developing a probabilistic model for assessing the extent of internal corrosion along the length of a pipeline. The probabilistic model can incorporate inspection data, so the model as well as the results can reflect observational data. The probabilistic model uses either Monte Carlo simulation or an approximate FORM solution to perform the probability integration. A Bayesian approach is used to update the model prediction with field data. Because the "true" corrosion rate model is unknown, three candidate corrosion rate models are used to obtain the probability estimate. The corrosion rate models are combined as a weighted average, where the weight factors are updated using the corrosion depth measured from inspection data.

Proposed Methodology

Corrosion Rate Model

The nature of corrosion growth largely depends on the presence of electrolyte such as water, concentration of species such as CO_2, O_2, H_2S, pH, and flow parameters such as temperature, pressure, and velocity. Here we focus on the internal region of a pipeline where the presence of widespread corrosion is prominent. Various empirical equations are available to represent the corrosion rate as a function of aforementioned parameters. Three candidate models were selected, M_1 represents the de-Waard Milliams model (de-Waard and Milliams, 1975), M_2 represents the de-Waard Lotz model, (de-Waard and Lotz, 1993) and M_3 represents the SwRI model, (Sridhar *et al*., 2001)

$$M_1: \frac{da}{dt} = k \times C_I \times 10^{\left(5.8 - \frac{1710}{T} + 0.67 \log_{10}(pCo_2)\right)} \quad mm/years \tag{6-1}$$

$$M_2: \frac{da}{dt} = k \times C_I \times CF \times 10^{\left(5.8 - \frac{1710}{T} + 0.67 \log_{10}(pCo_2)\right)} \quad mm/years \tag{6-2}$$

$$M_3:\ \frac{da}{dt} = k \times C_1 \times 0.0254 \times \begin{pmatrix} 8.7 + 9.86\times10^{-3}(O_2) - 1.48\times10^{-7}(O_2)^2 - 1.31(pH) + \\ 4.93\times10^{-2}(pCo_2)(pH_2S) - 4.82\times10^{-5}(pCo_2)(O_2) - \\ 2.37\times10^{-3}(pH_2S)(O_2) - 1.11\times10^{-3}(O_2)(pH) \end{pmatrix} \quad mm/years \tag{6-3}$$

Where the temperature correction factor for M_2 is given as

$$CF = 10\left(-6.7 + \frac{2400}{T} - 0.61\log_{10}(pCo_2)\right) ..when.. \frac{2400}{(6.7 + 0.61\log_{10}(pCo_2))} < T$$
$$else \tag{6-4}$$
$$CF = 1.0$$

These three models are referred to as DM, DL and SwRI respectively. In the Equations 6-1 to 6-4, *a* is the corrosion depth in *mm*, *t* is time in *seconds*, *T* is temperature in degree K, pCO_2 partial pressure of CO_2 in the mixture in *Pascal's*, pH_2S is partial pressure of H_2S in the mixture in *Pascal's*, O_2 is the concentration of O_2 in parts per million, *k* is the modeling error, C_1 is inhibitor correction factor, and *CF* is the temperature correction factor given by the following Eq. (6-4) (Bert *et al*., 2002). Although a complete discussion of the applicability of these models to pipeline systems is beyond the scope of this chapter it should be noted that the DM and DL models have been derived from experiments simulating production systems whereas the SwRI model simulates gathering lines.

Inhibitor Correction Model

Corrosion inhibitors can be added to the inlet of a pipeline to reduce the corrosion rate. Since the effect of inhibitor will diminish as a function of distance from the injection point, an exponential model is assumed to represent the reduction in corrosion rate with distance along pipe length. The inhibitor correction factor is represented by the following equation

$$C_I = 1 - e^{\left(-A\frac{L}{L_0}\right)} \tag{6-5}$$

where A, is the model parameter, L is the distance along the pipe length, and L_0 is the characteristic length to describe the effect of inhibitor. The effect of continuous inhibitor injection on corrosion in multiphase flow system was examined by Erickson *et al.* (1993). Their modeling showed that the inhibitor effectiveness in a condensate pipeline is a complex function of gas and liquid flow rate and pipeline elevation profile. However, they made a general observation that increasing condensation occurs as a function of distance away from the inlet end. Because the inhibitor does not partition to the condensed phase, the concentration of inhibitor decreases as the liquid flow increases due to condensation. The result is that the inhibitor effectiveness decreases as a function of distance away from the inlet end. The decay distance is a function of condensation and gas flow rates.

Water Accumulation

Flow in wet gas pipelines can be classified into four major types: (i) bubble flow occurs in the form of gas bubbles in a continuous liquid phase when the gas volume is low, (ii) annular flow occurs at high gas velocities in the form of a liquid layer contacting pipe wall and a gas core, (iii) slug flow occurs in the form of pockets of liquid followed by pockets of gas, and (iv) stratified flow occurs in the form of a liquid layer at the bottom of the pipe with oil or gas flowing above it. In the case of stratified flow, the shear stress between the liquid-vapor interfaces provides the mechanism for water to flow from one location to another along the pipe length. However, if the pipeline inclination angle is greater than the critical angle then water is assumed to accumulate. Water formation

occurs at all angles greater than critical angle because the shear stress is no longer sufficient to overcome gravity (Burwell *et al.*, 2004). The critical angle α is given by:

$$\alpha = \sin^{-1}\left(\frac{F\rho_g V_g^2}{(\rho_l - \rho_g)gD_i}\right) \tag{6-6}$$

where

$$V_g = \frac{4H_P}{\pi D_i^2}$$

$$H_p = \frac{S_p \times T \times Z \times 101325}{P \times 273}$$

$$\rho_g = \frac{P \times MW}{R \times T \times Z}$$

where F is the Froude number, ρ_g is the gas density in kg/m^3, V_g is the gas velocity in *m/s*, ρ_l is water density in kg/m^3, g is acceleration due to gravity in m/s^2, D_i is internal diameter of pipe in *mm*, H_p is high-pressure flow rate in m^3/s, S_p is flow rate at standard temperature and pressure m/s^2, Z is compressibility factor, MW is molecular weight of gas in $kg/mole$ and R is universal gas constant in $J/K/mole$. Typical values of these constants are given in Table 6-1.

Table 6-1: Typical wet gas pipeline flow parameters

Constant	Value
ρ_l	1000 kg/m^3
G	9.81 m/s^2
D_i	0.559 m
S_p	136.111 m/s^2
Z	0.83
MW	0.015 $kg/mole$
R	8.314 $J/K/mole$
Froude number, F	0.56 (θ>2 deg), 0.35 (θ <2 deg) 0.14θ +0.28 (0.5<θ<2 deg)
Pipe thickness	8.33 *mm*

Probabilistic Model

Corrosion Damage

The probability of corrosion damage at a specific location is the probability of corrosion depth exceeding a critical value times the probability that water is present at that location. The likelihood of water formation at a location is given by

$$P_w = P(\theta \geq \alpha) \tag{6-7}$$

where θ is inclination at a particular location. Figure 6-1 illustrates that there will always be some probability that the inclination angle will exceed the critical angle. The uncertain inclination angle arises from uncertainties in mapping measurements, cover depth and axial location (discussed later in the chapter). The uncertain critical angle arises from uncertainties in the flow velocity, pressure, temperature and pipe diameter. The corrosion probability at a location is calculated by using three candidate models

$$P_{cr} = P(a_{M1} \geq a_c)W_1 + P(a_{M2} \geq a_c)W_2 + P(a_{M3} \geq a_c)W_3 \tag{6-8}$$

Where $W_1 + W_2 + W_3 = 1$ and a_c is the critical corrosion depth, a_{Mi} is the corrosion depth predicted by i^{th} model, W_i is the weight factor for the i^{th} model, and $P(a_{Mi} \geq a_c)$ is the probability of exceeding the critical corrosion depth for the i^{th} model. For oil and gas lines the critical corrosion depth has been assumed to be 80% of wall thickness (Caleyo *et al.* 2002; Vinod *et al.,* 2003). The total corrosion probability at a location given that water is present at that location is given by

$$P_{tot} = P_w P_{cr} \tag{6-9}$$

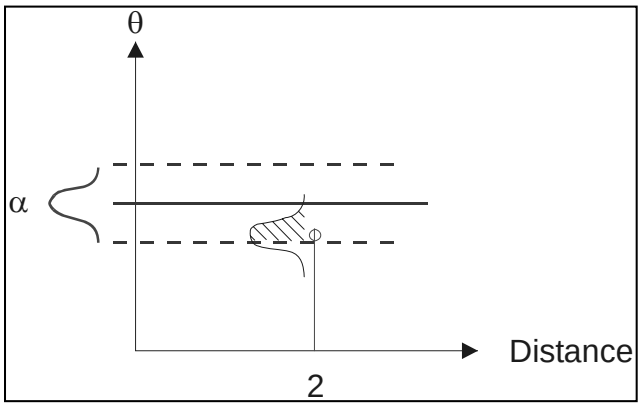

Figure 6-1: Uncertainty in inclination and critical angle

Input Uncertainties

Safety measures such as inspections and repairs are scheduled to reduce the chance of leaks and structural failure in face of uncertainties. These uncertainties include parameters affecting, for example, corrosion growth, and water flow and elevation data. These uncertainties should be accounted for by assessing the extent of corrosion damage at given location along pipe length and scheduling excavation and repairs. Probabilistic analysis can be used to account for randomness in these parameters. Table 6-2 presents random variables and their associated probability distributions for a demonstrative pipeline scenario.

Table 6-2: Typical wet gas pipeline corrosion growth parameters

Random variable (units)	Distribution type	Mean	Standard deviation
T (degree K)	Normal	289	28.9
% CO_2 (mole)	Lognormal	5	1
O_2 (ppm)	Lognormal	5000	1500
pH	Lognormal	6	1
% H_2S (mole)	Lognormal	0.05	0.005
P, (Pascal)	Lognormal	4080000	808000
k, Corrosion Model error	Lognormal	1.0	0.5
A, Inhibitor factor	Lognormal	1.0	0.5

Mapping Uncertainty

The uncertainty in pipeline inclination data occurs because of inaccuracies in elevation data present in digital maps and uncertainties in pipeline burial depth. The mapping inaccuracies are location specific and there is substantial evidence to suggest that it is positively correlated to the ruggedness of terrain (e.g., Holmes *et al.*, 2000; Riley *et al*., 1999; Sakude *et al*., 1988 and Tang *et al*., 2000). A linear equation between the terrain ruggedness index (TRI) and the accuracy in elevation can be obtained by a regression analysis on data from Tang *et al.* (2000) and Weng (2002) used the USGS database to obtain the maximum error of 11 meters and minimum error of three meters in the elevation data obtained from digital maps. The elevation data is used to calculate the terrain ruggedness index (this is the root mean square error between the elevation at a location and eight neighboring locations) for each location along the pipe. The regression equation developed above was used to obtain an estimate of elevation error at each location. The following equations are used

$$TRI = \sqrt{\frac{\sum_{j=i-4}^{j=i+4} \left(y_i - y_j\right)^2}{8}} \tag{6-10}$$

$$\varepsilon_y = C_1 \times TRI + C_2 \tag{6-11}$$

where TRI is terrain ruggedness index, ε_y is the error in elevation, and C_1 and C_2 are regression constants, y_i is the location at which *TRI* is to be determined and y_j's are adjacent locations around y_i. The error ε_y is used to calculate maximum and minimum inclination angles at these locations. We further assume that the inclination angle follows

a normal distribution with a 6σ range between the maximum and minimum inclination angles (this was chosen to capture the majority of the data).

Inspection Updating

There will be uncertainty in our initial prediction because of lack of accurate information on model weights, physics considered (or neglected) in competing models, and the assumed distribution of random variables. Data collected from inspections can be used to update the reliability estimate. Bayesian updating provides a systematic method for incorporating measured data with prior information to estimate future outcome (e.g., Rajasankar *et al*., 2003; Simola and Pulkkinen, 1998; and Zhang and Mahadevan, 2001). The underlying assumption in the approach taken is that the correct form of the corrosion rate model is unknown. Consequently, and as a demonstration of the methodology, three candidate models are considered. Based on inspection data, the weight factors are adjusted to reflect this additional information in the next prediction. We have used the reliability-updating model developed by Zhang and Mahadevan (2001). We further assume that there is no uncertainty in the detection process so that the detected damage is the actual damage at a location. The event of damage detected with size a_d is expressed as

$$D_A = a_{M_i} - a_d \tag{6-12}$$

where a_{M_i} is the corrosion depth predicted by i[th] model at the most probable point (MPP). The updated model weight and reliability in the event of a detected corrosion depth a_d can be expressed as

$$W_i \mid D_A = \frac{W_i \times \dfrac{\partial P_i\left(a_{M_i} - a_d \le 0\right)}{\partial a_{M_i}}\Big|_{a_{M_i}=a_d}}{\sum_{i=1}^{3} W_i \times \dfrac{\partial P_i\left(a_{M_i} - a_d \le 0\right)}{\partial a_{M_i}}\Big|_{a_{M_i}=a_d}} \tag{6-13}$$

$$P_{Updated} = \sum_{i=1}^{3} \frac{\dfrac{\partial P_i\left(a_{M_i} \geq a_c \cap a_{M_i} - a_d \leq 0\right)}{\partial a_{M_i}}\Big|_{a_{M_i}=a_d}}{\dfrac{\partial P_i\left(a_{M_i} - a_d \leq 0\right)}{\partial a_{M_i}}\Big|_{a_{M_i}=a_d}} \tag{6-12}$$

Equations 6-13 and 6-14 are solved numerically. Note that the updating only affects the component weighting of the component models. No adjustment to the probability distribution of the component models is performed.

Example 1: Determination of Critical Location Prior to Inspection

A typical gas transmission pipeline was chosen for demonstrating the proposed methodology. The pipeline elevation data at 1000 locations was used to calculate the inclination angles and the associated uncertainties in them using Equations 6-10 and 6-11. These are actual elevation data from which company-specific geographic information has been removed. The probability of water formation is obtained from Equation 6-7 and the probability of corrosion damage is obtained from Equation 6-8 using inputs in Tables 6-1 and 6-2 after a time period of 10 years. As a first illustration, we demonstrate the methodology by calculating the corrosion probability at each of the 1,000 locations. Since no information about pipeline corrosion is available in the beginning, we assume that all corrosion models represent corrosion growth in the pipeline with equal probability so that the model weights of each corrosion model in Equation 6-8 are 1/3. Figure 6-2 shows that the probability of water formation is at a maximum at location 971. Figure 6-3 shows that the probability of corrosion depth exceeding critical depth increases monotonically with pipe length. This is because the corrosion inhibitor reduces the corrosion rate in the beginning and its effectiveness diminishes with pipe length.

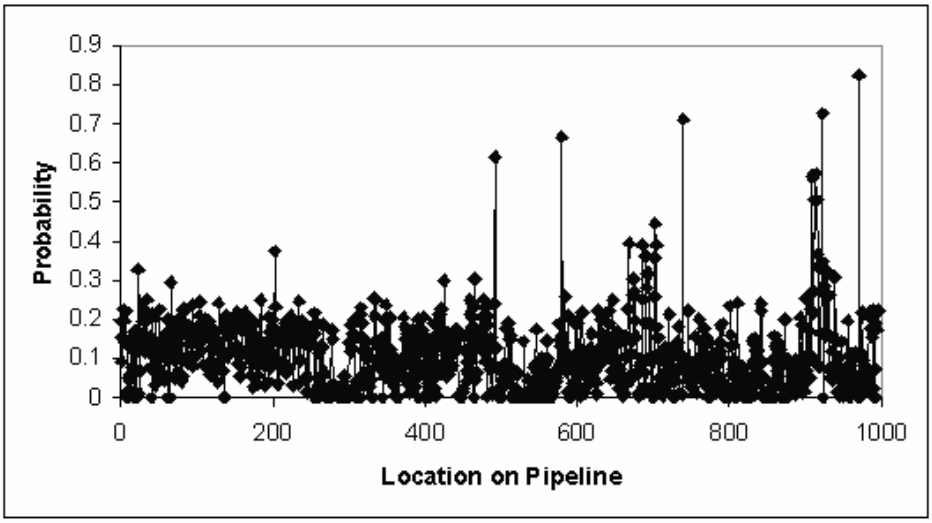

Figure 6-2: Probability of water formation along pipe length with highest probability observed at location 971

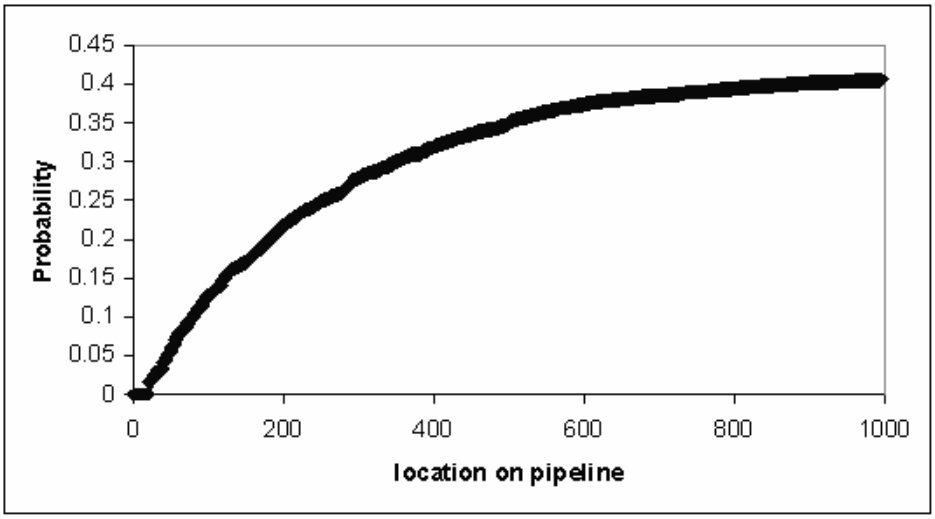

Figure 6-3: Probability of corrosion depth exceeding critical depth along pipe length assuming water is present at all locations

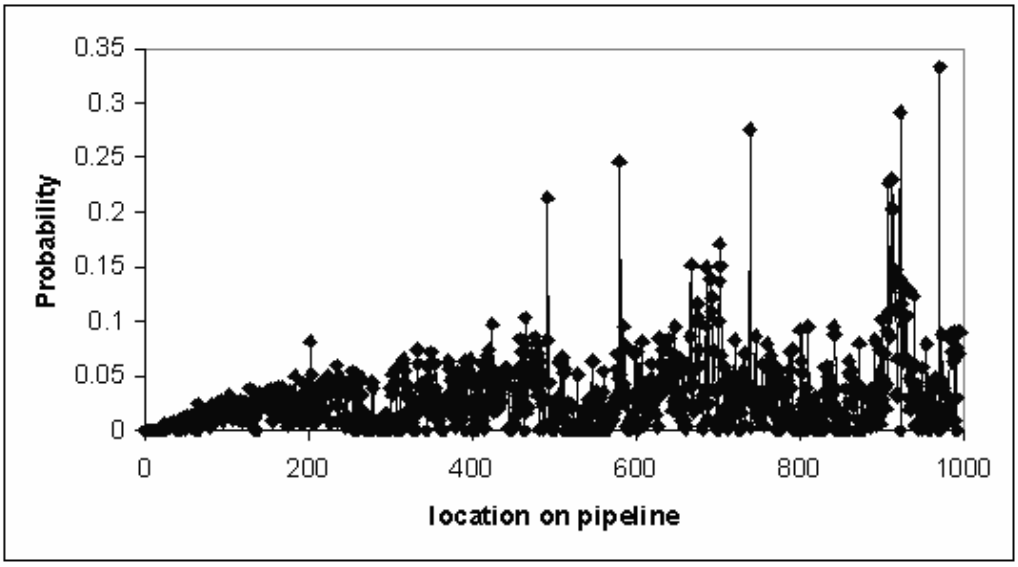

Figure 6-4: Total probability of corrosion exceeding critical depth along pipe length

As we can see from Figure 6-4, the probability of corrosion is maximum at location 971 (highest probability of water formation and far from the corrosion inhibitor injection). Consequently excavation and inspection is recommended at this location.

Example 2: Updating Corrosion Modeling with Inspection Data

In Example 1, three different corrosion models with equal model weights were used because there is no information regarding the accuracy of individual model prediction in a typical pipeline setting. The DM and DL models (derived for production systems) estimate corrosion rates that are higher than those obtained from the SwRI model. Also each model is based on different uncertain parameters. Inspections can be done to repair the damaged part of a pipeline with the data collected subsequently utilized with Bayesian analysis technique to improve reliability estimates. As more information from inspections becomes available, accuracy should improve as the most appropriate model or weighting of the three models is modified from the initial prediction. An example of the updating process is provided in Table 6-3 to show how several observations affect the model weights.

Table 6-3: Updating of model weights given assumed observations corresponding to input component models

Observed corrosion depth, *mm*	Observation derived from	Model weight W1 (DM)	Model weight W2 (DL)	Model weight W3 (SwRI)
0.05	SwRI	0.104	0.104	0.792
0.07	SwRI	0.019	0.019	0.962
0.11	SwRI	0.003	0.003	0.994
0.13	SwRI	0.0003	0.0003	0.9994
5.12	DM	0.500	0.500	0.000

The observations were made so that they corresponded to either the SwRI model (first four samples) or the DM model (last sample) at a given location. The analysis began with an equal weighting of 0.3333 for all three models. For the first four observations derived from the SwRI corrosion model, it is clear that the model weights rapidly approach 0.0 for both the DM and DL models while the SwRI goes to 1.0. The reason for this is the large disparity in the predictions between the competing models resulting from the differing intended applications for each model. The last observation corresponds to the DM model and there is no gradual transition in the weight factors. The reason for this is the probability associated with the SwRI model generating a 5.12 *mm* crack are exceptionally small compared to DM and DL. As such, the Bayesian updating immediately removes the SwRI model from active consideration in order to reflect the latest observation. Since the DM and DL models are equivalent for the conditions being considered, their corresponding weights each go to 0.50.

Typically pipelines are hundreds of miles long and excavating the entire length is impractical and uneconomical. Excavations can be scheduled at locations where the probability of corrosion is highest. Data obtained from each excavation can be used to update the reliability along the pipe length and to predict the next excavation location. This can continue until a specified level of reliability at each location on the pipeline is

obtained. Here we assume that if corrosion is detected at a location, it is repaired or replaced such that the location becomes defect free.

Table 6-4 shows the results of a series of inspections and model updates. Only a few locations are illustrated in the table. Additionally, the method outlined below is one approach for updating. Depending on the inspection methods and procedures, other types of updating can be performed. In the illustrative example shown in Table 6-4, the following sequences of steps are performed

(1) Before any inspections are performed, location 971 is predicted to have the highest probability with other locations up and downstream from it having a lower probability of corrosion exceeding certain depth.

(2) An inspection at location 971 is performed and the depth of corrosion is found to be 8.2 mm. Based on the predicted and detected corrosion depth at location 971, the model is updated and the next location of maximum probability is predicted to be location 923.

(3) An inspection is then performed at location 923, a defect depth of 7.5 mm is measured. This is then compared to model prediction and the model updated again. This updating then modifies the probabilities of corrosion downstream and upstream from this location.

(4) This process is repeated at the next highest probability location until all the highest probability locations upstream and downstream from 739 are inspected. Note that as the model is updated based on inspections, the previously inspected location probabilities will change. However, since they would have been

inspected already and mitigation measures adopted, the purpose of this assessment is considered to be fulfilled.

Table 6-4: Inspection locations along pipeline

Location of inspection	Detected corrosion depth (*mm*)	Maximum updated probability	Location of maximum updated probability
971	8.2	0.7247	923
923	7.5	0.7100	739
739	5.1	0.6662	580
⋮	⋮	⋮	⋮

Note that updating procedure may be modified to suite individual pipeline needs. Furthermore, modeling and updating may be adopted such that a certain proportion of pipeline is inspected in detail and downstream from these inspections, the updated model is used for locating further examinations.

Summary

A preliminary methodology to predict the most probable corrosion damage location along a pipeline and update this prediction using inspection data has been developed. The approach computes the probability of critical corrosion damage as a function of location along the pipeline using physical models for flow, corrosion rate, and inspection information as well as uncertainties in elevation data, pipeline geometry and flow characteristics. The probability of corrosion damage is computed as the probability that the corrosion depth exceeds a critical depth given the presence of electrolytes such as water. Water is assumed to be present at locations where the pipeline inclination angle is greater than the critical angle. Three candidate corrosion rate models were employed to reduce the chance of selecting the incorrect model. Monte Carlo simulation and the first-order reliability method (FORM) implemented in a spreadsheet model was used to perform the probability integration. Bayesian updating was used to incorporate inspection

information (e.g., in-line, excavation, etc.) and update the prediction of most probable damage location. This provides a systematic method for focusing costly inspections on only those locations with a high probability of damage and incorporating the results of the inspection in a manner that improves confidence in future predictions.

CHAPTER 7
CONCLUSIONS

The primary objective of this dissertation was to demonstrate the advantage of simultaneous design optimization of structure and inspection schedule. There is uncertainty in structural failure because of randomness in geometry, material properties, and loading. These uncertainties are readily incorporated into the design process by using statistical distributions and reliability methods. Here a methodology for cost optimal reliability-based structural design and inspection planning of aircraft structures subjected to fatigue damage growth was developed. An optimization problem was formulated to minimize the expected lifetime cost while maintaining a minimum acceptable reliability level. The effect of the structural design and the inspection schedule on the operational cost and reliability was explored. Calculating structural reliability in presence of inspection is computationally challenging because distribution of some of the parameters has to be updated after each inspection to simulate replacement. Exact evaluation using Monte Carlo simulation is time consuming because large sample size is required for estimating low probability of failure accurately. In this dissertation an approximate method using a combination of Monte Carlo simulations (MCS) and first-order reliability method (FORM) to expedite reliability calculations was presented. This method was used to perform combined optimization of structural design and inspection schedule of aircraft structures. The study led to the following conclusions

(1) The multiple safety measures used to design structure for stable fatigue crack growth lead to heavy design for structures designed using safe-life criterion.

(2) Large variability associated with estimating fatigue life reduces the effectiveness of safety measures. Safety measures are also more effective for fail-safe design than safe-life design. For the same reason certification tests are not very effective in improving reliability. Certification tests can be made more effective by reducing variability in crack sizes.

(3) Even if only their effect on fatigue is considered, inspections are cost effective in maintaining reliability levels through damage detection and replacement. From our examples, there was 25 % in lifetime cost due to inspections over a design without any inspections. Their advantages for detecting other types of damage, such as that due to corrosion, tool drops, and accidental impact, only add to their usefulness. As fuel cost rise, additional inspections become profitable and improvement in inspection effectiveness also makes them more attractive.

(4) Combined optimization of structural weight and inspection reduces the lifetime cost penalty associated with single type of inspection, thus allowing possible simplification of the inspection regime. When inspections are scheduled after the structure has been designed, mixture of inspection types may lead to additional cost savings.

(5) Designing structures for multiple load transfer capability (that is stiffened panels) can be much more cost effective and failure resistant than single load path when structure is designed without any inspections, however with inspections there is much lower gain from stiffeners.

(6) The variability associated with location and severity of corrosion damage in pipelines makes probabilistic design suitable for predicting location of maximum

damage in pipeline. Inspections are scheduled at locations of maximum probability of failure and results from inspections are used to update corrosion probabilities.

The methodology presented in this dissertation eases the computational burden associated with calculation of low failure probabilities. However this method suffers from the fact that probability distribution in the tail region is poorly approximated because only the mean and standard deviations are estimated. An alternative method is to use extreme value distributions (EVD's) to estimate the tail region of probability distribution and use it directly in reliability analysis. The may lead to more accurate reliability computations at slightly higher computational expense. The use of importance sampling to reduce the sample size of MCS may be helpful in reducing the computational expense.

The through the thickness crack model assumed in this work represents the worst case scenario and was chosen to demonstrate that inspections are cost effective for the worst case. Actual cracks present at the time of initiation may have different configurations but will finally evolve into a through the thickness crack. The methodology presented in this dissertation can be applied to different crack growth models. Furthermore, a simple structural design with constant amplitude loading is considered (fuselage) to facilitate the demonstration of the proposed reliability method. For structures with variable amplitude loading like wing panels, detailed load history effects can be included by using cycle counting techniques in combination with crack growth acceleration and retardation models.

APPENDIX A
DISPLACEMENT COMPATIBILITY ANALYSIS FOR CALCULATION OF STRESS INTENSITY OF STIFFENED PANEL

Introduction

This appendix presents detailed explanation and clarification of the displacement compatibility method developed by Swift (1984) to facilitate easy implementation and also serves as errata for printing errors in the original paper. These errors were corrected from private communication with the author. The figures and equations presented in this chapter have been extracted with permission from special technical publication STP 842, Damage Tolerance of Metallic Structures, Analysis Methods and Applications, copyright ASTM International, 100 Barr Harbor Drive, West Conshohocken, PA, 19428

As the crack propagates in a stiffened panel, load is transferred from the skin to the intact stiffeners by means of fasteners. The stress intensity factor at the crack tip can be obtained by displacement compatibility analysis. In this method the displacement in the cracked sheet at fastener location are made equal to the stiffener plus fastener displacement. The effect of stiffening is measured by the geometric factor ψ which is the ratio of stress intensity factor with stiffening to that without stiffening.

To demonstrate the application of the displacement compatibility analysis we consider a center cracked stiffened panel as shown in Figure A-1 with two intact stiffeners placed symmetrically across from crack center line and a broken stiffener along the crack centerline (y-axis). This is a typical example of a two bay crack with centre broken stiffener used to certify aircraft for damage tolerance.

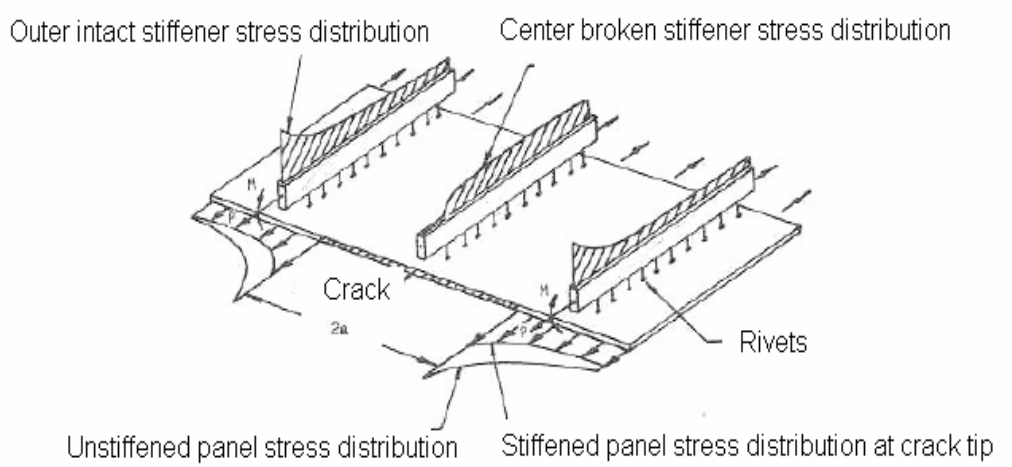

Figure A-1: Half-geometry of a center cracked stiffened panel with a central broken stiffener and two intact stiffeners placed symmetrically across from crack

Displacement Compatibility Method

The stress intensity factor at the crack tip of a stiffened panel is lower than that on an unstiffened panel because of the reduced stresses at the crack tip as shown in Figure A-1. The panel is assumed to be in a state of plane stress and the stiffeners are assumed to be one dimensional rods placed symmetrically across the crack with one broken stiffener along the crack centerline. The displacements[§§§] in the panel at fastener locations are obtained by superposition of five cases shown in Figure A-2.

(1) V_1, the displacement anywhere in the cracked sheet caused by the applied gross stress.

(2) V_2, the displacement in the uncracked sheet resulting from fastener loads, F.

(3) V_3, the displacement in the uncracked sheet resulting from broken fastener loads, P.

[§§§] The highlighted text in this appendix is different from original paper. The additional details were obtained from private communication with the author of the paper.

(4) V_4, the displacement in the cracked sheet resulting from stress applied to the crack face equal and opposite to the stresses caused by rivet loads.

(5) Stiffener displacement at location y_i resulting from direct fastener load.

The total number of fasteners on a single stiffener is *2n* equally distributed on either side of crack. Using symmetry we need to solve for fastener forces only in a quarter of the panel. For solving the matrix equation for fastener forces we number the index of fastener on central broken stiffener from *1* through *n* and those on intact stiffener from *n+1* through 2*n*.

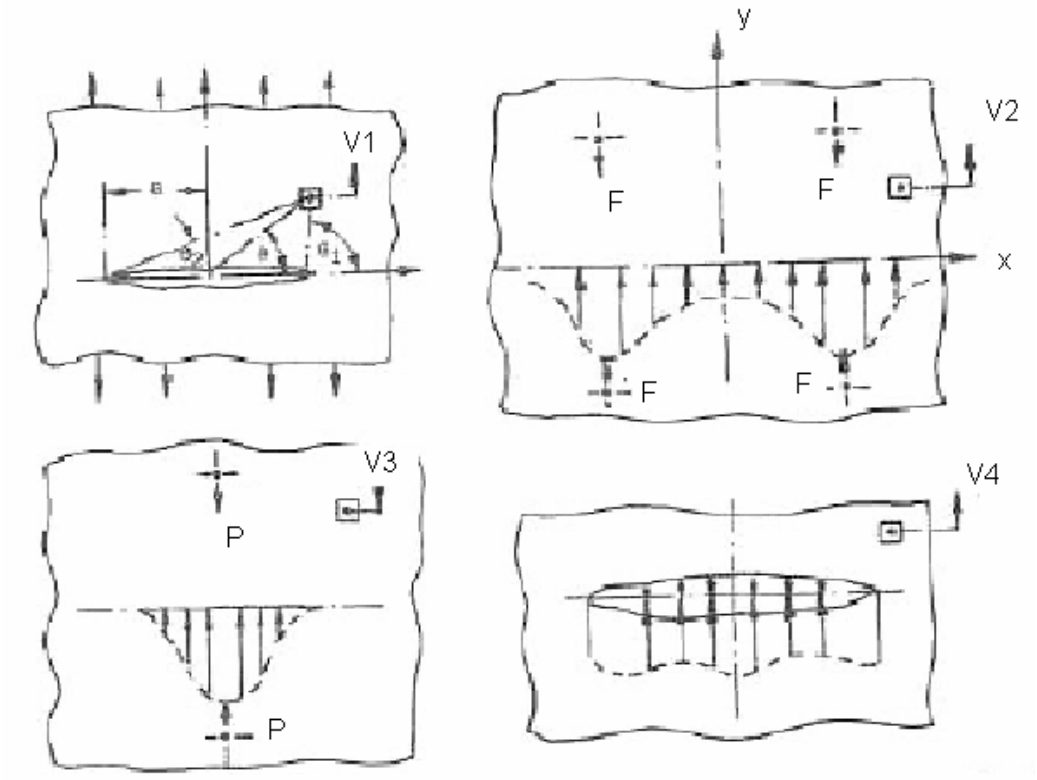

Figure A-2: Description of applied stress and resulting fastener forces and induced stress on stiffened panel

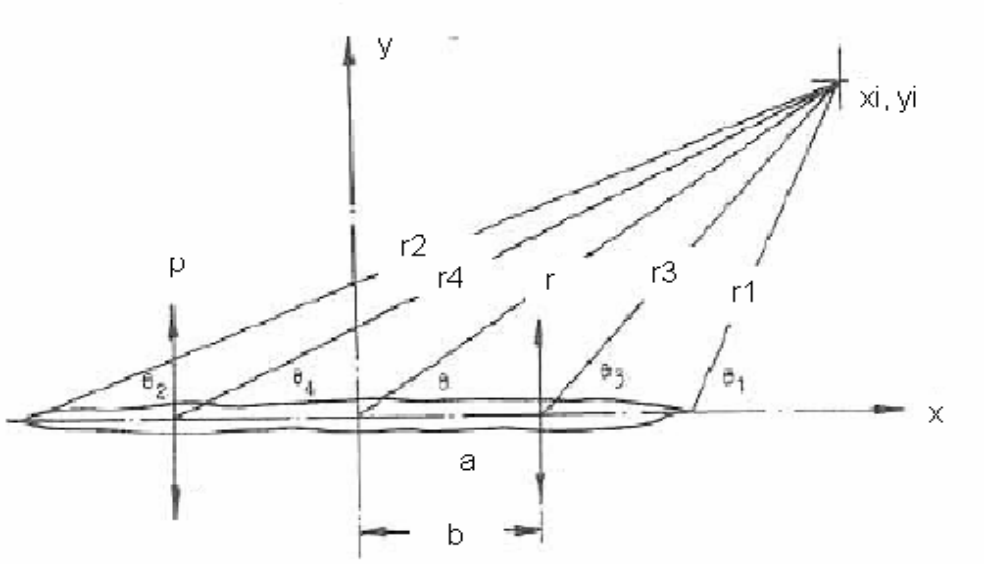

Figure A-3: Description of position coordinate of forces and displacement location with respect to crack centerline as *y* axis

where the variables are defined in nomenclature. Figure A-2 shows the displacement due to gross stress V_1, displacements due to concentrated fastener forces V_2 and V_3 and displacement due to stress at the crack tip.

Displacement V_1

The displacement at any location (*x, y*) in the cracked sheet resulting from overall gross stress can be determined using Westregaard's stress function (Westergaard, 1939) below

$$V_1 = \frac{\sigma}{E}\left[2\sqrt{r_1 r_2}\,\sin\left(\frac{\theta_1+\theta_2}{2}\right) - \frac{(1+v)yr\left[\cos\left(\theta-\frac{\theta_1}{2}-\frac{\theta_2}{2}\right)\right]}{\sqrt{r_1 r_2}} + vy \right] \qquad \text{(A-1)}$$

The variables as shown in Figures A-2 and A-3 are measured from the coordinate (x_i, y_i) of the point at which displacement is measured.

Displacement V_2 and V_3

The stress distribution anywhere in and infinite plate resulting from a concentrated force *F* can be determined from work of Love (1944). The displacement at any location (*x*, *y*) due to a concentrated force can be obtained as

$$V_F = \frac{F(1+\nu)}{4\pi tE}\left[\frac{3-\nu}{2}\log\left(x^2+y^2\right)+\frac{(1+\nu)x^2}{\left(x^2+y^2\right)}\right]+C \qquad \text{(A-2)}$$

where *x, y* is measured from point of application of force and *C* is a constant. Superposing the displacement due to four rivet load placed symmetrically opposite of the crack centerline the resulting displacement can be obtained as follows (the constant *C* cancels out)

$$V_2(x_i,y_i,x_j,y_j)=\frac{F(1+\nu)(3-\nu)}{16\pi Et}\left\{\begin{array}{l}(X_A+1)\log\left[\frac{(X_A+1)^2+Y_A^2}{(X_A+1)^2+Y_B^2}\right]-(X_A-1)\log\left[\frac{(X_A-1)^2+Y_A^2}{(X_A-1)^2+Y_B^2}\right]+\\(X_B+1)\log\left[\frac{(X_B+1)^2+Y_A^2}{(X_B+1)^2+Y_B^2}\right]-(X_B-1)\log\left[\frac{(X_B-1)^2+Y_A^2}{(X_B-1)^2+Y_B^2}\right]\\+4\left(\frac{1-\nu}{3-\nu}\right)\left[\begin{array}{l}Y_A\tan^{-1}\left(\frac{2Y_A}{Y_A^2+X_A^2-1}\right)+Y_A\tan^{-1}\left(\frac{2Y_A}{Y_A^2+X_B^2-1}\right)-\\Y_B\tan^{-1}\left(\frac{2Y_B}{Y_B^2+X_B^2-1}\right)-Y_B\tan^{-1}\left(\frac{2Y_B}{Y_B^2+X_A^2-1}\right)\end{array}\right]\end{array}\right\} \qquad \text{(A3-1)}$$

for the central broken stiffener, superposition of the two rivet forces placed symmetrically opposite of the crack centerline we get

$$V_3(x_i,y_i,x_j,y_j)=\frac{P(1+\nu)(3-\nu)}{16\pi Et}\left\{\begin{array}{l}(X_A+1)\log\left[\frac{(X_A+1)^2+Y_A^2}{(X_A+1)^2+Y_B^2}\right]-(X_A-1)\log\left[\frac{(X_A-1)^2+Y_A^2}{(X_A-1)^2+Y_B^2}\right]\\+4\left(\frac{1-\nu}{3-\nu}\right)\left[Y_A\tan^{-1}\left(\frac{2Y_A}{Y_A^2+X_A^2-1}\right)-Y_B\tan^{-1}\left(\frac{2Y_B}{Y_B^2+X_A^2-1}\right)\right]\end{array}\right\} \qquad \text{(A3-2)}$$

where

$$X_A = \left(\frac{2}{d}\right)(x_i - x_j),\ X_B = \left(\frac{2}{d}\right)(x_i + x_j),\ Y_A = \left(\frac{2}{d}\right)(y_i - y_j),\ Y_B = \left(\frac{2}{d}\right)(y_i + y_j)$$

the i^{th} term is the point at which displacement is required and the j^{th} term represents coordinates of the forces.

Displacement V_4

The displacements due to concentrated point forces at the rivets induce stresses along the crack length. The displacement in the cracked sheet resulting from this stress distribution is given as

$$V_4 = -\left[(1+\nu)\frac{y_j}{2\pi^2 Et}\right]\left[F_j\int_0^a \alpha(x_j, y_j, b)\varepsilon(x_i, y_i, b)db + P_j\int_0^a \alpha(x_j, y_j, b)\varepsilon(x_i, y_i, b)db\right] \quad \text{(A-4)}$$

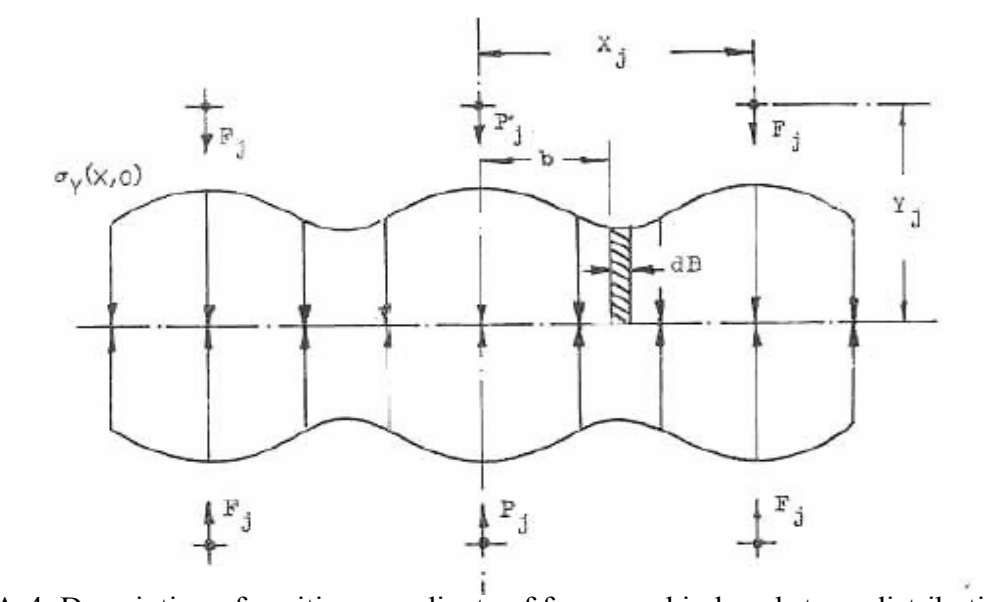

Figure A-4: Description of position coordinate of forces and induced stress distribution along the crack length

$$\alpha(x_j, y_j, b) = \left(\frac{3+\nu}{1+\nu}\right)\left[\frac{1}{(b-x_j)^2 + y_j^2} + \frac{1}{(b+x_j)^2 + y_j^2}\right] - \frac{2(b-x_j)^2}{\left[(b-x_j)^2 + y_j^2\right]^2} - \frac{2(b+x_j)^2}{\left[(b+x_j)^2 + y_j^2\right]^2} \quad \text{(A-5)}$$

$$\varepsilon\left(x_i, y_j, b, a\right) = \log\left[\frac{\left(a^2 - b^2\right) + \left(a^2 - b^2\right)^{0.5}\left(B_1C_1 + A_1D_1\right) + r_1r_2}{\left(a^2 - b^2\right) - \left(a^2 - b^2\right)^{0.5}\left(B_1C_1 + A_1D_1\right) + r_1r_2}\right]$$
$$- \frac{y_i(1+\nu)\left(a^2 - b^2\right)^{0.5}}{r_1r_2r_3^2r_4^2}\left\{\begin{array}{l}\left(x_i^2 - b^2 - y_i^2\right)\left[\begin{array}{l}x_i\left(A_1C_1 - B_1D_1\right) + \\ y_i\left(B_1C_1 + A_1D_1\right)\end{array}\right] \\ -2x_iy_i\left[\begin{array}{l}x_i\left(B_1C_1 + A_1D_1\right) - \\ y_i\left(A_1C_1 + B_1D_1\right)\end{array}\right]\end{array}\right\} \quad \text{(A-6)}$$

and $A_1 = \left(r_1 + x_i - a\right)^{0.5}, B_1 = \left(r_1 - x_i + a\right)^{0.5}, C_1 = \left(r_2 + x_i + a\right)^{0.5}, D_1 = \left(r_2 - x_i + a\right)^{0.5}$

the highlighted text in this appendix is different from original paper. The additional details were obtained from private communication with the author of the paper.

Intact Stiffener Displacement

The outer stiffener is assumed to be supported on three frames running normal to the stiffeners. The center frame is on the skin crack centerline. Stiffener extension at the fastener shear face is determined because of axial loads and bending from fastener loads and direct loads resulting from axial stresses. Stiffener bending is induced since the fastener shear faces are offset from the stiffener neutral axis. The average bending moment between each fastener, obtained through the use of the three moment equation is given by

$$M_{A_i} = \sum_{j=i}^{j=2n} CF_j - \left[\frac{3C}{2L^3}\sum_{j=n+1}^{j=2n} F_j\left(2Ly_j - y_j^2\right)\right]\left[L - \frac{y_{i-1} + y_i}{2}\right] \quad \text{(A-7)}$$

stiffener displacement caused by bending from fastener loads is given by

$$\delta_{M_i} = \frac{C}{EI}\sum_{i=n+1}^{i=i} M_{A_i}\left(y_i - y_{i-1}\right) \quad \text{(A-8)}$$

stiffener displacement caused by direct fastener loads is given by

$$\delta_{D_i} = \frac{1}{AE}\sum_{j=n+1}^{j=i} F_j y_j + \frac{y_i}{AE}\sum_{j=i+1}^{j=2n} F_j \quad \text{(A-9)}$$

stiffener displacement resulting from gross stress is given by

$$\delta_{G_i} = \frac{\sigma y_i}{E} \tag{A-10}$$

Broken Stiffener Displacement

The broken stiffener is supported at the frames that pass across the center of the panel along the crack length and at the edge of the stiffeners. Since the fasteners are not located at the neutral axis of the stiffeners there will be displacement due to bending moment also. The average bending moment between each fastener is given by

$$M_{A_i} = \sum_{j=1}^{j=i} CP_j - \left[\frac{C}{L}\sum_{j=1}^{j=n} P_j\left(\frac{5}{4} - \frac{3y_j^2}{4L^2}\right)\right]\left[\frac{y_{i+1} + y_i}{2}\right] \tag{A-11}$$

stiffener displacement resulting from bending from fastener loads is given by

$$\delta_{M_i} = \frac{C}{EI}\sum_{i=i}^{i=n-1} M_{A_i}\left(y_{i+1} - y_i\right) \tag{A-12}$$

stiffener displacement resulting from direct load is given by

$$\delta_{D_i} = \frac{1}{AE}\left(y_n - y_i\right)\sum_{j=1}^{j=i} P_j + \frac{1}{AE}\sum_{j=i+1}^{j=n-1} P_j\left(y_n - y_j\right) \tag{A-13}$$

Fastener Displacement

The elastic displacement in shear can be represented by the empirical relation

$$\delta_R = \frac{F}{ED}\left[H_1 + H_2\left(\frac{D}{t_1} + \frac{D}{t_2}\right)\right] \tag{A-14}$$

where the symbols are defined in nomenclature and the parameters for aluminum and steel are given below.

H_1: 5.0 for aluminum and 1.666 for steel fasteners

H_2: 0.8 for aluminum and 0.86 for steel fasteners

Compatibility of Displacements

For displacement compatibility the total skin displacement at any fastener location should be equal to the stiffener plus fastener displacement at that location. This gives 2*n*

by 2*n* matrix equation to be solved for unknown fastener forces. For central broken stiffener, the center of the stiffener undergoes displacement, so we fix the n^{th} fastener on this stiffener as datum and subtract the displacement at the n^{th} location from displacements at all the other fasteners on this stiffener. The compatibility equation is given by

$$\begin{aligned}
&\sum_{j=n+1}^{j=2n} F_j\left[v_2\left(x_n, y_n, x_j, y_j\right) - \frac{(1+\nu) y_j}{2\pi^2 Et} \int_0^a \alpha\left(x_j, y_j, b\right) \varepsilon\left(x_i, y_i, b\right) db \right] \\
&- \sum_{j=1}^{j=n} P_j\left[v_3\left(x_n, y_n, x_j, y_j\right) - \frac{(1+\nu) y_j}{2\pi^2 Et} \int_0^a \alpha\left(x_j, y_j, b\right) \varepsilon\left(x_i, y_i, b\right) db \right] \\
&+ \delta R_n - \delta D_i - \delta M_i - \delta R_i \\
&- \sum_{j=n+1}^{j=2n} F_j\left[v_2\left(x_i, y_i, x_j, y_j\right) - \frac{(1+\nu) y_j}{2\pi^2 Et} \int_0^a \alpha\left(x_j, y_j, b\right) \varepsilon\left(x_i, y_i, b\right) db \right] \\
&\sum_{j=1}^{j=n} P_j\left[v_3\left(x_i, y_i, x_j, y_j\right) - \frac{(1+\nu) y_j}{2\pi^2 Et} \int_0^a \alpha\left(x_j, y_j, b\right) \varepsilon\left(x_i, y_i, b\right) db \right] \\
&= \sigma V_1\left(x_i, y_i\right) - \sigma V_1\left(x_n, y_n\right)
\end{aligned} \tag{A-15}$$

Additional equation is obtained from the equilibrium of broken stiffener. The summation of fastener forces on the broken stiffener should be equal to the gross stress times the broken stiffener area.

$$\sum_{i=1}^{n} P_i = \sigma A_s \tag{A-16}$$

for outer intact stiffeners the datum is fixed at the center of stiffener since it does not undergo displacement.

$$\begin{aligned}
&\delta R_i + \delta D_i + \delta M_i \\
&- \sum_{j=n+1}^{j=2n} F_j\left[v_2\left(x_i, y_i, x_j, y_j\right) - \frac{(1+\nu) y_j}{2\pi^2 Et} \int_0^a \alpha\left(x_j, y_j, b\right) \varepsilon\left(x_i, y_i, b\right) db \right] \\
&\sum_{j=1}^{j=n} P_j\left[v_3\left(x_i, y_i, x_j, y_j\right) - \frac{(1+\nu) y_j}{2\pi^2 Et} \int_0^a \alpha\left(x_j, y_j, b\right) \varepsilon\left(x_i, y_i, b\right) db \right] \\
&= \sigma V_1\left(x_i, y_i\right) - \delta G_i
\end{aligned} \tag{A-17}$$

using Equations A-15 and A-16 for calculating displacement at *n* fasteners on the central broken stiffener and Equation A-17 for *n* fastener on outer intact stiffener 2*n* fastener forces are determined from 2*n* equations. The stress intensity factor due to equal and opposite pair of fastener forces placed symmetrically across the crack centerline (*x*-axis) is given as

$$K = \left(\frac{2Fy\sqrt{\pi a}}{\pi t}\right)\left[\left(\frac{3+\nu}{2}\right)I_1 - (1+\nu)I_2\right] \tag{A-18}$$

and the total stress intensity due to fastener forces is

$$K_F = \sum_{i=1}^{n}\left(\frac{2Py\sqrt{\pi a}}{\pi t}\right)\left[\left(\frac{3+\nu}{2}\right)I_1 - (1+\nu)I_2\right] + \sum_{i=n+1}^{2n}\left(\frac{2Fy\sqrt{\pi a}}{\pi t}\right)\left[\left(\frac{3+\nu}{2}\right)I_1 - (1+\nu)I_2\right] \tag{A-19}$$

where

$$I_1 = \frac{\beta}{y\left(\sqrt{\left(y^2+a^2-x^2\right)^2+4x^2y^2}\right)}$$

$$I_2 = \frac{\left[\left(a^2+x^2\right)y^2+\left(a^2-x^2\right)^2\right]\beta^2+x^2y^2\left(y^2-a^2+x^2\right)}{2y\beta\left[\left(y^2+a^2-x^2\right)^2+4x^2y^2\right]^{1.5}} \tag{A-20}$$

$$\beta = \frac{1}{\sqrt{2}}\left[\left(y^2+a^2-x^2\right)+\sqrt{\left(y^2+a^2-x^2\right)^2+4x^2y^2}\right]^{0.5}$$

The total stress intensity is obtained by superposition of stress intensity due to far field stress on an unstiffened plate, plus that due to each set of fasteners (paying attention to load direction. If a stiffener is broken then the fastener forces on that stiffener will be tensile otherwise for intact stiffener they are compressive).

$$K_{total} = K_F + \sigma\sqrt{\pi a} \tag{A-21}$$

The geometric factor ψ is the ratio of this stress intensity factor with stiffeners to that of an unstiffened panel. A complete description of procedure can be found in Swift (1984).

Effectiveness of Stiffeners in Reducing Crack Tip Stress Intensity

The effectiveness of stiffeners in reducing crack growth rate increases with stiffener area and decreases with stiffener spacing. If stiffener area is very small or stiffener spacing is very large compared to critical crack length, the effectiveness of stiffeners in reducing crack growth will be compromised. Stiffeners will however continue to be very effective in arresting cracks, besides they provide protection against buckling and pillowing effect due to bending loads in fuselage. To demonstrate this, the stress intensity $K = \psi\sigma\sqrt{\pi a}$ is plotted in Figure A-5 for unstiffened and stiffened panel made of 7075-T6 Aluminum alloy.

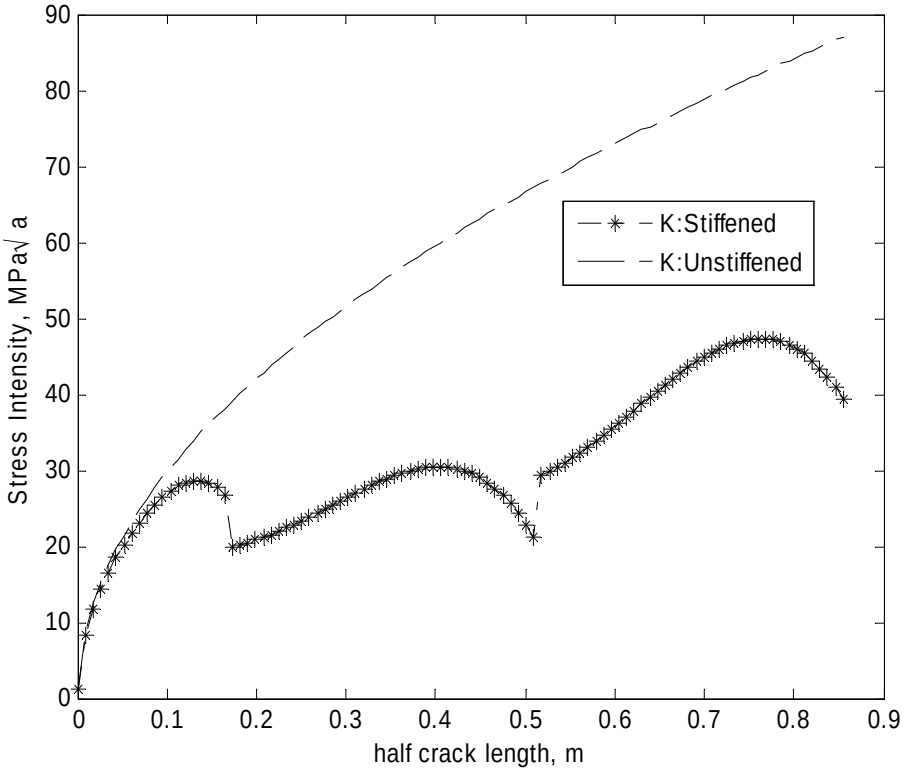

Figure A-5: Comparison of stress intensity factor for a panel with skin thickness = 2.34 *mm* and stiffener area of 2.30×10^{-3} *meter*^{2}

From Figure A-5 it can be seen that stiffeners have arrested the crack. The critical stress intensity factor for 7075-T6 aluminum is $36.58\,MPa\sqrt{meter}$. To demonstrate a case where stiffening will not be very effective we plot the stress intensity for another design in Figure A-6.

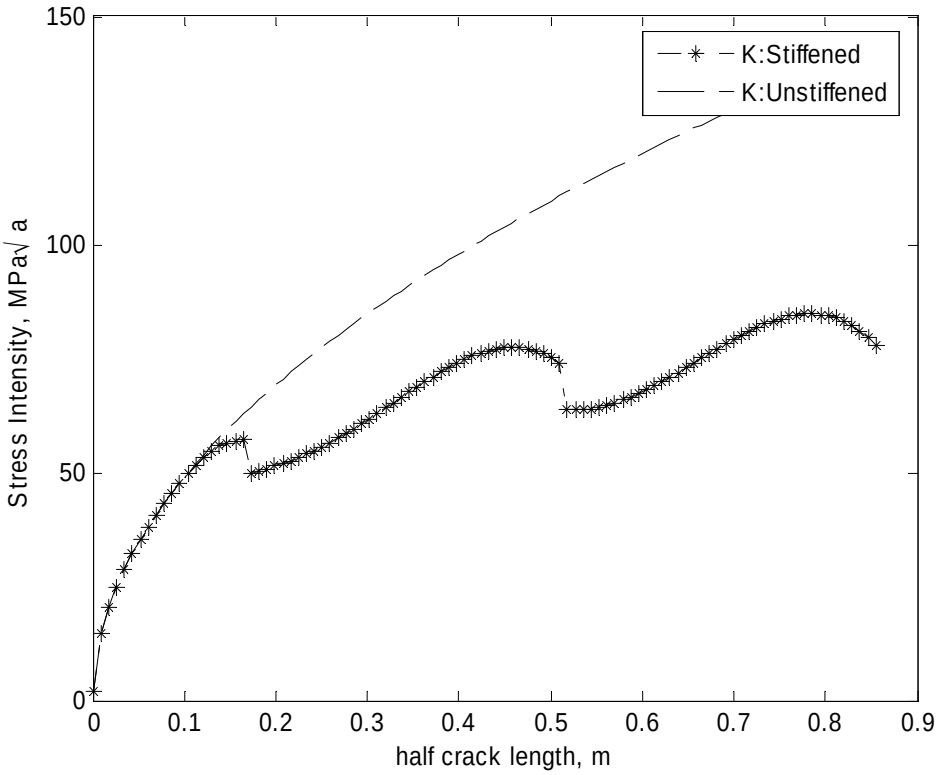

Figure A-6: Comparison of stress intensity factor for a panel with skin thickness = 1.81 *mm* and stiffener area of 7.30×10^{-4} $meter^2$

APPENDIX B
CALCULATING CRACK GROWTH FOR STIFFENED PANELS USING NUMERICAL INTEGRATION AND RESPONSE SURFACE

The main computational expense associated with reliability based design for fatigue cracking is that for most structural design problems there is no analytical expression to track crack size as a function of applied load cycles. Crack growth can only be determined using computationally intensive methods. For the stiffened panel design the number of fatigue cycles accumulated in growing a crack from initial size a_i to final size a_N can be obtained by integrating a crack growth rate equation f, between the initial crack a_i and final crack a_N. Alternatively, the final crack size a_N after N fatigue cycles can be determined by solving Equation B-1.

$$N = \int_{a_i}^{a_N} \frac{da}{f\left(\Delta K\left(\psi\right), m\right)} \tag{B-1}$$

where

a is crack length

f represents the crack growth rate function

m represents one or more material parameters depending on crack growth model

ΔK is the cyclic stress intensity range

ψ is the effect of structural geometry

Accurate numerical integration will require us to determine the stress intensity factor K at large number of integration points using detailed finite element analysis or displacement compatibility method (Appendix A), which is cost prohibitive.

To reduce the computational burden associated with evaluating the stress intensity factor we develop response surface approximations (RSA's) for the geometric factor due to stiffening (ψ). The geometric factor ψ accounts for the effect of stiffening and depends on crack length *a*, panel dimension, stiffener dimension and stiffener spacing. Stiffeners can break during crack growth if stiffener strength is exceeded thereby increasing the stress intensity factor. For accurate computation of ψ at each integration point (crack size), the state of the stiffeners (broken or intact) was also incorporated into the estimation of ψ by having four RSA's for each stiffener states.

Using symmetry, for a given crack length and stress, only the following are considered (a) all stiffeners intact (b) two inner stiffener broken (c) four inner stiffener broken (d) all stiffeners broken. Typical response curves for geometric factor ψ and stiffened panel dimensions are shown in Figure B-1. Calculating crack growth during the reliability based optimization can be extremely time consuming. To reduce the computational cost we use cubic response surface approximation (RSA) to estimate ψ at crack tip and maximum force on stiffener as a function of plate thickness, stiffener area and crack length.

A Latin hypercube design of experiments in these three variables with 600[****] sampling points is used (200 for each of the three regimes of crack length). To take into account the state of stiffener (broken or intact) in computing fatigue life, we first obtain the maximum number of stiffeners that could have been broken at the given state of

[****] To improve the accuracy of RSA's, three different approximations were obtained for each case above (a, b, c and d) for crack lengths between (1) center of plate to first stiffener (2) first stiffener to second stiffener (3) second stiffener to third stiffener. In all we have 12 RSA's for ψ and stiffener force. The original reason for the large number of points was to improve the accuracy of single cubic RSA that was fitted to the geometric factor curve in Figure B-1 in our previous paper (Kale *et al.,* 2005). With three individual RSA's accurate results can be achieved with fewer points. For example, with 150 sample points the error in the reliability index is of the order of 3%

structure (structural design, crack length). The maximum stress on each stiffener is then calculated using the three RSA's for maximum stress on each stiffener $F^{\max}_{FirstStiffener}$, $F^{\max}_{SecondStiffener}$, $F^{\max}_{ThirdStiffener}$. If this stress exceeds yield stress of material than the stiffener is broken. Depending on state of stiffener the appropriate RSA for ψ is used, e.g., if none of the stiffeners are broken than $\psi = \psi_{0\_broken}$ is used to estimate the stress intensity factor at that crack length.

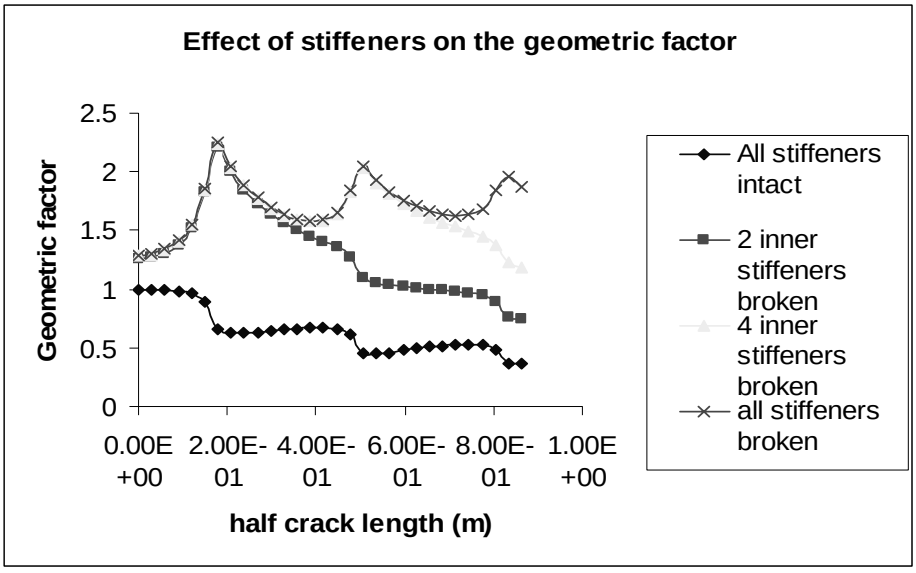

Figure B-1: Typical response curves for effect of stiffening on geometric factor ψ for a stiffener area of 1.5 mm^2 and skin thickness of 1.5 mm

APPENDIX C
ACCURACY ESTIMATES OF RESPONSE SURFACE APPROXIMATIONS

Response Surface Approximations for Geometric Factor ψ

The response surface approximation (RSA) for geometric factor ψ due to stiffening is obtained by first computing it for some selected design points in the domain using the displacement compatibility analysis. The design of experiments for fitting the RSA for ψ was obtained by constructing Latin hypercube design in three variables namely plate thickness, stiffener area and crack length with 600 sampling points and calculating ψ and stiffener forces at each point. A cubic equation is then fitted by minimizing the least square error between predicted and actual value.

To achieve accurate results we partition the design domain and construct several RSA's depending on structural design concept. For safe-life design without any inspections, the stiffener area and skin thickness will be higher than the inspection based design. Table C-1 shows the bounds on design variables used to construct the design of experiment for estimating ψ for safe-life design calculation. The bounds on stiffener area and skin thickness were obtained by successive windowing. Table C-2 show the error estimate for the RSA's used to approximate ψ and stiffener stress for safe-life design.

Table C-1: Bounds on design variables used to evaluate response surface approximation for safe life design (this design domain is used for calculating results in Table 3-10)

Design variable	Lower bound	Upper bound
Skin thickness	2.04 *mm*	4.08 *mm*
Stiffener area	1.5×10^{-3} $meter^2$	3.0×10^{-3} $meter^2$
Crack length	0.86 *meters*	0.1 *mm*

Table C-2: Error estimate of analysis response surfaces used to obtain safe-life stiffened panel design (these RSA's are used in crack growth calculations for safe-life design of stiffened panels in Table 3-10), ψ-RSA and F-RSA

Error estimates → Normalized values ↓	Typical value	e_{av}	e_{rms}	R^2	R^2_{adj}
ψ_{0_broken}	0.5 – 1.0	0.004,0.007, 0.006	0.006, 0.01, 0.009	0.95 , 0.95, 0.96	0.94, 0.94,0.96
ψ_{1_broken}	>1	0.006, 0.008, 0.007	0.009, 0.012, 0.01	0.98, 0.98, 0.91	0.97, 0.98, 0.90
ψ_{2_broken}	>1	0.006, 0.009, 0.01	0.009, 0.01, 0.014	0.98, 0.98, 0.97	0.97, 0.97, 0.98
ψ_{3_broken}	>1	0.006, 0.01, 0.01	0.009, 0.013, 0.012	0.98, 0.98, 0.97	0.98, 0.97, 0.97
$F^{\max}_{FirstStiffener}$	>1	0.009, 0.02,0.04	0.012, 0.03,0.05	0.99, 0.99,0.99	0.98, 0.99,0.99
$F^{\max}_{SecondStiffener}$	>1	0.002, 0.02, 0.04	0.004, 0.03, 0.05	0.99, 0.98, 0.99	0.99, 0.97, 0.99
$F^{\max}_{ThirdStiffener}$	>1	0.006,0.003, 0.04	0.008, 0.001, 0.05	0.99, 0.99, 0.97	0.99,0.99,0 .96

Since addition of inspections leads to reduction in structural sizes, we use closer bounds on the design of experiments to construct RSA for inspection based design. These bounds are shown in Table C-3. The upper bound on thickness is based on maximum possible plate thickness for unstiffened panel optimum with inspection (2.56 *mm* + thickness equivalent to cost of 3 inspections); bounds on stiffener area were reduced based on successive windowing. Table C-4 shows the error estimate of the RSA's.

Table C-3: Bounds on design variables used to evaluate response surface approximation for inspection based design. (This design domain is used to calculate results for inspection based design shown in Table 3-12 through 3-14)

Design variable	Lower bound	Upper bound
Skin thickness	1.0 *mm*	3.0 *mm*
Stiffener area	$3.0 \times 10^{-4}\ m^2$	$2.0 \times 10^{-3}\ m^2$
Crack length	0.86 *m*	0.1 *mm*

Table C-4: Error estimate of analysis response surfaces used to obtain inspection based stiffened panel design (these RSA's are used in crack growth calculations for inspection based design of stiffened panels in Table 3-12 through 3-14), ψ-RSA and F-RSA

Error estimates → Response↓	Nominal value	e_{av}	e_{rms}	R^2	R^2_{adj}
ψ_{0_broken}	0.5 – 1.0	0.004, 0.009, 0.008	0.007, 0.013, 0.011	0.96,0.95, 0.97	0.94, 0.94, 0.96
ψ_{1_broken}	>1	0.009, 0.011, 0.008	0.014, 0.016, 0.012	0.98, 0.98,0.93	0.98,0.98, 0.92
ψ_{2_broken}	>1	0.009, 0.015, 0.011	0.014, 0.019, 0.016	0.99, 0.98, 0.98	0.98, 0.97, 0.98
ψ_{3_broken}	>1	0.01, 0.014, 0.012	0.015, 0.02, 0.017	0.99, 0.98, 0.98	0.98,0.97, 0.98
$F^{\max}_{FirstStiffener}$	>1	0.005, 0.024, 0.027	0.008, 0.032, 0.036	0.99, 0.99, 0.99	0.99,0.99,0.99
$F^{\max}_{SecondStiffener}$	>1	0.0023, 0.017, 0.033	0.0051, 0.022, 0.043	0.99, 0.98, 0.99	0.99, 0.98, 0.99
$F^{\max}_{ThirdStiffener}$	>1	0.0014, 0.0018, 0.04	0.002, 0.0024, 0.05	0.99, 0.99, 0.97	0.99, 0.99, 0.96

Response Surface Approximation for Reliability Index (Beta)

This section presents the accuracy estimates of design response surface to estimate the reliability index as a function of design variables. These RSA's are constructed by fitting a cubic equation to data at sampled locations. Table C-5 presents the RSA for reliability index for the stiffened panel safe-life design. The bounds on the design variables are presented in Table C-1 and RSA is calculated by fitting data to 100 sample points.

Table C-5: Error estimate of design response surfaces (this is used to estimate reliability index as a function of design variables for safe-life design calculations in Table 3-10), β_d-RSA

Response, reliability index	Nominal target value	e_{av}	e_{rms}	R^2	R^2_{adj}
Beta	5.0 – 6.0	0.18	0.35	0.95	0.93

Computational cost of reliability analysis with inspection schedule is reduced by using a cubic response surface approximation to predict the crack size mean and standard deviation after an inspection as a function of skin thickness, stiffener area, standard deviation in applied stress, initial crack mean, initial crack standard deviation and crack growth time. For accurate results we estimate the crack size mean and standard deviation after the first inspection using the RSA in Table C-7 as a function of skin thickness, stiffener area, inspection interval and standard deviation in stress (the initial crack size distribution is fixed for first inspection). The reliability index for first inspection is also approximated by a cubic RSA in same variables as shown in Table C-9. A minimax LHS design of experiment with 200 level of each design variable is used. For all inspections following the first one we estimate the crack size mean and standard deviation after inspections using the RSA in Table C-8 as a function of skin thickness, stiffener area, inspection interval and standard deviation in stress, initial crack mean and initial crack standard deviation. The reliability index is approximated by a cubic RSA in same variables is shown in Table C-10. A minimax LH design of experiments with 400 level of each design variable is used. The range of each variable is shown in Table C-6. These RSA's are used for calculations in Tables 3-12 through 3-14.

Table C-6: Bounds on design variables used to evaluate response surface for crack sizes parameters after inspection and reliability index

Design variable	Lower bound	Upper bound
Skin thickness	1.0 *mm*	3.0 *mm*
Stiffener area	3.0×10^{-4} *meter*^{2}	2.0×10^{-3} *meter*^{2}
Initial crack mean μ_{ai}	0.2 *mm*	1.0 *mm*
Initial crack standard deviation σ_{ai}	0.2 *mm*	1.0 *mm*
Crack growth time	5000 *flights*	20000 *flights*
Standard deviation in *Stress*	2 *MPa*	10 *MPa*

Table C-7: Error estimate of crack size response surfaces used to estimate the crack size distribution parameters after the first inspection (response surface is constructed by normalizing variables, stiffener area, plate thickness and inspection time and standard deviation in stress), μ_{ai}-RSA, σ_{ai}-RSA

Response	Nominal target value , *mm*	$e_{av,}$	e_{rm}	R^2	R^2_{adj}
Mean a_i after inspection	0.2 – 1.0	0.015	0.013	0.99	0.99
Standard deviation of a_i after inspection	0.2 – 1.0	0.027	0.036,	0.96	0.95

Table C-8: Error estimate of crack size response surfaces used to estimate the distribution after inspection (response surface is constructed by normalizing variables), σ_{ai}-RSA

Response	Nominal target value , *mm*	$e_{av,}$	e_{rm}	R^2	R^2_{adj}
Mean a_i after inspection	0.2 – 1.0	0.006	0.008	0.99	0.99
Standard deviation of a_i after inspection	0.2 – 1.0	0.016	0.023,	0.98	0.98

Table C-9: Error estimate of reliability index response surfaces used to schedule first inspection (design variables are stiffener width, plate thickness and inspection time), β_d-RSA

Response, reliability index	Nominal target value	e_{av}	e_{rms}	R^2	R^2_{adj}
Beta	5.0	0.17	0.24	0.99	0.98

Table C-10: Error estimate of reliability index response surfaces, β_d-RSA

Response, reliability index	Nominal target value	e_{av}	e_{rms}	R^2	R^2_{adj}
Beta	5.0	0.18	0.28	0.98	0.97

APPENDIX D
COST OF STRUCTURAL WEIGHT

Fuel cost and material manufacturing cost may account for more than 80% of the total life cycle cost. We calculated the fuel cost based on data obtained from Venter (1998). The fuel cost is assumed to be \$0.89 a gallon and it is assumed that a pound of structural weight will cost 0.1 pounds of fuel in a flight. This leads to a fuel cost of \$0.0134 per pound per flight (assuming a gallon of jet fuel weighs 6.7 pounds). In this dissertation a slightly higher value of \$0.015 per pound per flight is used for convenience.

The material manufacturing cost was obtained by scaling down the material cost of the composite (\$250) from Venter (1998) to \$150 per pound for aluminum from previous paper (Kale *et al*., 2003). The scaling down is based on a rough estimate only to demonstrate the methodology rather than performing true cost calculation. The rough cost estimate of about \$110 per pound was obtained from Petit *et al.* (2000). They obtained the cost estimate for stiffened metallic fuselage panels for the B777 series aircraft. The structure used in Petit *et al.* (2000) consists of a 3.04×3.04 m^2 structural component with 14 stringers, 7 frames and 7 fail safe straps bonded to each frame. The fuselage length is $l = 62$ m, the radius is $r = 3.2$ m and the skin thickness is 1.6 mm. The total manufacturing cost for the fuselage structure is \$2.78 million. The computation of the total volume of a single structural component for weight calculation is given in Table D-1.

Table D-1: Area of structural dimensions for cost calculation

Structural component	Area, m^2	Number of components	Total area m^2	Total volume, m^3 Total area × Width
Stringer	2×10^{-4}	14	28×10^{-4}	85.64×10^{-4}
Frame	3×10^{-4}	7	21×10^{-4}	63.84×10^{-4}
Tear strap	0.96×10^{-4}	7	6.77×10^{-4}	20.48×10^{-4}

(Source: Petit *et al.,* 2000)

Single panel skin area = 9.24 m^2. The total fuselage surface area is $2\pi rl = 1246m^2$

This corresponds to 135 panels. The skin panel volume is, skin area times thickness = 9.24×0.0016 m^3. Assuming aluminum density, ρ = 2670 kg/m^3

Total fuselage weight = number of panels × (stringer volume+ frame volume + strap volume + skin volume) × ρ = 11512 kg

Cost per unit weight = $\frac{2{,}780{,}000}{11{,}512} = \$241$ per kg or \$110 per pound

APPENDIX E
PSEUDO CODE FOR COMBINED OPTIMIZATION OF STRUCTURE AND INSPECTION SCHEDULE

Introduction

Combined optimization of structure and inspection schedule can be done by performing a one dimensional search on structural size for fixed number of inspection. When only one inspection type is used to generate optimum inspection schedule this is straightforward since the cost function varies monotonically with thickness for fixed number of inspections. The use of multiple inspection types leads to several local minima for fixed number of inspection depending on the inspection type sequence used for generating the inspection schedule. For example, to obtain minimum cost for a schedule consisting of two inspections generated using four inspection types; it will require structural optimization for 16 inspection schedules (4×4). Since the number of inspection that will lead to minimum cost is unknown, several iterations on structural sizes and number of inspections are required to obtain optimum design and inspection schedule. This is computationally expensive. To solve this problem we perform a one dimensional minimization on structural thickness in small steps. At each step we reduce thickness by an amount equivalent to cost of cheapest inspection. For reducing total lifecycle cost, at most one inspection can be added for this structure after iteration. This expedites the optimization. The pseudo code is shown below.

(1) Start the one dimensional minimization using safe life design as initial guess $t^{i}_{guess} = t_{safe\ life}$, initialize thickness

$i = 0$, initialize iteration counter

$N_{allowable} = 0$, set the allowable number of inspections to zero (safe life design does not require any inspection

(2) Reduce the thickness by an amount equivalent to cost of cheapest inspection and obtain optimum inspection schedule such that the number of inspections in the schedule is at most equal to one additional inspection from optimum of previous step.

$i = i + 1$, update iteration counter

$t^{i}_{guess} = t^{i-1}_{guess} - \Delta t$, decrease thickness by fixed amount

$N^{i}_{\min} \le N_{allowable} + 1$

Obtain cost of inspection schedule $C^{i}_{\min}$

Obtain total minimum cost at i^{th} iteration C^{i}_{Total}

(3) Find all the inspection type sequences with cost bounded between the costs of inspection at current iteration and that at previous iteration. The constraints for generating inspection sequence is given below.

$C^{i-1}_{\min} \le C^{new}_{\min} \le C^{i}_{\min}$
$N^{i-1}_{\min} \le N^{new}_{\min} \le N^{i}_{\min}$

(4) Obtain the minimum thickness required to maintain the threshold reliability level for each inspection type sequence obtained in step 3. This gives the minimum cost at i^{th} iteration. Obtain optimum structural design t^{i}_{opt}, number of inspections N^{i}_{opt}, minimum cost C^{i}_{Total} and cost of inspections, C^{i}_{opt}.

(5) If the structural thickness has reached a minimum allowable value,[††††] find the structural design and inspection schedule with minimum total cost from optimum of each iteration else update the variables as shown below and go to step 2.

Update variables at i^{th} iteration

$$t^i_{guess} = t^i_{opt}$$
$$N^i_{\min} = N^i_{opt}$$
$$C^i_{\min} = C^i_{opt}$$
$$N_{allowable} = N^i_{opt}$$

Optimization of Inspection Types

Optimization of an inspection schedule with different inspection types is computationally time-consuming because the inspection time and type of each subsequent inspection depends on the inspection time and type of previous inspections. As an illustration, if four inspection types are to be chosen to schedule four inspections for minimum cost, this will require a reliability analysis on 4×4×4×4 = 256 different type sequence. However, in a typical optimization problem, the number of inspections required to satisfy reliability constraint is unknown and is obtained directly from reliability analysis (optimization of inspection times for fixed reliability). The computational cost may be prohibitive if a brute force approach is used. We seek a mix of inspection types and reduce the number of sequence by eliminating impossible or clearly sub-optimal inspection types. The terminology used in the algorithm presented in Chapter 4 is described below.

[††††] For aircraft structures the minimum structural thickness is about 1.0 *mm*. Typically, if the cost starts increasing at successive thickness reduction, the iterations can be terminated

(1) Baseline inspection schedule (N_{kb}, C_{kb}). Optimum number of inspections of k^{th} type and N_{kb} and the corresponding cost C_{kb} if only the k^{th} inspection type is used to optimize the inspection schedule for a given reliability constraint.

(2) Combination sequence. Number of inspection of each type that can be used to generate the inspection schedule (time of inspection). For example, a combination represented by [N_1 =1, N_2 = 2, N_3 = 1, N_4 = 2] means that there is one inspection of type 1, two inspections of type 2, one inspection of type 3 and two inspections of type 4 in an inspection schedule. In all on them there are 6 inspections available to generate the inspection schedule.

(3) Inspection type sequence. The order in which the various inspections are done. For example, a combination sequence represented by [N_1 =0, N_2 =1, N_3 = 1, N_4 = 1] can have six different orders in which an inspection of each type can be conducted. These are (1) I_2, I_3, I_4 , (2) I_2, I_4, I_3 , (3) I_3, I_2, I_4 , (4) I_3, I_4, I_2 , (5) I_4, I_2, I_3 , (6) I_4, I_3, I_2. The order of the inspection type is important in generating the optimum inspection schedule for minimum cost, because the reduction in the probability of failure of one sequence can be different from others, probability of detection P_d being a function of crack size and crack size being a function of time.

(4) Constraint 1. $N_k < \left\lfloor \frac{C_{\min}}{I_{ck}} \right\rfloor$ where [] is a rounded up integer. This constraint essentially means that the maximum number of inspections of the k^{th} type that can occur in a combination sequence should be such that the cost due to inspection of the k^{th} type is less than or equal to the minimum cost C_{min}.

(5) Constraint 2: $N_{1b} < \sum_{k=1}^{4} N_k < N_{4b}$ The reason for this constraint is that N_{1b} is the optimum number of inspections obtained using the most effective inspection type. A total number of inspections in a combination sequence $\sum_{k=1}^{4} N_k$ less than N_{1b} is a direct violation of the reliability constraint. N_{4b} is the optimum number of inspections obtained using the least effective inspection type. The total number of inspection in a combination sequence $\sum_{k=1}^{4} N_k$ greater than N_{4b} is a direct violation of the cost constraint.

APPENDIX F
EFFECT OF CRACK SIZE PROBABILITY DISTRIBUTION ON FAILURE PROBABILITY AND INSPECTION INTERVAL

Intuitively it appears that when we increase the standard deviation of a distribution, we increase the probability of extreme values of the random variable. This appendix shows that this is not always true for the lognormal distribution used here to model initial crack size. Consequently, we can run into situations as in Table F-1 where increase in mean and standard deviation of the initial crack sizes can lead to increase in inspection interval. In Table F-1 we generated inspection times for a structural size of 2.48 *mm* for a required reliability level of 10^{-7}.

Table F-1: Inspection schedule and crack size distribution after inspection (a_h = 1.27 *mm*) for an unstiffened plate thickness of 2.48 *mm* and a threshold probability of 10^{-7}

Number of inspections, *N*	Inspection time (flights)	Inspection interval (flights) $S_n - S_{n-1}$	Crack size distribution after inspection (Mean,*mm*, cov)
0			Initial crack distribution (0.200 *mm*, 0.35)
1	14569	14569	(0.33,1.39)
2	18991	4422	(0.29,1.06)
3	25952	6961	(0.32,1.31)
4	30128	4176	(0.36,1.16)
5	38167	8037	

Table F-1 shows the inspection times in column 2 and inspection interval in column 3. The crack size mean and standard deviation after the inspection is shown in column 4 (these values are different for each row because the crack growth time is different for each inspection interval and because the detected cracks are replaced by new component with much smaller cracks after an inspection). From Table F-1, third inspection interval

6961 flights is smaller than fifth inspection interval 8037 flights even though the crack size distribution parameter before the third interval (mean = 0.29 *mm*, cov = 1.06) is benign than the parameters before fifth interval (mean = 0.36 *mm*, cov = 1.16). That is, by just looking at the mean and standard deviation from Table F-1 it appears that larger cracks are growing slower which is counter intuitive because crack grows faster with crack length (e.g., Paris law).

This counterintuitive nature of the lognormal distribution is illustrated by keeping the mean of the distribution at 1.0, varying the standard deviation and calculating the probability that the variable is greater than 2.0.

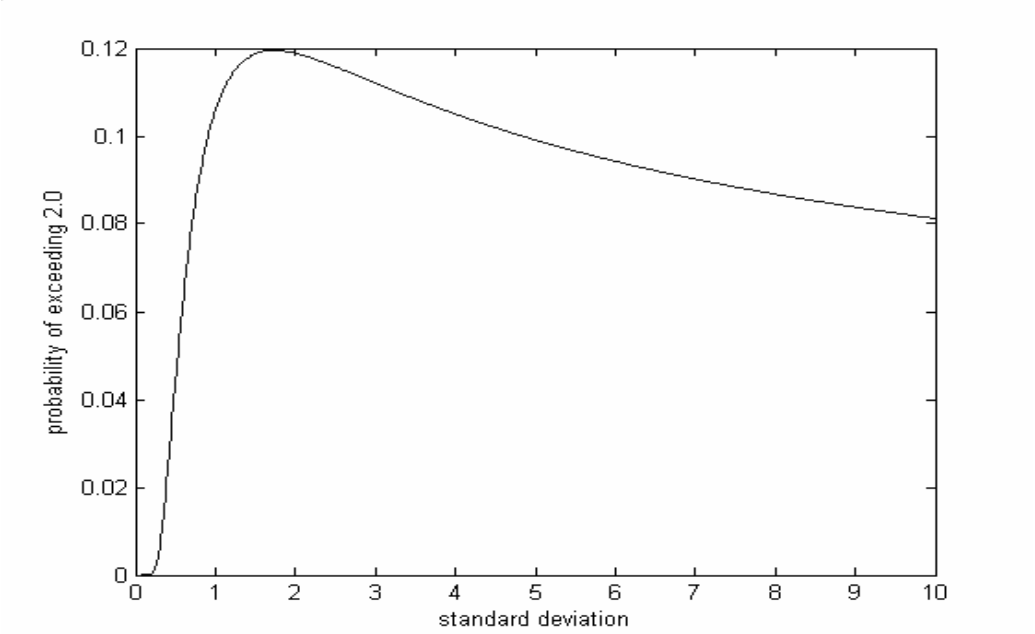

Figure F-1: Probability of exceeding 2.0 for a lognormally distributed random variable with a mean of 1.0. Note that large standard deviation decreases probability

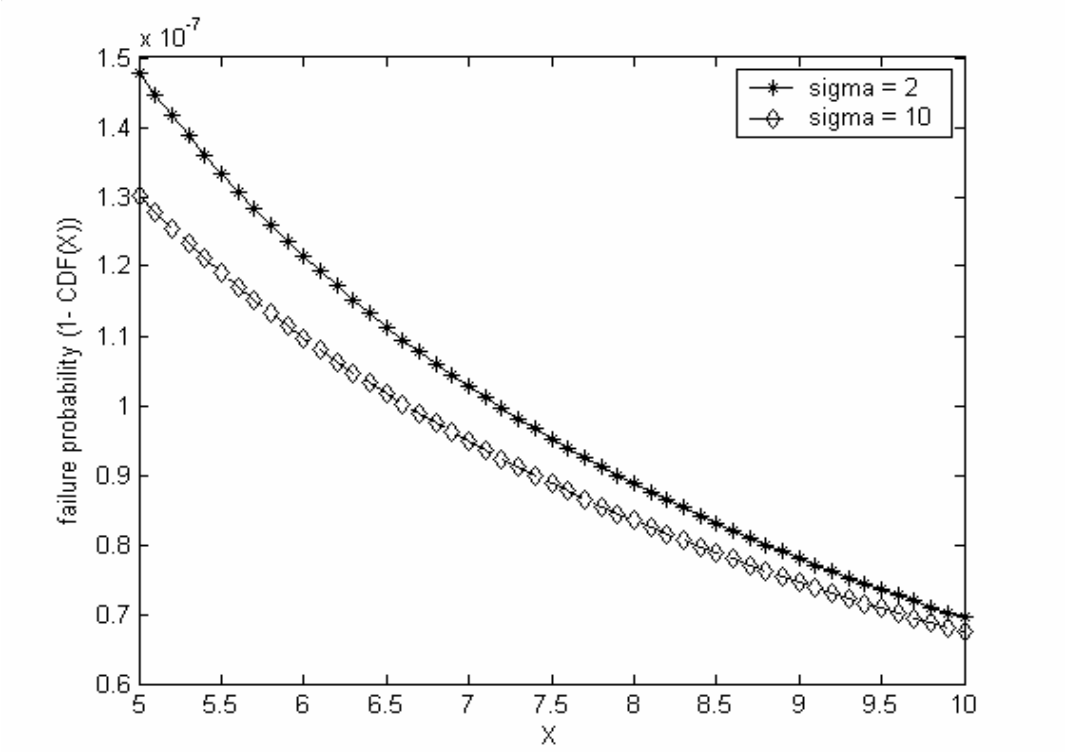

Figure F-2: Comparison of failure probability (1- CDF) of two probability distributions with mean 10^{-5} and standard deviation of 2 and 10 units

Figure F-2 illustrates the cumulative density function of two distributions with standard deviation of 1.8 and 10.0 units. It can be seen that the failure probability of the distribution with higher standard deviation is lesser than that of the distribution with lower standard deviation.

APPENDIX G
WHY ARE AIRPLANES SO SAFE STRUCTURALLY? EFFECT OF VARIOUS SAFETY MEASURES ON STRUCTURAL SAFETY

This chapter is close to Acar *et al.* (2005). A preliminary methodology to investigate the interaction of error, variability and testing in structural design was developed by me using Monte Carlo simulation method. This work was done in collaboration with Erdem Acar who improved the work by developing analytical approximation for calculating failure probability and investigated the effectiveness of certification testing and its effect on distribution of errors. Erdem's contribution to this work in fully acknowledged.

Introduction

In the past few years, there has been growing interest in applying probability methods to aircraft structural design (e.g., Lincoln, 1980; Wirsching, 1992; Aerospace Information Report 5080 (Society of Automotive Engineers, 1997) and, Long and Narciso, 1999). However, many engineers are skeptical of our ability to calculate the probability of failure of structural designs for the following reasons. First, data on statistical variability in material properties, geometry and loading distributions are not always available in full (e.g., joint distributions), and it has been shown that insufficient information may lead to large errors in probability calculations (e.g., Ben-Haim and Elishakoff, 1990 and Neal *et al.*, 1992). Second, the magnitude of errors in calculating loads and predicting structural response is not known precisely, and there is no consensus on how to model these errors in a probabilistic setting. As a result of these concerns, it is

possible that transition to probability based design will be gradual. In such circumstances it is important to understand the impact of existing design practices on safety. This chapter is a first attempt to explore the effects of various safety measures taken during aircraft structural design using the deterministic design approach based on FAA regulations.

The safety measures that we include here are (1) the use of safety factors, (2) the use of conservative material properties (A-basis), and (3) the use of final certification tests. These safety measures are representative rather than all inclusive. For example, the use of A-basis properties is a representative measure for the use of conservative material properties. We do not include in this discussion the additional safety due to structural redundancy and due to conservative design load specification. The use of A-Basis property rather than B-basis is due to the fact that we did not include redundancy. FAA suggests that (FAR 25.613) when there is a single failure path, A-Basis properties should be employed, but in case of multiple failure paths, B-Basis properties are to be used. The effect of the three individual safety measures and their combined effect on the probability of structural failure of the aircraft are demonstrated. We use Monte Carlo simulations to calculate the effect of these safety measures on the probability of failure of a structural component.

We start with a structural design employing all considered safety measures. The effects of variability in geometry, loads, and material properties are readily incorporated by the appropriate random variables. However, there is also uncertainty due to various errors such as modeling errors in the analysis. These errors are fixed but unknown for a given airplane. To simulate these epistemic uncertainties, we transform the error into a

random variable by considering the design of multiple aircraft models. As a consequence, for each model the structure is different. It is as if we pretend that there are hundreds of companies (Airbus, Boeing, etc.) each designing essentially the same airplane, but each having different errors in their structural analysis. This assumption is only a device to model lack of knowledge or errors in probabilistic setting. However, pretending that the distribution represents a large number of aircraft companies helps to motivate the probabilistic setting.

For each model we simulate certification testing. If the airplane passes the test, then an entire fleet of airplanes with the same design is assumed to be built with different members of the fleet having different geometry, loads, and material properties based on assumed models for variability in these properties. That is, the uncertainty due to variability is simulated by considering multiple realizations of the same design, and the uncertainty due to errors is simulated by designing different structures to carry the same loads. We consider only stress failure due to extreme loads, which can be simulated by an unstiffened panel designed under uniaxial loads. No testing of components prior to certification is analyzed for this simple example.

Structural Uncertainties

A good analysis of different sources of uncertainty is provided by Oberkampf *et al.* (2002). Here we simplify the classification, with a view to the question of how to control uncertainty. We propose in Table G-1 a classification that distinguishes between (1) uncertainties that apply equally to the entire fleet of an aircraft model and (2) uncertainties that vary for the individual aircraft. The distinction is important because safety measures usually target one or the other. While type 2 are random uncertainties

that can be readily modeled probabilistically, type 1 are fixed for a given aircraft model (e.g., Boeing 737-400) but they are largely unknown.

That is, the uncertainty in the failure of a structural member can also be divided into two types: systemic errors and variability. Systemic errors reflect inaccurate modeling of physical phenomena, errors in structural analysis, errors in load calculations, or use of materials and tooling in construction that are different from those specified by the designer. Systemic errors affect all the copies of the structural components made and are therefore fleet-level uncertainties. They can reflect differences in analysis, manufacturing and operation of the aircraft from an ideal. The ideal aircraft is an aircraft designed assuming that it is possible to perfectly predict structural loads and structural failure for a given structure, that there are no biases in the average material properties and dimensions of the fleet with respect to design specifications, and that there exists an operating environment that on average agrees with the design specifications. The other type of uncertainty reflects variability in material properties, geometry, or loading between different copies of the same structure and is called here individual uncertainty.

Table G-1: Uncertainty classification

Type of uncertainty	Spread	Cause	Remedies
Systemic error (modeling errors)	Entire fleet of components designed using the model	Errors in predicting structural failure and differences between properties used in design and average fleet properties.	Testing and simulation to improve math model and the solution.
Variability	Individual component level	Variability in tooling, manufacturing process, and flying environments.	Improve tooling and construction. Quality control.

Safety Measures

Aircraft structural design is still done, by and large, using code-based design rather than probabilistic approaches. Safety is improved through conservative design practices that include use of safety factors and conservative material properties. It is also improved by tests of components and certification tests that can reveal inadequacies in analysis or construction. In the following we detail some of these safety measures.

Safety Margin. Traditionally all aircraft structures are designed with a safety factor to withstand 1.5 times the limit loads without failure.

A-Basis Properties. In order to account for uncertainty in material properties, the Federal Aviation Administration (FAA) recommends the use of conservative material properties. This is determined by testing a specified number of coupons selected at random from a batch of material. The A-basis property is determined by calculating the value of a material property exceeded by 99% of the population with 95% confidence.

Component and Certification Tests. Component tests and certification tests of major structural components reduce stress and material uncertainties for given extreme loads due to inadequate structural models. These tests are conducted in a building block procedure. First, individual coupons are tested, and then a sub assembly is tested followed by a full-scale test of the entire structure. Since these tests cannot apply every load condition to the structure, they leave uncertainties with respect to some loading conditions. It is possible to reduce the probability of failure by performing more tests to reduce uncertainty or by extra structural weight to reduce stresses. If certification tests were designed together with the structure, it is possible that additional tests would become cost effective because they would allow reduced structural weight.

We simulate the effect of these three safety measures by assuming the statistical distribution of the uncertainties and incorporating them in approximate probability calculations and Monte Carlo simulation. For variability the simulation is straightforward. However, while systemic errors are uncertain at the time of the design, they will not vary for a single structural component on a particular aircraft. Therefore, to simulate the uncertainty, we assume that we have a large number of nominally identical aircraft being designed (e.g., by Airbus, Boeing, Bombardier, etc.), with the errors being fixed for each aircraft. This creates a two-level Monte Carlo simulation, with different aircraft models being considered at the upper level, and different instances of the same aircraft at the lower level.

To illustrate the procedure we consider a simple example of an unstiffened panel designed for strength under uniaxial tensile loads. This will still simulate reasonably well more complex configurations, such as stiffened panels subject to stress constraints. Aircraft structures have more complex failure modes, such as fatigue and fracture, which require substantially different treatment and the consideration of the effects of inspections (see Kale *et al.*, 2003). However, this simple example serves to further our understanding of the interaction between various safety measures. The procedure is summarized in Figure G-1, which is described in detail in the next section.

Panel Example Definition

Design and Certification Testing

We assume that we have N different aircraft models, i.e., we have N different companies producing a model with systemic errors. We consider a generic panel to represent the entire aircraft structure. The true stress (σ_{true}) is found from the equation

$$\sigma_{true} = \frac{P}{wt} \tag{G-1}$$

where P is the applied load on the panel of width w and thickness t. In a more general situation, Eq. (G-1) may apply to a small element in a more complex component.

When errors are included in the analysis, the true stress in the panel is different from the calculated stress. We include the errors by introducing an error factor e while computing the stress as

$$\sigma_{calc} = (1+e)\sigma_{true} \tag{G-2}$$

Positive values of e yield conservative estimates of the true stress and negative values yield unconservative stress estimation. The other random variables account for variability. Combining Eqs. (G-1) and (G-2), the stress in the panel is calculated as

$$\sigma_{calc} = (1+e)\frac{P}{wt} \tag{G-3}$$

The design thickness is determined so that the calculated stress in the panel is equal to material allowable stress for a design load P_d multiplied by a safety factor S_F, hence the design thickness of the panel is calculated from Eq. (G-3) as

$$t_{design} = (1+e)\frac{S_F P_d}{w\sigma_a} \tag{G-4}$$

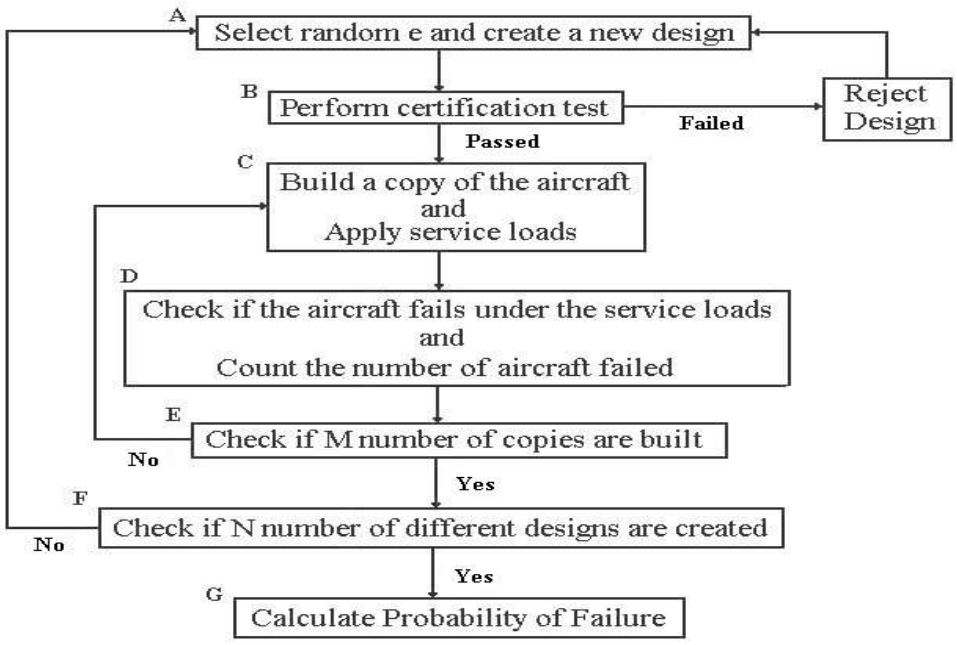

Figure G-1: Flowchart for Monte Carlo simulation of panel design and failure

where the panel width, w, is taken here to be 1.0 meter, and σ_a is the material stress allowable obtained from testing a batch of coupons according to procedures that depend on design practices. Here, we assume that A-basis properties are used (Appendix H). During the design process, the only random quantities are σ_a and e. The thickness obtained from Eq. (G-4) (step A in Fig. (G-1)) is the nominal thickness for a given aircraft model. The actual thickness will vary due to individual–level manufacturing uncertainties.

After the panel has been designed (that is, thickness determined) from Eq. (G-4), we simulate certification testing for the aircraft. Here we assume that the panel will not be built with complete fidelity to the design due to variability in geometry (width and thickness). The panel is then loaded with the design axial force of (S_F times P_d), and the stress in the panel is recorded. If this stress exceeds the failure stress (itself a random

variable, see Table G-2.) then the design is rejected, otherwise it is certified for use. That is, the airplane is certified (step B in Fig. G-1) if the following inequality is satisfied

$$\sigma - \sigma_f = \frac{S_F P_d}{wt} - \sigma_f \le 0 \tag{G-5}$$

and we can build multiple copies of the airplane. We subject the panel in each airplane to actual random maximum (over a lifetime) service loads (step D) and decide whether it fails using Eq. (G-6).

$$P \ge R = t\, w \sigma_f \tag{G-6}$$

Here, P is the applied load, and R is the resistance or load capacity of the structure in terms of the random width w, thickness t and failure stress σ_f. A summary of the distributions for the random variables used in design and certification is listed in Table G-2.

Table G-2: Distribution of random variables used for panel design and certification

Variables	Distribution	Mean	Scatter
Plate width (w)	Uniform	1.0	(1%) bounds
Plate thickness (t)	Uniform	t_{design}	(3%) bounds
Failure stress (σ_f)	Lognormal	150.0	8 % coefficient of variation
Service load (P)	Lognormal	100.0	10 % coefficient of variation
Error factor (e)	Uniform	0.0	10% to 50%

This procedure of design and testing is repeated (steps A-B) for N different aircraft models. For each new model, a different random error factor e is picked for the design, and different allowable properties are generated from coupon testing (Appendix H). Then in the testing, different thicknesses and widths, and different failure stresses are generated at random from their distributions.

Effect of Certification Tests on Distribution of Error Factor *e*

One can argue that the way certification tests reduce the probability of failure is by changing the distribution of the error factor *e*. Without certification testing, we assume symmetric distribution of this error factor. However, designs based on unconservative models are more likely to fail certification, and so the distribution of *e* becomes conservative for structures that pass certification. In order to quantify this effect, we calculated the updated distribution of the error factor *e*. The updated distribution is calculated analytically by Bayesian updating by making some approximations, and Monte Carlo simulations are conducted to check the validity of those approximations.

Bayesian updating is a commonly used technique to obtain updated (or posterior) distribution of a random variable upon obtaining new information about the random variable. The new information here is that the panel has passed the certification test. Using Bayes' Theorem, the updated (posterior) distribution $f^U(\theta)$ of a random variable θ is obtained from the initial (prior) distribution $f^I(\theta)$ based on new information as

$$f^U(\theta) = \frac{P(\in|\theta)\, f^I(\theta)}{\int_{-\infty}^{\infty} P(\in|\theta)\, f^I(\theta) d\theta} \tag{G-8}$$

where $P(\in|\theta)$ is the conditional probability of observing the experimental data $\in$ given that the value of the random variable is θ. For our case, the posterior distribution $f^U(e)$ of the error factor *e* is given as

$$f^U(e) = \frac{P(C|e)\, f^I(e)}{\int_{-b}^{b} P(C|e)\, f^I(e) de} \tag{G-9}$$

where C is the event of passing certification, and $P(C|e)$ is the probability of passing certification for a given e. Initially, e is assumed to be uniformly distributed. The procedure of calculation of $P(C|e)$ is described in Appendix J, where we approximate the distribution of the geometrical variables, t and w as lognormal, taking advantage of the fact that their coefficient of variation is small compared to that of the failure stress (see Table G-2).

We illustrate the effect of certification tests for the panels designed with A-Basis material properties. An initial and updated distribution plot of error factor e with 50 % bound is shown in Fig. G-2 Monte Carlo simulation with 50,000 aircraft models is also shown. Figure G-2 shows that the certification tests greatly reduce the probability of negative error, hence eliminating most unconservative designs. As seen from the figure, the approximate distribution calculated by the analytical approach matches well the distribution obtained from Monte Carlo simulations.

Probability of Failure Calculation by Analytical Approximation

The stress analysis represented by Eq. (G-1) is trivial, so that the computational cost of Monte Carlo simulation of the probability of failure is not high. However, it is desirable to obtain also analytical probabilities that may be used for more complex stress analysis and to check the Monte Carlo simulations. In order to take advantage of simplifying approximations of the distribution of the geometry parameters, it is convenient to perform the probability calculation in two stages, corresponding to the inner and outer loops of Fig. G-1. That is, we first obtain expressions for the probability of failure of a single aircraft model (that is, given e and allowable stress). We then calculate the probability of failure over all aircraft models.

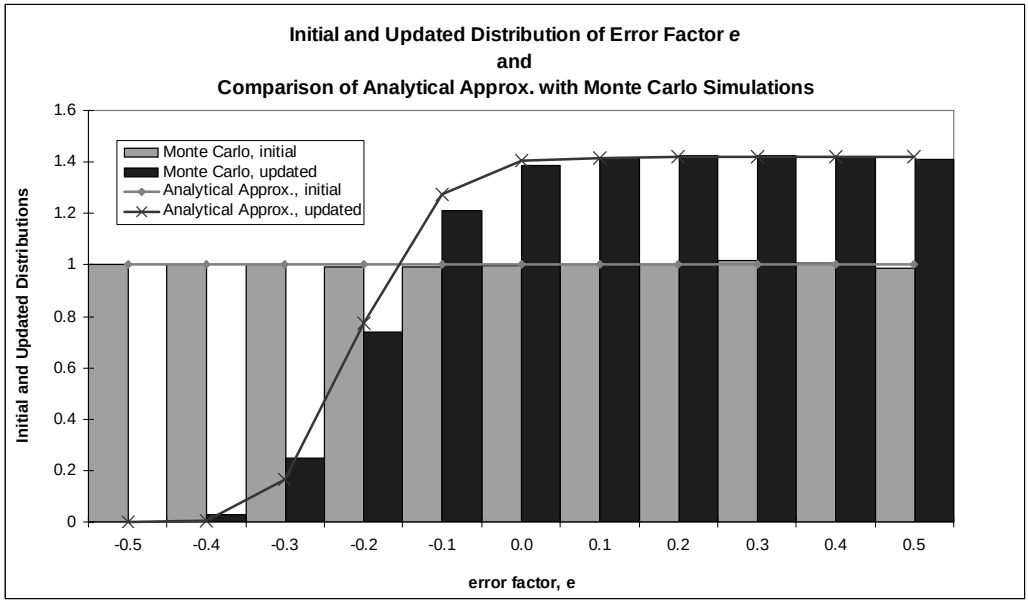

Figure G-2: Initial and updated probability distribution functions of error factor *e* Error bound is 50% and Monte Carlo simulation done with a sample of 50,000.

The mean value of the probability of failure over all aircraft models is calculated as

$$\hat{P}_f = \int P_f(t_{design})\, f(t_{design})\, dt_{design} \tag{G-10}$$

where t_{design} is the non-deterministic distribution parameter, and $f(t_{design})$ is the probability density function of parameter t_{design}.

It is important to have a measure of variability in this probability from one aircraft model to another. The standard deviation of failure probability gives a measure of this variability. In addition, it provides information on how accurate is the probability of failure obtained from Monte Carlo simulations. The standard deviation can be calculated from

$$\sigma_{P_f} = \left[\int \left(P_f(t_{design}) - \hat{P}_f \right)^2 f(t_{design})\, dt_{design} \right]^{1/2} \tag{G-11}$$

Probability of Failure Calculation by Monte Carlo Simulations

The inner loop in Fig. G-1 (steps C-E) represents the simulation of a population of M airplanes (hence panels) that all have the same design. However, each panel is different due to variability in geometry, failure stress, and loading (step D). We subject the panel in each airplane to actual random maximum (over a lifetime) service loads (step E) and calculate whether it fails using Eq. (G-6).

For airplane model that pass certification, we count the number of panels failed. The failure probability is calculated by dividing the number of failures by the number of airplane models that passed certification, times the number of copies of each model.

The analytical approximation for the probability of failure suffers due to the approximations used, while the Monte Carlo simulation is subject to sampling errors, especially for low probabilities of failure. Using large samples, though, can reduce the latter. Therefore, we compared the two methods for a relatively large sample of 10,000 aircraft models with 100,000 instances of each model. In addition, the comparison is performed for the case where mean material properties (rather than A-basis properties) are used for the design, so that the probability of failure is high enough for the Monte Carlo simulation to capture it accurately. Table G-3 shows the results for this case.

Table G-3: Comparison of probability of failures (P_f's) for panels designed using safety factor of 1.5, mean value for allowable stress and error bound of 50%

Value	Analytical approximation	Monte Carlo simulation*	% error
Average Value of P_f without certification (P_{nt})	1.715×10^{-1}	1.726×10^{-1}	0.6
Standard Deviation of P_{nt}	3.058×10^{-1}	3.068×10^{-1}	0.3
Average Value of P_f with certification (P_t)	3.166×10^{-4}	3.071×10^{-4}	3.1
Standard Deviation of P_t	2.285×10^{-3}	2.322×10^{-3}	1.6
Average Value of Initial error factor (e^i)	0.0000	-0.00024	---
Standard Deviation of e^i	0.2887	0.2905	0.6
Average Value of Updated error factor (e^{up})	0.2468	0.2491	0.9
Standard Deviation of e^{up}	0.1536	0.1542	0.4

* N = 10,000 and M = 100,000 is used in the Monte Carlo Simulations

The last column of Table G-3 shows the percent error of the analytical approximation compared to Monte Carlo simulations. It is seen that the analytical approximation is in good agreement with the values obtained through Monte Carlo simulations. It is remarkable that the standard deviation of the probability of failure is almost twice the average value of the probability (the ratio, the coefficient of variation, is about 178%) before certification, and about seven times larger after certification. This indicates huge variability in the probability of failure for different aircraft models, and this is due to the large error bound, *e=50%*. With 10,000 different aircraft models (*N*), the standard deviation in the Monte Carlo estimates is about 1%, and the differences between the Monte Carlo simulation and the analytical approximation are of that order.

Effect of Three Safety Measures on Probability of Failure

We next investigate the effect of other safety measures on failure probability of the panels using Monte Carlo simulations. We performed the simulation for a range of variability in error factor *e* for 5000 airplane models (*N* samples in outer loop) and 20,000 copies of each airplane model (*M* samples in inner loop). Here, we compare the probability of failure of a structure designed with three safety measures (safety factor, conservative material property and certification testing) to that of a structure designed without safety measures.

Table G-4: Probability of failure for different bounds on error *e* for panels designed using safety factor of 1.5 and A-basis property for allowable stress. Numbers in parenthesis denote the coefficient of variation of the quantity. Average design thickness without certification is 1.271.

Error Bound ***e***	Average design thickness after certification*	Certification failure rate %	Probability of failure after certification (P_t) x10^{-4}	Probability of failure without certification (P_{nt}) x10^{-4}	Probability ratio (P_t/P_{nt})	Probability difference (P_{nt}-P_t)
50%	1.453 (0.19)	29.3	1.664 (7.86)	449.0 (2.74)	3.706×10^{-3}	4.473×10^{-2}
40%	1.389 (0.17)	24.3	1.586 (6.92)	89.77 (3.22)	1.767×10^{-2}	8.818×10^{-3}
30%	1.329 (0.15)	16.3	1.343 (5.28)	9.086 (3.46)	1.479×10^{-1}	7.742×10^{-4}
20%	1.283 (0.12)	6.2	0.304 (4.81)	0.477 (3.51)	6.377×10^{-1}	1.727×10^{-5}
10%	1.272 (0.07)	1.2	0.027 (4.71)	0.029 (4.59)	9.147×10^{-1}	2.490×10^{-7}

*Average over N=5000 models

Table G-4 presents the results when all safety measures are used for different bounds on the error. The second column shows the mean and standard deviation of design thicknesses generated for panels that passed certification. These panels correspond to the outer loop of Fig. G-1. The variability in design thickness is due to the randomness in the error *e* and in the stress allowable. The average thickness before certification was 1.269, so that the column shows the conservative effect of certification testing. When the error bound is 10% then 98.8% of the panels pass certification (third column in Table G-4), and the average thickness is increased by only 0.24% due to the certification process. On the other hand, when the error bound is 50%, 29% of the panels do not pass certification, and this raises the average thickness to 1.453. Thus, the increase in error bound has two opposite effects. Without certification testing, increasing the error bound greatly increases the probability of failure. For example, when the error bound changes from 30% to 50%, the probability of failure without certification changes from

0.00091 to *0.0449*, or by a factor of 49. On the other hand, with the increased average thickness, after certification the probability increases only from $1.343x10^{-4}$ to $1.664x10^{-4}$.

The effectiveness of the certification tests can be expressed by two measures of probability improvement. The first measure is the ratio of the probability of failure with the test, P_t, to the probability of failure without tests, P_{nt}. The second measure is the difference of these probabilities. The ratio is a more useful indicator for low probabilities of failure, while the difference is more meaningful for high probabilities of failure. However, when P_t is high, the ratio can mislead. That is, an improvement from a probability of failure of 0.5 to 0.1 is more substantial than an improvement in probability of failure of 0.1 to 0.01, because it "saves" more airplanes. However, the ratio is more useful when the probabilities are small, and the difference is not very informative.

Table G-4 shows that certification testing is more important for large error bounds *e*. For these higher values the number of panels that did not pass certification is higher, thereby reducing the failure probability for those that passed certification. While the effect of component tests (building block tests) is not simulated, their main effect is to reduce the error magnitude *e*. This is primarily due to the usefulness of component tests in improving analytical models and revealing unmodeled failure modes. With that in mind, we note that the failure probability for the 50% error range is 1.7×10^{-4}, and it reduces to 2.7×10^{-6} for the 10% error range-that is, by a factor of 63.

The actual failure probability of aircraft panels is expected to be of the order of 10^{-8} per flight, much lower than the best number in the fourth column of Table G-4. However, the number in Table G-4 is for a lifetime for a single structural component. Assuming about 10,000 flights in the life of a panel and 100 independent structural components, this

10^{-5} failure probability for a panel will translate to a per flight probability of failure of 10^{-7} per airplane. This factor of 10 discrepancy is exacerbated by other failure modes like fatigue that have not been considered. However, other safety measures, such as conservative load specifications may account for this discrepancy.

Table G-5: Probability of failure for different bounds on error *e* for panels designed using safety factor of 1.5 and mean value for allowable stress. Numbers in parenthesis denote the coefficient of variation of the quantity. Average design thickness without certification is 1.000.

Error bound ***e***	Average design thickness after certification *	Certification failure rate+ %	Probability of Failure after certification (P_t) x 10^{-4}	Probability of failure without certification (P_{nt}) x10^{-4}	Probability ratio (P_t/P_{nt})	Probability difference (P_{nt}-P_t)
50%	1.243 (0.13)	50.1	3.420 (5.82)	1681 (1.81)	2.035×10^{-3}	1.677×10^{-1}
40%	1.191 (0.11)	50.1	4.086 (6.78)	969.0 (1.99)	4.217×10^{-3}	9.649×10^{-2}
30%	1.139 (0.09)	50.8	5.616 (5.45)	376.6 (2.00)	1.495×10^{-2}	3.700×10^{-2}
20%	1.086 (0.07)	50.7	6.253 (3.19)	92.67 (1.83)	6.748×10^{-2}	8.642×10^{-3}
10%	1.029 (0.05)	51.0	9.209 (1.70)	19.63 (1.25)	4.690×10^{-1}	1.043×10^{-3}

*Average over N=5000 models +With only 5000 models, the standard deviation in the certification failure rate is about 0.71%. Thus, all the number in this column are about 50% as may be expected when mean material properties are used.

Table G-5 shows results when average rather than conservative material properties are used. It can be seen from Table G-5 that the average thickness determined using the mean value of allowable stress is lower than that determined using the A-basis value of allowable stress (Table G-4). This is equivalent to adding an additional safety factor over an already existing safety factor of 1.5. For the distribution (lognormal with 8% coefficient of variation) and number of batch tests (40 tests) considered in this chapter, a typical value of the safety factor due to A-Basis property is around 1.27.

Without the A-basis properties, the stress in the certification test is approximately equal to the average ultimate service stress, so that about 50% of the panels fail certification. When the errors are large, this raises substantially the average thickness of the panels that pass certification, so that for an error bound of 50% the certification test is equivalent to a safety factor of 1.243. Large errors produce some super-strong and some super-weak panels (see Fig. G-3). The super-weak panels are mostly caught by the certification tests, leaving the super-strong panels to reduce the probability of failure. Another way of looking at this effect is to note that when there are no errors, there is no point to the tests. Indeed, it can be seen that the probability of failure without certification tests improves with reduced error bound *e*, but that the reduced effect of the certification tests reverses the trend. Thus for this case we obtain the counter-intuitive results that larger errors produce safer designs. Comparing the first row of Table G-5 to Table G-3 we see the effect of the smaller sample for the Monte Carlo simulations. Table G-3 was obtained with 10,000 models and 100,000 copies per model, while Table G-5 was obtained with 5000 models, and 20,000 copies per model. The difference in the probability of failure after certification between the two tables is about 11 percent. However, the two values straddle the analytical approximation.

The effects of building block type of tests that are conducted before certification are not included in this study. These tests reduce the errors in analytical models. For instance, if there is 50% error in the analytical model the building block type of tests may reduce this error to lower values. Hence, the difference between the rows of Table G-4 may be viewed as indicating the benefits of reducing the error by building block tests.

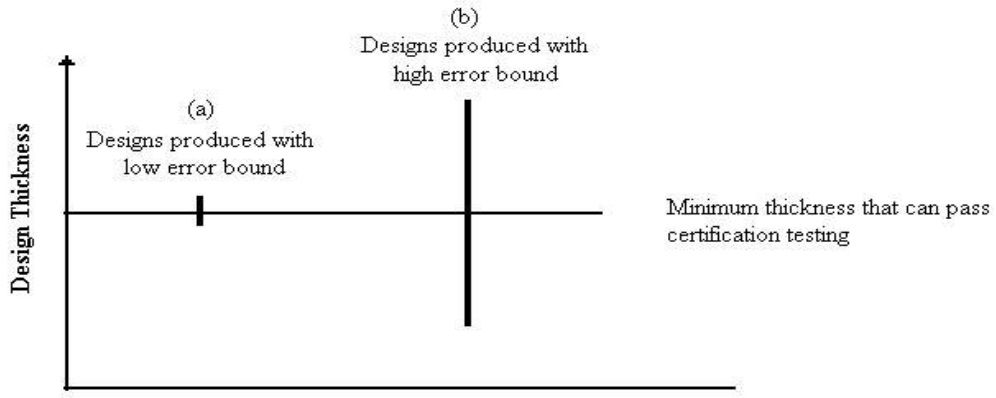

Figure G-3: Design thickness variation with low and high error bounds. (Note that after certification testing only the designs above the minimum thickness are built and flown. Those on the right have a much higher average design thickness than those on the left).

Table G-6: Probability of failure for different bounds on error *e* for safety factor of 1.0 and A-basis property for allowable stress. Numbers in parenthesis denote the coefficient of variation of the quantity. Average design thickness without certification is 0.847.

Error bound ***e***	Average design thickness after certification *	Certification failure rate %	Failure probability after certification (P_t) x10^{-2}	Failure probability with no certification (P_{nt}) x10^{-2}	Probability ratio (P_t/P_{nt})	Probability difference (P_{nt}-P_t)
50%	0.969 (0.19)	29.4	6.978 (2.12)	29.49 (1.31)	2.366×10^{-1}	2.251×10^{-1}
40%	0.929 (0.17)	25.0	7.543 (1.98)	24.56 (1.38)	3.071×10^{-1}	1.702×10^{-1}
30%	0.886 (0.15)	16.6	8.923 (1.73)	17.11 (1.43)	5.216×10^{-1}	8.184×10^{-2}
20%	0.855 (0.11)	5.7	8.171 (1.40)	9.665 (1.34)	8.454×10^{-1}	1.494×10^{-2}
10%	0.847 (0.06)	1.3	4.879 (0.97)	4.996 (0.97)	9.767×10^{-1}	1.163×10^{-3}

*Average over N=5000 models

Table G-6 shows the effect of not using a safety factor. Although certification tests improve the reliability, again in a general trend of high improvement with high error, the lack of safety factor of 1.5 limits the improvement. Comparing Tables G-4 and G-6 it can be seen that the safety factor reduces the probability of failure by two to four orders of magnitudes. It is interesting to note that the effect of the error bound on the probability of

failure after certification is not monotonic, and this phenomenon is discussed in Appendix I.

Table G-7: Probability of failure for different error bounds for panels designed using safety factor of 1.0 and mean value for allowable stress. Average design thickness without certification is 0.667.

Error bound ***e***	Average design thickness after certification *	Certification failure rate %	Probability of Failure after certification (P_t)	Probability of failure without certification (P_{nt})	Probability ratio (P_t/P_{nt})	Probability difference (P_{nt}-P_t)
50%	0.830 (0.12)	50.1	0.125 (1.39)	0.505 (0.83)	2.463×10^{-1}	3.808×10^{-1}
40%	0.796 (0.11)	50.2	0.158 (1.20)	0.504 (0.79)	3.140×10^{-1}	3.459×10^{-1}
30%	0.761 (0.09)	50.4	0.205 (0.92)	0.503 (0.72)	4.075×10^{-1}	2.981×10^{-1}
20%	0.727 (0.08)	50.9	0.285 (0.64)	0.503 (0.58)	5.653×10^{-1}	2.189×10^{-1}
10%	0.686 (0.05)	50.7	0.412 (0.34)	0.500 (0.34)	8.228×10^{-1}	8.869×10^{-2}

*Average over N=5000 models

Table G-7, shows results when the only safety measure is certification testing. Certification tests can reduce the probability of failure of panels by 38%, the highest improvement corresponds to the highest error. As can be expected, without certification tests and safety measures, the probability of failure is near 50%.

Tables G-4 through G-7 illustrates the probability of failure for a fixed 8 % coefficient of variation in failure stress. The general conclusion that can be drawn from these results is that the error bound *e* is one of the main parameters affecting the efficacy of certification tests to improve reliability of panels. Next, we will explore how another parameter, variability, influences the efficacy of tests. This is accomplished by changing the coefficient of variation of failure stress σ_f between 0 – 16% and keeping the error bound constant.

Table G-8: Probability of failure for uncertainty in failure stress for panels designed using safety factor of 1.5, 50% error bounds *e* and A-basis property for allowable stress. Numbers in parenthesis denote the coefficient of variation of the quantity.

cov of σ_f	Average design thickness without certification *	Average design thickness after certification *	Certification failure rate %	Probability of failure after certification (P_t) x10^{-4}	Probability of failure without certification (P_{nt}) x 10^{-4}	Probability ratio (P_t/P_{nt})	Probability difference (P_{nt}-P_t)
0 %	0.998 (0.29)	1.250 (0.11)	50.2	0.017 (6.85)	1699 (1.87)	1.004×10^{-5}	1.698×10^{-1}
4%	1.127 (0.29)	1.347 (0.15)	38.9	0.087 (7.20)	970.4 (2.35)	8.973×10^{-5}	9.703×10^{-2}
8 %	1.269 (0.29)	1.453 (0.19)	29.3	1.664 (7.86)	449.0 (2.74)	3.706×10^{-3}	4.473×10^{-2}
12 %	1.431 (0.29)	1.574 (0.22)	20.9	13.33 (7.71)	206.1 (3.08)	6.469×10^{-2}	1.927×10^{-2}
16%	1.616 (0.30)	1.723 (0.25)	14.1	22.52 (5.54)	107.3 (3.24)	2.100×10^{-1}	8.476×10^{-3}

*Average over N=5000 models

Table G-9: Probability of failure for uncertainty in failure stress for panels designed using safety factor of 1.5, 30% error bound *e* and A-basis properties

cov of σ_f	Average design thickness without certification *	Average design thickness after certification *	Certification failure rate %	Probability of failure after certification (P_t) x10^{-4}	Probability of failure without certification (P_{nt}) x 10^{-4}	Probability ratio (P_t/P_{nt})	Probability difference (P_{nt}-P_t)
0 %	1.001 (0.17)	1.148 (0.08)	50.1	0.026 (4.79)	223.8 (2.50)	1.163×10^{-4}	2.238×10^{-2}
4 %	1.126 (0.17)	1.232 (0.11)	31.6	0.146 (6.03)	35.25 (2.97)	4.149×10^{-3}	3.511×10^{-3}
8 %	1.269 (0.17)	1.329 (0.15)	16.3	1.343 (5.28)	9.086 (3.46)	1.479×10^{-1}	7.742×10^{-4}
12 %	1.431 (0.18)	1.459 (0.17)	7.2	2.404 (3.87)	4.314 (3.45)	5.572×10^{-1}	1.911×10^{-4}
16%	1.617 (0.18)	1.630 (0.18)	3.3	2.513 (3.73)	3.102 (3.54)	8.099×10^{-1}	5.896×10^{-5}

Table G-10: Probability of failure for uncertainty in failure stress for panels designed using safety factor of 1.5, 10% error bounds *e* and A-basis properties

cov of σ_f	Average design thickness without certification *	Average design thickness after certification *	Certification failure rate %	Probability of failure after certification (P_t) x10^{-4}	Probability of failure without certification (P_{nt}) x 10^{-4}	Probability ratio (P_t/P_{nt})	Probability difference (P_{nt}-P_t)
0 %	1.000 (0.06)	1.048 (0.03)	50.3	0.075 (2.91)	1.745 (1.78)	4.304×10^{-2}	1.669×10^{-4}
4 %	1.126 (0.06)	1.131 (0.06)	5.9	0.053 (3.85)	0.070 (3.56)	7.548×10^{-1}	1.716×10^{-6}
8%	1.269 (0.06)	1.272 (0.07)	1.2	0.027 (4.71)	0.029 (4.59)	9.147×10^{-1}	2.490×10^{-7}
12 %	1.431 (0.07)	1.432 (0.07)	0.8	0.049 (4.30)	0.051 (4.23)	9.623×10^{-1}	1.926×10^{-7}
16%	1.623 (0.08)	1.624 (0.08)	0.5	0.085 (3.50)	0.083 (3.55)	9.781×10^{-1}	1.853×10^{-7}

*Average over N=5000 models. See Tables G-8 through G-10 rows 3, 4, 5 with 8 – 16% standard deviation in failure stress.

The increase in the variability in failure stress has a large effect on the allowable stress because A-basis properties specify an allowable that is below 99% of the sample. Increased variability reduces the allowable stress and therefore increases the design thickness. It is seen from Tables G-8 through G-10 that when the variability increases from 0% to 16%, the design thickness increases by more than 60%. This greatly reduces the probability of failure without certification. However, the probability of failure with certification still deteriorates. That is, the use of A-basis properties fails to fully compensate for the variability in material properties. This opposite behavior of the probability of failure before and after certification is discussed in more detail in Appendix I.

The variability in failure stress greatly changes the effect of certification tests. Although the average design thicknesses of the panels increase with the increase in

variability, we see that when the variability is large, the value of the tests is reduced because the tested aircraft can be greatly different from the airplanes in actual service. We indeed see from the Tables G-8 through G-10 that the effect of certification tests is reduced as the variability in the failure stress increases. Recall that the effect of certification tests is also reduced when the error *e* decreases. Indeed, Table G-8 shows a much smaller effect of the tests than Table G-10. Comparing the second and third columns of Tables G-8 through G-10 we see that as the bound of error decreases, the change in the average value of design thicknesses of the panels become less which is an indication of loss in the efficacy of certification tests.

Up to now, both the probability difference (P_{nt}-P_t) and the probability ratio (P_t/P_{nt}) seem to be good indicators of efficacy of tests. To allow easy visualization, we combined the errors and the variability in a single ratio (Bound of *e*) / $V_R(\sigma/\sigma_f)$ ratio (ratio of error bound *e* to the coefficient of variation of the stress ratio). The denominator accounts for the major contributors to the variability. The value in the denominator is a function of four variables; service load *P*, width *w*, thickness *t*, and failure stress σ_f. Here, *P* and σ_f have lognormal distributions but *w* and *t* are uniformly distributed. Since the coefficient of variations of *w* and *t* is very small, they can also be treated as lognormally distributed to make calculation of the denominator easy while plotting the graphs. Since the standard deviations of the variables are small, the denominator is now the square root of the sum of the squares of coefficient of variations of the four variables mentioned above, that is

$$V_R(\sigma/\sigma_f) \cong \sqrt{V_R^2(P) + V_R^2(w) + V_R^2(t) + V_R^2(\sigma_f)} \qquad (11)$$

The effective safety factor is the ratio of the design thickness of the component when safety measures (such as usage of A-basis values for material properties and safety factor) are applied to the thickness of the component when no safety measures are taken.

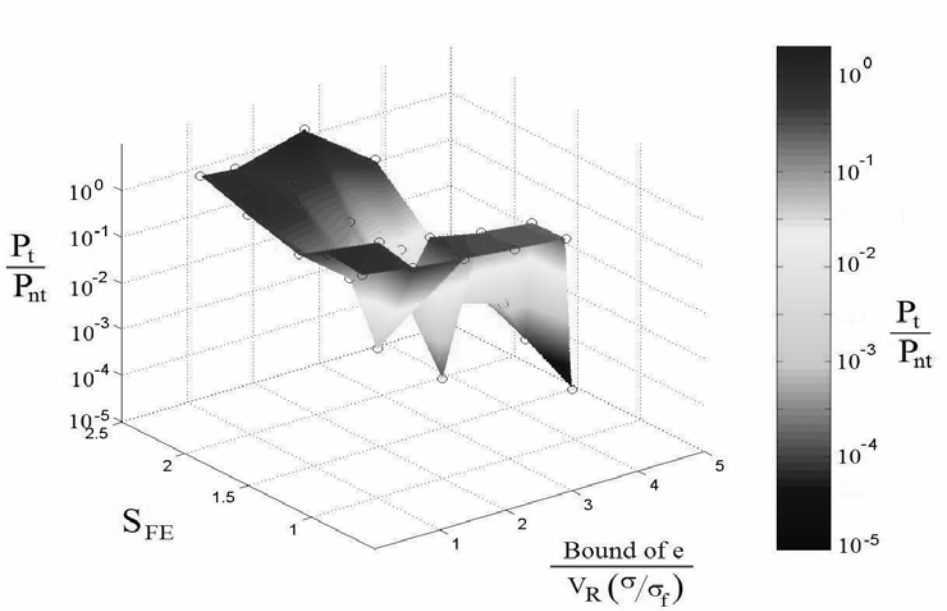

Figure G-4: Influence of effective safety factor, error, and variability on the probability ratio (3-D view)

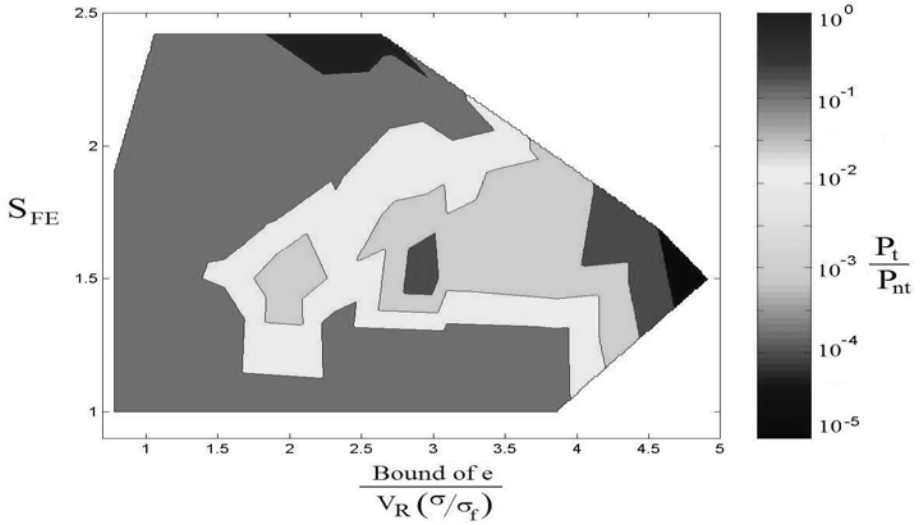

Figure G-5: Influence of effective safety factor, error and variability on the probability ratio (2-D contour plot)

Figures G-4 and G-5, present the P_t/P_{nt} ratio in visual formats. It can be seen that as expected, the ratio decreases as the (Bounds on e)/$V_R(\sigma/\sigma_f)$ ratio increases. However,

these two figures do not give a clear indication of how certification tests are influenced by the effective safety factor.

Figures G-6 and G-7 show the probability difference, P_{nt}-P_t. In these cases, the dependence on the effective safety factor is monotonic. As expected, it is seen that as the effective safety factor increases, the improvement in the safety of component decreases; meaning that the certification tests become less useful. The probability difference is more descriptive as it is proportional to the number of aircraft failures prevented by certification testing. The probability ratio lacks such clear physical interpretation, even though it is a more attractive measure when the probability of failure is very small. Considering the results presented by Figures G-4 through G-7, the probability difference (P_{nt}-P_t) is the more appropriate choice for expressing the effectiveness of tests.

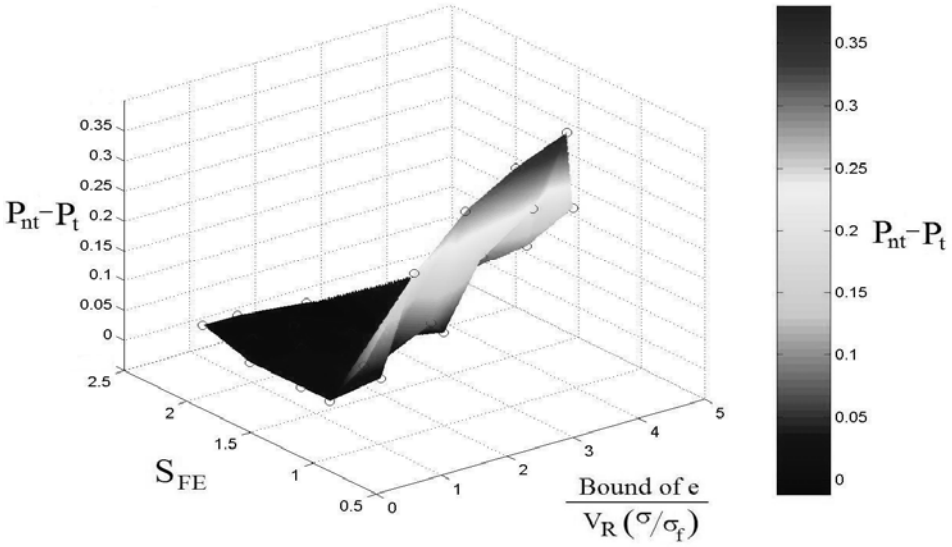

Figure G-6: Influence of effective safety factor, error and variability on the probability difference (3-D view)

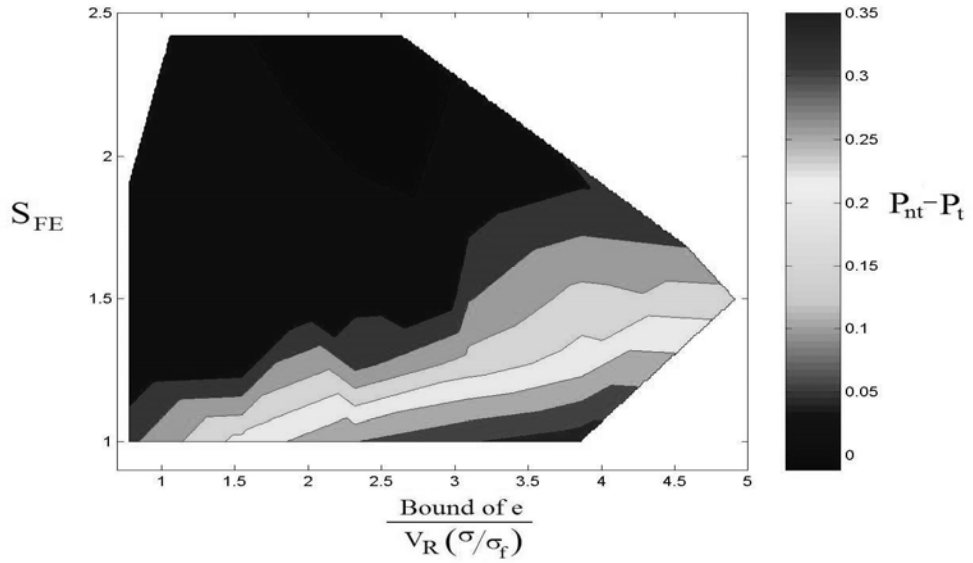

Figure G-7: Influence of effective safety factor, error and variability on the probability difference (2-D contour plot)

Concluding Remarks

We have used a simple example of point stress design for yield to illustrate the effects of several safety measures taken in aircraft design: safety factors, conservative material properties, and certification tests. Analytical calculations and Monte Carlo simulation were performed to account for both fleet-level uncertainties (such as errors in analytical models) and individual uncertainties (such as variability in material properties).

It was seen that an increase of the systemic errors in the analysis causes an increase in the probability of failure. We found that the systemic errors can be reduced by the use of certification tests, thereby reducing the probability of failure. Also we found that design thicknesses of the panels increased as the bounds of systemic errors increased.

We found that the effect of certification tests is most important when errors in analytical models are high and when the variability between airplanes is low. This leads to the surprising result that in some situations larger error variability in analytical models reduces the probability of failure if certification tests are conducted. For the simple

example analyzed here, the use of conservative (A-basis) properties was equivalent to a safety factor of up to 1.6, depending on the scatter in failure stresses.

The effectiveness of the certification tests is expressed by two measures of probability improvement. The ratio of the probability of failure with the test, P_t, to the probability of failure without tests, P_{nt}, is useful when P_t is small. The difference is more meaningful when the probability is high. Using these measures we have shown that the effectiveness of certification tests increases when the ratio of error to variability is large and when the effective safety factor is small.

The effect of building-block type tests that are conducted before certification was not assessed here. However, these tests reduce the errors in the analytical models, and on that basis we determined that they can reduce the probability of failure by one or two orders of magnitude.

The calculated probabilities of failure with all the considered safety margins explain why passenger aircraft are so safe structurally. They were still somewhat high — about 10^{-7}—compared to the probability of failure of actual aircraft structural components—about 10^{-8}. This may be due to additional safety measures, such as conservative design loads or to the effect of design against additional failure modes.

APPENDIX H
CALCULATION OF CONSERVATIVE MATERIAL PROPERTIES

The conservative material properties are specified by the probability level and confidence level of the probability distribution of material property. For example the A-basis value is the value exceeded by 99% of the population with 95% confidence. This is given by

$$\text{A-basis} = \mu - \sigma \times k_1 \tag{H-1}$$

where μ is the mean, σ is the standard deviation and k_1 is the tolerance coefficient for normal distribution given by Equation H-2.

$$k_1 = \frac{z_{1-p} + \sqrt{z_{1-p}^2 - ab}}{a} \tag{H-2}$$

$$a = 1 - \frac{z_{1-\gamma}^2}{2(N-1)} \; ; \; b = z_{1-p}^2 - \frac{z_{1-\gamma}^2}{N} \tag{H-3}$$

where, N is the sample size and z_{1-p} is the critical value of normal distribution that is exceeded with a probability of $1- p$. The tolerance coefficient k_1 for a lognormal distribution is obtained by first transforming the lognormally distributed variable to a normally distributed variable. Equation H-1 and H-2 can be used to obtain an intermediate value. This value is then converted back to the lognormally distributed variable using inverse transformation.

In order to obtain the A-basis values, 40 panels are randomly selected from a batch. Here the uncertainty in material property is due to allowable stress. The mean and standard deviation of 40 random values of allowable stress is calculated and used in

determining the A-basis value of allowable stress. For instance, when the failure stress is lognormal with 8% coefficient of variation and 40 tests are performed, the coefficient of variation of A-basis value is about 3 percent.

APPENDIX I
CONFLICTING EFFECTS OF ERROR AND VARIABILITY ON PROBABILITY OF FAILURE

As explained in the discussion of Table G-5 and Figure G-3, large errors coupled with certification tests can improve the average (over all companies) safety of an aircraft model. This was most apparent when mean material properties are used for design (Table G-5) because for this case airplanes would be tested at their average failure load, so that fifty percent will fail certification. A large error bound means a wide variation in design thicknesses. Certification testing fails most of the airplane models with unconservative designs and passes a group of airplane models with high average thickness (that is, over-designed planes).

When the additional safety factor of conservative material properties is used, as in Table G-6, the picture is more complex. Certification is still done at the same loads, but the test airplane is designed for higher loads because of the conservative material properties. For high errors, many airplanes will still fail certification, but small errors will be masked by the conservative properties. Thus in Table G-6, the certification failure rate varies from 29.4% for the largest errors to 1.3% for the smallest errors. At the highest error bound (50%), the certification process increases the average thickness from 0.847 to 0.969, and this drops to 0.866 for 30% error bound. This substantial drop in average certified model thicknesses increases the probability of failure. Below an error bound of 30%, the change in thickness is small, and then reducing errors reduces the probability of

failure. This is because small negative errors are not caught by certification, but they still reduce the effective safety factor.

A similar phenomenon is observed when the variability is changed in Tables G-8 through G-10. When the coefficient of variation in failure stress is increased from 0% to 16%, the average design thickness before certification increases by about 60% and so the probability of failure without certification is reduced by factors of 16-70. Note that for the smallest error bound (Table G-10), the drop occurs from zero to 8% coefficient of variation. At the higher coefficients of variation the probability of failure before certification increases again as the increased design thickness does not suffice to compensate for the large variation between airplanes .Once certification is included in the process, variability is mostly detrimental. Certification does not amount to much for large variability, because the certified airplane can be very different from the production aircraft. For large error bounds (Table G-8) there are large errors that can be masked during certification by the high material safety factor. Thus in Table G-8, while the probability of failure without certification is reduced by a factor of 16, the probability of failure with certification is increased by a factor of 1320 as the coefficient of variation in the failure stressed is increased from 0 to 16%. For small errors (Table G-10) the picture is more mixed as the non-monotonic behavior without certification is mirrored with certification.

APPENDIX J
CALCULATIONS OF *P(C|E),* THE PROBABILITY OF PASSING CERTIFICATION TEST

An analytical method to obtain failure probability following certification test is presented here. This method was developed by Erdem Acar. This method was used to validate the results from Monte Carlo Simulation and update the distribution of errors following certification tests.

$$P(C \mid e) = P(\sigma_f > \sigma) = P\left(\sigma_f > \frac{S_F P_d}{wt}\right) = P\left(\sigma_f wt > S_F P_d\right) = P(R > S) \tag{J-1}$$

where

$$R = \sigma_f \; t \; w \text{ and } S = S_F \, P_d. \tag{J-2}$$

S is a deterministic value, and since the coefficient of variations of *t* and *w* is small compared to the coefficient of variation of σ_f, we assume *t* and *w* can be assumed lognormal, so *R* can be treated as lognormal. In order to take advantage of the properties of lognormal distribution for calculating the distribution parameters, we can take *S* as a lognormally distributed random variable with zero coefficient of variation. Hence, both *R* and *S* are lognormally distributed random variables with distribution parameters λ_R, ζ_R, λ_S and ζ_S. Then,

$$\lambda_S = \ln(S_F P_d) \text{ and } \zeta_S = 0 \tag{J-3}$$

$$\lambda_R(e) = \lambda_{\sigma_f} + \lambda_t(e) + \lambda_w \text{ and } \zeta_R^2 = \zeta_{\sigma_f}^2 + \zeta_t^2 + \zeta_w^2 \tag{J-4}$$

where

$$\lambda_t(e) = \ln(t_{design}(e)) - 0.5\zeta_t^2 = \ln\left((1+e)\frac{S_F P_d}{w\sigma_a}\right) - 0.5\zeta_t^2 \quad \text{(J-5)}$$

Then, *P(C|e)* can be calculated as

$$P(C \mid e) = P(R > S) = \Phi\left(\frac{\lambda_R(e) - \lambda_S}{\sqrt{\zeta_R^2 + \zeta_S^2}}\right) = \Phi(\beta(e)) = \int_{-\infty}^{\beta(e)} \frac{1}{\sqrt{2\pi}} \exp\left(-\frac{x^2}{2}\right) dx \quad \text{(J-6)}$$

Mean and Standard Deviation of Probability. Failure is predicted to occur when the resistance of the structure (*R*) of the problem is less than the load (*P*), see Equation J-7. Then, the probability of failure is given as:

$$P_f = \Pr(R < P) \quad \text{(J-7)}$$

The load *P* is lognormally distributed, and as explained in above in this appendix, the distribution of *R* can also be approximated by a lognormal distribution, which allows us to immediately obtain the probability of failure of a single aircraft model. To calculate the probability of failure over all aircraft models, we take into account the fact that that t_{design} is a random variable. Then, the expected value of probability of failure is given as:

$$\hat{P}_f = \int P_f(t_{design})\, f(t_{design})\, dt_{design} \quad \text{(J-8)}$$

where t_{design} is the non-deterministic distribution parameter, and $f(t_{design})$ is the probability density function of parameter t_{design}. The standard deviation of failure probability can be calculated from

$$\sigma_{P_f} = \left[\int \left(P_f - \hat{P}_f\right)^2 f(P_f)\, dP_f\right]^{1/2} \quad \text{(J-9)}$$

where

$$P_f = P_f(t_{design})$$
$$f(P_f) = f(t_{design})\left|\frac{dt_{design}}{dP_f}\right| \tag{J-10}$$
$$dP_f = \frac{1}{dt_{design}/dP_f}\,dt_{design}$$

Hence, Equation J-9 can be re-written as

$$\sigma_{P_f} = \left[\int \left(P_f(t_{design}) - \hat{P}_f\right)^2 f(t_{design})\,dt_{design}\right]^{1/2} \tag{J-11}$$

As seen from Equations J-8 and J-11, the mean and standard deviation of the probability of failure can be expressed in terms of the probability density function (pdf) *f* of the design thickness, t_{design}. Therefore, we can perform the failure probability estimations to after calculating the pdf of t_{design}. The random variables contributing to t_{design} are (see Equation J-2) *e*, *w* and σ_a. Since the variations of w and σ_a are small compared to *e*, we neglect their contribution and calculate the pdf of t_{design} from the pdf of error factor *e* from

$$f(t_{design}) = f_e(e)\frac{de}{dt_{design}} \tag{J-12}$$

where $f_e(e)$ is the updated pdf of *e*.

LIST OF REFERENCES

Acar, E., Kale, A. A., and Haftka, R. T., "Why are Airplanes so Safe Structurally? Effect of Various Safety Measures on Structural Safety of Aircraft," *Journal of Aircraft*, 2005, (In press).

Ahammed, M., Melchers, R. E., "Probabilistic Analysis of Pipelines Subjected to Pitting Corrosion Leaks," *Engineering Structures*, Vol. 17, No. 2, 1995, pp. 74-80.

Ahammed, M., Melchers, R. E., "Probabilistic Analysis of Underground Pipelines Subjected to Combined Stresses and Corrosion," *Engineering Structures*, Vol. 19, No. 12, 1997, pp. 988-994.

Ahmed, A., Bakuckas, J. G., Bigelow, C. A., Tan, P. W., "Initiation and Distribution of Fatigue Cracks in a Fuselage Lap Joint Curved Panel," *Proceedings of the 6th Joint FAA/DoD/NASA Conference on Aging Aircraft*, CA, 2002.

Ang, A. H-S., Tang, W. H., *Probability Concepts in Engineering Planning and Design*, Vol. 2- Decision, Risk and Reliability, John Wiley and Sons Inc., New York, 1975.

Arietta, A. J., Striz, A. G.,"Modelling of Aircraft Fatigue Load Environment," *38th Aerospace Sciences Meeting and Exhibit*, AIAA-00-0973, Reno, 2000.

Arietta, A. J., Striz, A. G., "Optimal Design of Aircraft Structures with Damage tolerance Requirements," *Structural and Multidisciplinary Optimization*, Vol. 30, No. 2, 2005, pp. 155-1631.

Backman, B., "Structural Design Performed to Explicit Safety Criteria Containing Uncertainties," *42nd AIAA/ASME/ASCE/AHS/ASC Structures, Structural Dynamics, and Materials Conference and Exhibit*, AIAA-01-1241, Seattle, 2001.

Belytschko, T., Lewis, E. E., Moran, B., Harkness, H. H., Platt, M., *Durability of Metal Aircraft Structures*, Atlanta Technology Publications, Atlanta, 1992.

Ben-Haim, Y., Elishakoff, I., *Convex Models of Uncertainty in Applied Mechanics*, Elsevier, New York, 1990.

Bert, F. M., John, R. C., Rippon, I. J., Maarten, J. J., Thomas, S., Kapusta, S., D., Magdy, M. G., Whitham, T., "Improvements on de Waard-Milliams Corrosion Prediction and Applications to Corrosion Management," *Corrosion Conference*, Paper No. 02235, National Association of Corrosion Engineers, Denver, 2002.

Bich, N. N., Eng, P., "An Approach to Corrosion Mitigation for Wet Gas Pipelines," *4th International Pipeline Conference*, Alberta, Canada, 2002.

Bristow, J. W., "The Meaning of Life". *The Aeronautical Journal*, Paper No. 2470, 2000, pp. 264-270.

Brot, A., "Probabilistic Inspection Strategies for Minimizing Service Failures," *FAA/NASA International Symposium on Advanced Structural Integrity Methods for Airframe Durability and Damage Tolerance, NASA Conference*, Part I, Langely Research Center, Hampton, 1994, pp. 99-109.

Burwell, D., Sridhar, N., Moghissi, O. P, "Internal Corrosion Direct Assessment of Dry Gas Transmission Pipelines," *Corrosion Conference*, Paper No. 04195, National Association of Corrosion Engineers, Houston, 2004.

Caleyo, F., Gonzalez, J. L., Hallen, J. M., "A Study on the Reliability Assessment Methodology for Pipelines ith Active Corrosion Defects," *International Journal of Pressure Vessels and Piping*, Vol. 79, 2002, pp. 77-86.

de Waard, C., Milliams, D. E., "Carbonic Acid Corrosion of Steel," *Journal of Corrosion Science*, Vol. 31, No. 5, 1975, pp. 177-181.

de Waard, C., Lotz, U., "Prediction of CO2 Corrosion of Carbon Steel," *Corrosion Conference*, Paper No. 69, National Association of Corrosion Engineers, Houston, 1993.

Department of Defense, *Joint Service Specification Guide-2006*, Air Force Research Lab, Wright Patterson Air Force Base, Dayton, 1998.

Elber, W., "Fatigue Crack Closure Under Cyclic Tension," *Engineering Fracture Mechanics*, Vol. 2, 1970, pp. 37-45.

Enright, M.P., Frangopol, D. M., "Reliability Based Lifetime Maintenance of Aging Highway Bridges," *Proceedings of SPIE 5th International Symposium on Nondestructive Evaluation and Health Monitoring of Aging Infrastructure*, Newport beach, 2000, pp. 4-13.

Erickson, D., Buck, E., Kolts, J., "Corrosion Inhibitor Transport in a Wet-Gas Pipeline," *Materials Performance*, Vol. 32, No. 9, 1993, pp. 32-49.

Federal Aviation Regulations, *Airworthiness Standards: Transport Category Airplanes*, Part 25, Sec. 25.613, Material Strength Properties and Material Design Values, 2005.

Fujimoto, Y., Kim, S. C., Hamada, K., Huang, F., "Inspection Planning Using Genetic Algorithm for Fatigue Deteriorating Structures," *Proceedings of the International Offshore and Polar Engineering Conference*, Vol. 4, Golden, 1998, pp. 461-468.

Garbatov, Y., Soares, C. G., "Cost and Reliability Based Strategies for Fatigue Maintenance Planning of Floating Structures," *Reliability Engineering and Systems Safety*, Vol. 73, No. 3, 2001, pp. 293-301.

Gartland, P. O., Johnsen, R., Ovstetun, I., "Application of Internal Corrosion Modeling in the Risk Assessment of Pipelines," *Corrosion Conference*, National Association of Corrosion Engineers, San Diego, 2003.

Gruber, M. L., Mazur, C. J., Wilkins, K. E., Worden, R. E., "Investigation of Fuselage Structure Subjected to Widespread Fatigue Damage," Report No. AR-95/47, Department of Transportation/Federal Aviation Administration, 1996.

Harkness, H. H, "Computational Methods for Fracture Mechanics and Probabilistic Fatigue," Ph.D. Dissertation, Dept. of Mechanical Engineering, Northwestern Univ., Evanston, IL, 1994.

Harkness, H. H., Fleming, M., Moran, B., Belytschko, T., "Fatigue Reliability Method with In-Service Inspections," *FAA/NASA International Symposium on Advanced Structural Integrity Methods for Airframe Durability and Damage Tolerance, NASA Conference*, Part I, Langely Research Center, Hampton, 1994, pp. 307-325.

Harlow, D. G., Wei, R. P, "A Probability Model for the Growth of Corrosion Pits in Aluminum Alloy Induced by Constituent Particle," *Engineering Fracture Mechanics*, Vol. 59, No. 3, 1998, pp. 305-325.

Hellevik, S., G., Langen, I., Sørensen, J. D., "Cost Optimal Reliability Based Inspection and Replacement Planning of Piping Subjected to CO_2 Corrosion," *International Journal of Pressure Vessels and Piping*, Vol. 76, No. 8, 1999, pp. 527-538.

Holmes, K. W., Chadwick, O. A., Kyriakidis, P. C., "Error in USGS 30 –Meter Digital Elevation Model and its Impact on Terrain Modeling," *Journal of Hydrology*, Vol. 233, 2000, pp. 154-173.

Hong, H. P., "Inspection and Maintenance Planning of Pipeline Under External Corrosion Considering Generation of New Defects," *Structural Safety*, Vol. 21, 1999, pp. 203-222.

Jackson, P., *Jane's All The World's Aircraft 1995-1996*, ISBN 0-710612621, ınternational Thomson Publishing Company, New York, 1996.

Kale, A. A, Haftka, R. T., Papila, M., Sankar, B. V., "Tradeoff for Weight and Inspection Cost for Fail-Safe Design," *44th AIAA/ASME/SDM Conference*, AIAA-2003-1501, Norfolk, 2003.

Kale, A. A., Haftka, R. T., Sankar, B. V., "Tradeoff of Structural Weight and Inspection Cost in Reliability Based Optimum Design Using Multiple Inspection Types," *10th AIAA/ ISSMO Multidisciplinary Analysis and Optimization Conference*, AIAA-2004-4404, Albany, 2004.

Kale, A. A., Thacker, B. H., Sridhar, N., Waldhart, C. J., "A Probabilistic Model for Internal Corrosion of Gas Pipelines." *International Pipeline Conference*, Paper No. IPC04-0483, Calgary, Alberta, Canada, 2004.

Kale, A. A., Haftka R. T., Sankar B. V., "Reliability Based Design and Inspections of Stiffened Panels," *46th AIAA/ASME/SDM Conference*, AIAA-2005-2145, Austin, 2005.

Kale, A. A., Haftka, R. T., "Effect of Safety Measures on Reliability of Aircraft Structure Subjected to Damage Growth," *Proceedings of ASME- IDECT-2005: 31st ASME Design Automation Conference, Simulation-Based Design under Uncertainty*, Paper No. 85384, Long Beach, 2005.

Lin, K. Y., Rusk, D. T., Du J., "An Equivalent Level of Safety Approach to Damage Tolerant Aircraft Structural Design," *41st AIAA/ASME/ASCE/AHS/ASC Structures, Structural Dynamics, and Materials Conference and Exhibit*, AIAA-00-1371, Atlanta, 2000.

Lincoln, J.W., "Method for Computation of Structural Failure Probability for an Aircraft," Report No. ASD-TR-80-5035, Wright Patterson Air Force Base, OH, 1980.

Long, M.W., Narciso, J. D., "Probabilistic Design Methodology for Composite Aircraft Structures," Report No. AR-99/2, Department of Defense, Federal Aviation Administration, 1999.

Love, A. E. H., *A Treatise on the Mathematical Theory of Elasticity,* 4th Ed., Dover Publications, New York, 1944, pp. 209-214.

Madsen, H. O., Krenk, S., Lind, N. C., *Methods of Structural Safety*, Prentice Hall, Inc., New Jersey, 1986.

Mathworks Inc., *MATLAB Version 6.5.0*, Natick, MA, 1994-2002

Melchers, R. E., *Structural Reliability Analysis and Prediction*, Wiley, New York, 1987.

Miner, M. A., "Cumulative Damage in Fatigue," *Journal of Applied Mechanics*, Vol. 12, 1945, pp. A159-A164.

Muhlbauer, W. K., *Pipeline Risk Management Manual*, 2nd Ed., Gulf Publishing Company, Houston, 1996.

Myers, R. H., Montgomery, D. C., *Response Surface-Process and Product Optimization Using Designed Experiments*, Wiley, New York, 1995.

Neal, D. M., Matthews, W. T., and Vangel, M. G., "Uncertainties in Obtaining High Reliability from Stress-Strength Models," *Proceedings of the 9th DOD-/NASA/FAA Conference on Fibrous Composites in Structural Design*, DOT/FAA/CT 92-95, Part I, Lake Tahoe, 1992, pp. 503-521.

Nees, C. D., Canfield, R. A., "Methodology for Implementing Fracture Mechanics in Global Structural Design of Aircraft," *Journal of Aircraft*, Vol. 35, No. 1, 1998, pp 131-138.

Nguyen, B., Heaver, E., "Assessment and Control of Top Side/Riser/ Pipeline Corrosion of a Subsea Gas Re-Injection System," *Corrosion Conference*, Paper No. 03637, National Association of Corrosion Engineers, San Diego, 2003.

Niu, M. C., *Airframe Structural Design*, *In: Fatigue, Damage Tolerance and Fail-Safe Design,* Conmilit Press Ltd., Hong Kong, 1990, pp. 538-570.

Oberkampf, W. L., Deland, S. M., Rutherford, B. M., Diegert, K. V., and Alvin, K. F., "Error and Uncertainty in Modeling and Simulation," *Reliability Engineering and Systems Safety*, Vol. 75, 2002, pp. 333-357.

Palmberg, B., Blom, A. F., Eggwertz, S., "Probabilistic Damage Tolerance Analysis of Aircraft Structures". *Probabilistic Fracture Mechanics and Reliability*, Vol. 10, 1987, pp. 275-291.

Papila, M., "Accuracy of Response Surface Approximations for Weight Equations Based on Structural Optimization," Ph.D. Dissertation, Dept. of Mechanical and Aerospace Engineering, University of Florida, Gainesville, FL, 2001.

Paris, P. C., Erdogan, F., "A Critical Analysis of Crack Propagation Laws", *Journal of Basic Engineering*, Vol. 85, 1960, pp. 528-534.

Paris, P. C., "The Growth of Fatigue Cracks Due to Variations in Load," Ph.D. Dissertation, Dept. of Mechanical Engineering, Leigh University, Bethlehem, PA, 1962.

Petit, R. G., Wang, J. J., Toh, C., "Validated Feasibility Study of Integrally Stiffened Metallic Fuselage Panels for Reducing Manufacturing Costs," Report No. CR-2000-209342, NASA, 2000.

Philipchuk, J. M., "Relationship Between Field Measurements and Corrosion Leaks," *International Gas Research Conference*, San Diego, 1998.

Provan, J. W., *Probabilistic Fracture Mechanics and Reliability*, 1st Ed., Martinus Nijhoff, Boston, 1987.

Provan, J.W., Farhangdoost, K., ”A New Stochastic Systems Approach to Structural Integrity,” *FAA/NASA International Symposium on Advanced Structural Integrity Methods for Airframe Durability and Damage Tolerance, NASA Conference*, Part I, Langely Research Center, Hampton, 1994, pp 603-619.

Qu, X., “Reliability-Based Structural Optimization Using Response Surface Approximations and Probabilistic Sufficiency Factor,” Ph.D. Dissertation, Dept. of Mechanical and Aerospace Engineering, University of Florida, Gainesville, FL, 2004.

Rahman, S., Rice, R., “Assessment of the Reliability of the Commercial Aircraft Fleet Considering the Potential Adverse Effects of Multiple Repairs and Multiple Site Damage,” Preliminary Technical Interchange Report. DOT/FAA, Aging Aircraft Program, 1992.

Rajasankar, J., Iyer, N. R., Apparao, T. V. S. R., “Structural Integrity Assessment of Offshore Tubular Joints Based on Reliability Analysis”, *International Journal of Fatigue*, Vol. 25, 2003, pp. 609-619.

Richardson, D. J., Williamson, G. C., “Results From a Predictive Flow Model Used to Assess Internal Corrosion Likelihood and the Subsequent Development of a Risk-Based Integrity Plan for a Natural Gas Gathering System,” *Corrosion Conference*, Paper No. 02247, National Association of Corrosion Engineers, Denver, 2002.

Riha, D. S., Thacker, B. H., Millwater, H. R., Wu, Y.-T., and Enright, M. P., “Probabilistic Engineering Analysis Using the NESSUS Software,” *41st Structural Dynamics and Materials Conference*, AIAA-2000-1512, Atlanta, 2000.

Riley, S. J., DeGloria, S.D., Elliot, R., “A Terrain Ruggedness Index That Quantifies Topographic Heterogeneity,” *Intermountain Journal of Sciences*, Vol. 5, 1999, pp. 23-27.

Rummel, W. D., Matzkanin, G. A., *Non destructive Evaluation Capability Data Book,* 3rd Ed., Nondestructive Testing Information Analysis Center, Austin, 1997.

Sakude, M. T., Schiavone, G., Morelos-Borja, H., Martin, G., Cortes, A., “Recent Advances on Terrain Database Correlation Testing,” *SPIE Aerosense Conference,* Institute for Simulation and Training, Orlando, 1988.

Schijve J., *Fatigue in Structures and Materials*, Kluwer Academic Publishers, MA, 2001.
Shih, P., Mahadevan, S.,”Corrosion Fatigue and Multiple Site Damage Reliability Analysis,” *International Journal of Fatigue*, Vol. 68, 2003, pp. 1493-1507.

Simola, K., Pulkkinen, U., “Models for Non-Destructive Inspection Data,” *Reliability Engineering and Systems Safety*, Vol. 60, 1998, pp. 1-12.

Sinclair, G. B., Pierie, R. V., “On Obtaining Fatigue Crack Growth Parameters From the Literature,” *International Journal of Fatigue*, Vol. 12, No. 1, 1990, pp. 57-62.

Society of Automotive Engineers, "Integration of Probabilistic Methods into the Design Process," Aerospace Information Report No. 5080, SAE, PA, 1997.

Sridhar, N., Dunn, D. S., Anderko, A. M., Lencka, M. M., Schutt, H. U., "Effect of Water and Gas Composition on the Internal Corrosion of Gas pipelines-Modeling and Experimental Studies," *Corrosion*, Vol. 57, No. 3, 2001, pp. 221-235

Swift, T., "Fracture Analysis of Stiffened Structure," *American Society for Testing of Materials, Special Technical Publication, ASTM STP 842*, 1984, pp. 69-107.

Takus, D. A., Profozich, D. M., "Arena Software Tutorial," *Proceedings of the Winter Simulation Conference*, Atlanta, 1997.

Tang, G., Wenzhong, S., Mudan, Z., Zhang Y., "Modeling Slope Uncertainty Derived From DEMS: A Case Study in China Loess Plateau Area," Report No. 49971065, National Nature Science Foundation of China, 2000.

Thacker, B. H., Popelar, C. F., McClung, R. C., "A New Probabilistic Method for Predicting the Long Life Reliability of Pipelines," *Proceedings of International Conference on Pipeline Reliability*, Calgary, Alberta, Canada, 1992.

Tisseyre, M., Plantec, J. Y., Beaufils, J. Y., Boetsch, R., "Aerospatiale Probabilistic Methods Applied to Aircraft Maintenance," *Proceedings of the 17th International Committee on Aeronautical Fatigue, Durability and Structural Reliability of Airframes*, Stockholm, Sweden, 1994, pp. 589-617.

Tober G. and Klemmt W.B., "NDI Reliability Rules used by Transport Aircraft-European View Point," *15th World Congress on Non Destructive Testing*, Paper No. 739, Rome, Italy, 2000.

Toyoda-Makino, M., "Cost-Based Optimal History Dependent Strategy for Random Fatigue Cracks Growth," *Probabilistic Engineering Mechanics*, Vol. 14, 1999, pp. 339-347

Venter, G., "Non-Dimensional Response Surfaces for Structural Optimization with Uncertainty," Ph.D. Dissertation, Dept. of Mechanical and Aerospace Engineering, Univ. of Florida, Gainesville, FL., 1998.

Vermeulen, B., Tooren, M. J., "Design Case Study for a Comparative Performance Analysis of Aerospace Materials," *Journal of Materials and Design*, Vol. 27, No. 1, 2004, pp. 10-20.

Vinod, G., Bidhar, S. K., Kushwaha, H. S., Verma, A. K., Srividya, A., "A Comprehensive Framework for Evaluation of Piping Reliability due to Erosion-Corrosion for Risk-Informed In-service Inspection," *Reliability Engineering and Systems Safety*, Vol. 82, No. 2, 2003, pp. 187-193.

Walker, E. K., "The Effect of Stress Ratio During Crack Propagation and Fatigue for 2024-T3 and 7075-T6. The Effect of Environment and Complex Load History on Fatigue Life," *American Society for testing of Materials, ASTM STP-462*, 1970, pp. 1-15.

Wei, R. P., Harlow, D. G., "Corrosion Enhanced Fatigue and Multi Site Damage," *43rd AIAA/ASME/ASCE/AHS/ASC Structures, Structural Dynamics, and Materials Conference*, AIAA-2002-1398, Denver, 2002.

Weir, T. W., Simmons, G. W., Hart, R. G., Wei, R. P., "A Model for Surface Reaction and Transport Controlled Fatigue Crack Growth," *Scripta Metallurgica*, Vol. 14, 1980, pp. 357-364.

Weng, *Quantifying Uncertainty of Digital Elevation Models Derived from Topographic Maps, In: Advances in Spatial Data Handling,* Springer-Verlag, New York, 2002, pp. 403-418.

Westergaard, H. M., "Bearing Pressure and Cracks," *Journal of Applied Mechanics*, Vol., No. 1, 1939, pp. 49-53.

Wheeler, D. E., "Spectrum Loading and Crack Growth," *Journal of Basic Engineering*, Vol. 94, 1972, pp. 181-186.

Willenborg, J., Engle, R. M., Wood, H. A., "A Crack Growth Retardation Model Using and Effective Stress Concept," Report No. 71-1-F1312, Air Force Flight Dynamics Laboratory, Wright-Patterson Air Force Base, OH, 1971.

Wirsching, P. H., "Probabilistic Structural Analysis Methods for Select Space Propulsion System Components," NASA Contractor Report No. 189159, Vol. III., NASA Lewis Research Center, OH, 1992.

Wu, J. Y., Millwater, R. Y., Enright, M. P., Chell, G. G., Kuhlman, C. J., Leverant G. R., "Probabilistic Method for Design Assessment of Reliability with Inspection (DARWIN)." *41st AIAA/ASME/ASCE/AHS/ASC Structures, Structural Dynamics, and Materials Conference and Exhibit*, AIAA-00-1371, Atlanta, 2000.

Wu, J., Shin, Y., "Probabilistic Damage Tolerance Methodology for Reliability Design and Inspection Optimization," *45th AIAA/ASME/ASCE/AHS/ASC Structures, Structural Dynamics, and Materials Conference and Exhibit*, AIAA-04-1789, Palm Springs, 2003.

Wu, J., Shin, Y., "Probabilistic Function Evaluation System (ProFES) for Maintenance Optimization," *46th AIAA/ASME/ASCE/AHS/ASC Structures, Structural Dynamics and Materials Conference 13th AIAA/ASME/AHS Adaptive Structures Conference*, AIAA-2005-2214, Austin, 2005.

Yu, J. C., "Stress Intensity Factor for an Edge Crack in a Stiffened Sheet," *American Society for Testing of Materials, ASTM STP 945*, 1988, pp. 247-258.

Zhang, R., Mahadevan, S., "Model Uncertainty and Bayesian Updating in Reliability Based Inspection," *Structural Safety*, Vol. 22, No. 2, 2000, pp. 145-160.

Zhang, R., Mahadevan, S., "Reliability Based Reassessment of Corrosion Fatigue Life," *Structural Safety*, Vol. 23, No. 1, 2001, pp. 77-91.

BIOGRAPHICAL SKETCH

Amit Anand Kale was born on 25th of October 1978 at Bhopal in India. He received a Bachelor of Technology degree in aerospace engineering in May 2000 from the Indian Institute of Technology, Kharagpur. He then joined Deneb Robotics Inc, India, as a software programmer. After working for a year he joined the Department of Mechanical and Aerospace Engineering at the University of Florida to pursue doctoral studies in August 2001. While at the University of Florida he completed a four month internship at Southwest Research Institute.